AD_____

Award Number: W81XWH-09-1-0198

TITLE: Tumor-Selective Targeting of Androgen Receptor Expression by Novel Small-Molecule Agents

PRINCIPAL INVESTIGATOR: Ching-Shih Chen, Ph.D.

CONTRACTING ORGANIZATION: Ohio State University
Columbus, OH 43210

REPORT DATE: May 2013

TYPE OF REPORT: Final

PREPARED FOR: U.S. Army Medical Research and Materiel Command
Fort Detrick, Maryland 21702-5012

REPORT DOCUMENTATION PAGE

Form Approved
OMB No. 0704-0188

1. REPORT DATE	2. REPORT TYPE	3. DATES COVERED
May 2013	Final	1 May 2009 – 30 April 2013

4. TITLE AND SUBTITLE

Tumor-Selective Targeting of Androgen Receptor Expression by Novel Small-Molecule Agents

5a. CONTRACT NUMBER

5b. GRANT NUMBER
W81XWH-09-1-0198

5c. PROGRAM ELEMENT NUMBER

6. AUTHOR(S)

Ching-Shih Chen

E-Mail: chen.844@osu.edu

5d. PROJECT NUMBER

5e. TASK NUMBER

5f. WORK UNIT NUMBER

7. PERFORMING ORGANIZATION NAME(S) AND ADDRESS(ES)

Ohio State University
Columbus, OH 43210

8. PERFORMING ORGANIZATION REPORT NUMBER

9. SPONSORING / MONITORING AGENCY NAME(S) AND ADDRESS(ES)
U.S. Army Medical Research and Materiel Command
Fort Detrick, Maryland 21702-5012

10. SPONSOR/MONITOR'S ACRONYM(S)

11. SPONSOR/MONITOR'S REPORT NUMBER(S)

12. DISTRIBUTION / AVAILABILITY STATEMENT
Approved for Public Release; Distribution Unlimited

13. SUPPLEMENTARY NOTES

14. ABSTRACT

This project is aimed at test the hypothesis that targeting androgen receptor (AR) expression by small-molecule agents represents a potentially successful strategy to block prostate tumor growth and to delay prostate progression. Based on our finding that the AR-ablative agent CG-12 blocked AR expression through the inhibition of glucose uptake, we embarked on the lead optimization of CG-12 to generate novel glucose transporter inhibitors with high potencies in suppressing AR signaling in LNCaP and VCaP cells. These agents inhibited AR expression through β-TrCP-mediated Sp1 downregulation, leading to transcriptional repression of the AR gene. By using a structurally optimized derivative, CG-5, the present study demonstrates the therapeutic relevance of targeting the Warburg effect to prostate cancer therapy, in part, through the blockade of AR signaling. Oral CG-5 exhibits in vivo efficacy in suppressing LNCaP-abl xenograft tumor growth in nude mice, and in suppressing the progression of pre-neoplastic prostatic intraepithelial neoplasia progression in TRAMP mice, which correlated with the drug's ability to modulate biomarkers associated with AR signaling.

15. SUBJECT TERMS
None provided

16. SECURITY CLASSIFICATION OF:			17. LIMITATION OF ABSTRACT	18. NUMBER OF PAGES	19a. NAME OF RESPONSIBLE PERSON
a. REPORT	b. ABSTRACT	c. THIS PAGE			USAMRMC
U	U	U	UU	55	19b. TELEPHONE NUMBER *(include area code)*

Table of Contents

Final Report* for Award Number W81XWH-09-1-0198
Tumor-Selective Targeting of Androgen Receptor Expression by Novel Small-Molecule Agents

Submitted by Ching-Shih Chen
Division of Medicinal Chemistry, College of Pharmacy, The Ohio State University
Parks Hall, 500 West 12th Avenue, Columbus, OH 43210
Tel: 614-688-4008; Fax: 614-688-8556; E-mail: chen.844@osu.edu

A. INTRODUCTION

Despite the general success of anti-androgen therapy, prostate cancer cells develop the castration-resistant phenotype through various evasive mechanisms. Alternative strategies for targeting AR signaling in hormone-refractory prostate cancer (HRPC) include (1) exclusion of AR activity by inhibiting dimerization or DNA binding, (2) inhibition of androgen synthesis, and (3) silencing of AR expression. A recent example is the drug abiraterone acetate, an oral, irreversible inhibitor of cytochrome P450C17, currently undergoing clinical trials in advanced prostate cancer. The hypothesis to be tested in this proposal is that **targeting AR expression by small-molecule agents represents a potentially successful strategy to block prostate tumor growth and to delay prostate progression.**

In about one third of HRPC patients, the AR gene is amplified, leading to increased AR expression and enhanced AR activation by low levels of androgens. Moreover, androgen-refractory tumors may contain mutations in the AR gene, which increase the number of ligands that can activate the receptor including other steroids as well as anti-androgens. Mounting evidence implicates intact AR signaling as a key factor in the recurrent growth of human prostate tumors after androgen depletion, and defines a need for therapeutic strategies that include the direct targeting of AR to improve the treatment of androgen-independent prostate cancer and ultimately to increase the survival of HRPC patients. In the PI's lab, we have developed OSU-CG12, a small-molecule agent capable of suppressing AR gene expression at μM concentrations by targeting Sp1 protein stability in a tumor-selective manner. Pursuant to this finding, the focus of this project is threefold.

Aim 1. Lead optimization of OSU-CG12 via combinatorial synthesis.
Aim 2. To validate the mechanism by which lead OSU-CG12 derivatives mediate AR ablation.
Aim 3. To assess the *in vivo* effect of lead OSU-CG12 derivatives on blocking prostate tumor progression in the LNCaP-C4-2 xenograft model.

In this Final Report, our results in each of the three specific aims are summarized as follows.

B. BODY

B.1. Lead optimization of OSU-CG12 via combinatorial synthesis (Aim 1)

D. Wang, P.-C. Chu, C.N. Yang, R. Yan, Y.-C. Chung, S. K. Kulp, and **C.-S. Chen** (2012) "Development of a Novel Class of Glucose Transporter Inhibitors" ***J. Med. Chem***. 55, 3827-3836

Pursuant to our finding that OSU-CG12 suppressed the expression of AR through the inhibition of glucose uptake (Aim 2), we embarked on the lead optimization of CG-12, of which the strategy is depicted in Fig. 1.

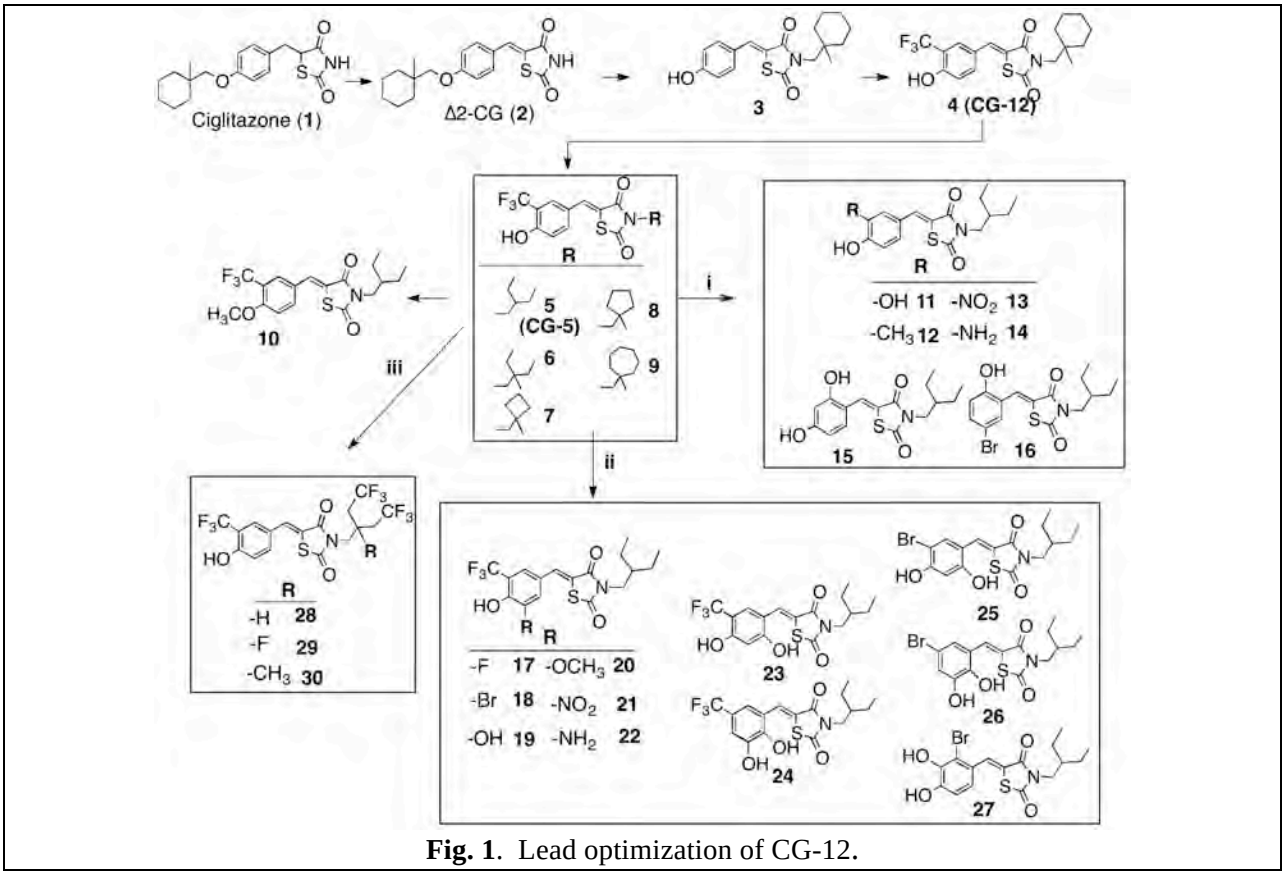

Fig. 1. Lead optimization of CG-12.

Among these derivatives, CG-30 represented the optimal agent in suppressing [^{3}H]-2-deoxyglucose entry and viability of LNCaP cells (Fig. 2).

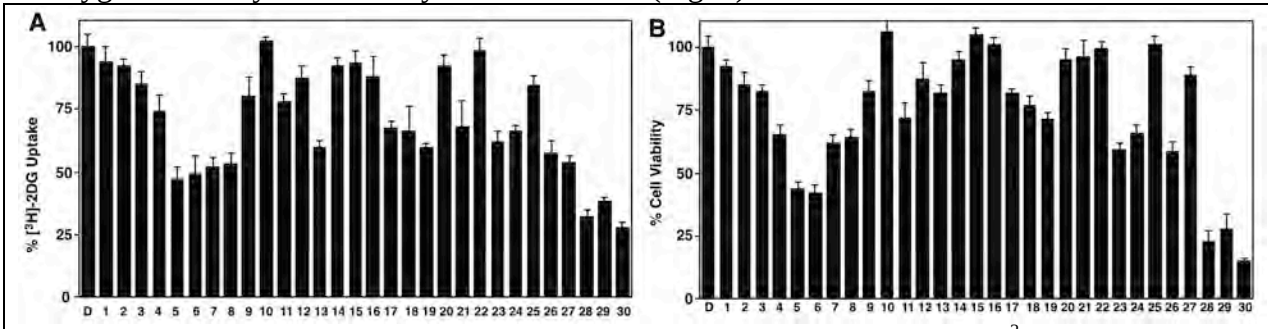

Fig. 2. (A) Inhibitory effects of compounds **1** – **30**, each at 5 μM, on the uptake of [^{3}H]2-DG into LNCaP cells in Krebs-Ringer phosphate buffer at 37°C after 30 min of drug treatment. Column, mean; bars, SD (N = 3). (B) The corresponding effects of compounds **1** – **30** on the viability of LNCaP cells by MTT assays in 10% FBS-containing RPMI 1640 medium after 72 h of drug treatment. Column, mean; bars, SD (N = 6).

Dose-response analysis confirmed the high potency of compound **30** in blocking [^{3}H]2-DG uptake into LNCaP cells with IC_{50} of 2.5 μM, while the IC50 values of other compounds examined were as follows: **28**, 3.5 μM; **5**, 6 μM; **4**, 9 μM; **2**, 52 μM; **1**, 78 μM (Fig. 3).

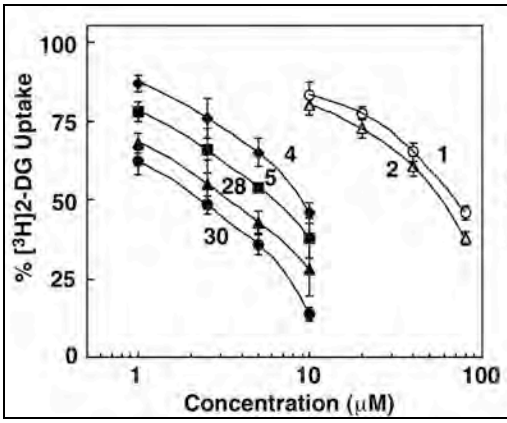

Fig. 3. Dose-dependent inhibitory effects of compounds **1**, **2**, **4**, **5**, **28**, and **30** on the uptake of [^{3}H]2-DG into LNCaP cells in Krebs-Ringer phosphate buffer at 37°C after 30 min of drug treatment. Points, mean; bars, SD (N = 3).

Examinations of the dose-dependent suppressive effects of compounds **28** and **30** versus compounds **1**, **2**, **4**, and **5** on the viability of LNCaP cells revealed differential antiproliferative potencies that paralleled the respective inhibitory activities in glucose uptake (Fig. 4A). After 72 h of exposure in 10% fetal bovine serum (FBS)-containing medium, the IC_{50} values for individual compounds were: **30**, 1.5 μM; **28**, 2.2 μM; **5**, 4.2 μM; **4**, 6 μM; **2**, 28 μM; **1**, 60 μM. It is noteworthy that despite the high potency of the optimal agent compound **30** in suppressing the viability of LNCaP cells, normal human prostate epithelial cells (PrECs) and human mammary epithelial cells (HMECs) were resistant to the cytotoxic effect of compound **30** even at 10 μM (Fig. 4B). This drug-induced cell death was, at least in part, attributable to apoptosis, as evidenced by a dose-dependent increase in poly(ADP-ribose) polymerase (PARP) cleavage in response to compound **30** (Fig. 4C). Western blot analysis indicates that compound **30** (CG-30) dose dependently increased β-TrCP expression, leading to the downregulated expression of its substrates cyclin D1 and Sp1, as well as the Sp1 target AR (Fig. 4C).

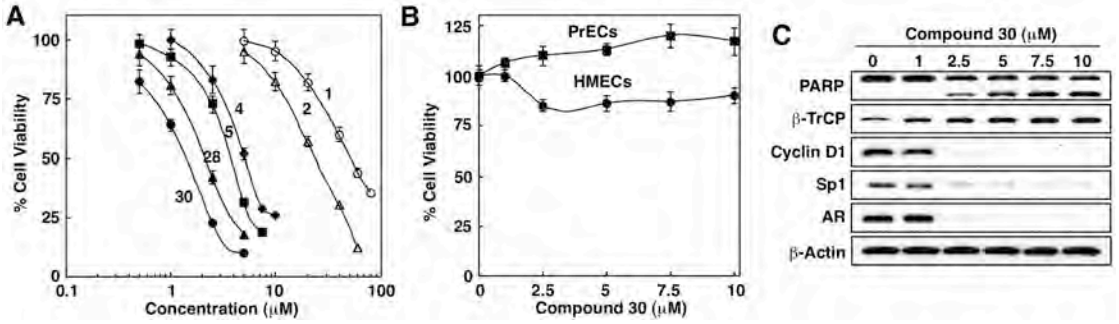

Fig. 4. (A) Dose-dependent suppressive effects of compounds **1**, **2**, **4**, **5**, **28**, and **30** on the viability of LNCaP cells by MTT assays in 10% FBS-containing RPMI 1640 medium after 72 h of drug treatment. Points, mean; bars, SD (N = 6). (B) Dose-dependent effect of compound **30** on the viability of normal prostate epithelial cells (PrECs) and human mammary epithelial cells (HMECs) after 72 h of treatment. Points, mean; bars, SD (N = 6). (C) Western blot analysis of the dose-dependent effects of compound **30** on PARP cleavage, β-TrCP, the β-TrCP substrates cyclin D1 and Sp1, and AR.

However, in vivo efficacy study of various structurally optimized OSU-CG12 derivatives, including CG-5, CG-28, and CG-30, indicates that daily oral CG-5 at 100 mg/kg was effective in suppressing the growth of C4-2 xenograft tumors in nude mice, while CG-28 and CG-30 were ineffective due to the poor bioavailability of these compounds (Aim 3). Thus, in the subsequent mechanistic studies, we used CG-5 as a proof-of-concept compound to validate the mode of mechanism of glucose transporter inhibitors in blocking AR signaling.

B.2. To validate the mechanism by which lead OSU-CG12 derivatives mediate AR ablation (Aim 2)

The effect of CG-5 on the expression of AR and its downstream targets was examined by using both immunoblotting and quantitative real-time PCR (qPCR) in LNCaP versus VCaP cells, as depicted by Fig. 5A and B, respectively. As shown, CG-5 was effective in inhibiting AR expression in LNCaP, and, to a lesser extent, VCaP cells. Nevertheless, the potencies of CG-5 to downregulate the expression of AR downstream targets, at both protein and mRNA levels, were comparable in both cell lines. It is noteworthy that VCaP cells harbors *TMPRSS2-ERG* fusion, which is significantly associated with prostate cancer-specific mortality. From a clinical perspective, the ability of CG-5 to block the transcription of *TMPRSS2-ERG* gene through the inhibition of AR signaling is of therapeutic relevance to prostate cancer treatment.

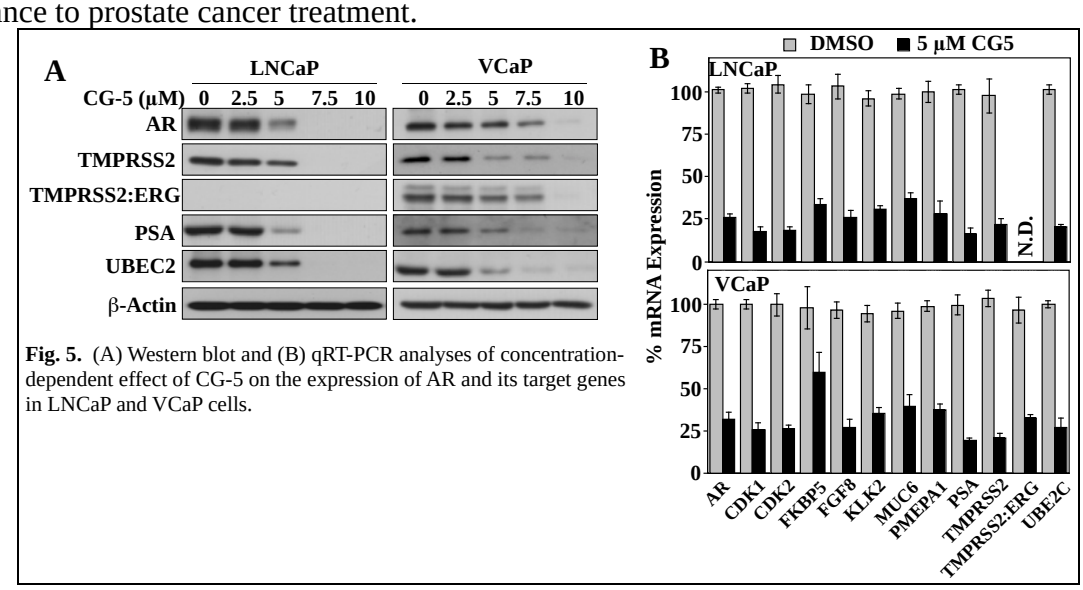

Fig. 5. (A) Western blot and (B) qRT-PCR analyses of concentration-dependent effect of CG-5 on the expression of AR and its target genes in LNCaP and VCaP cells.

Mode of mechanism of CG-5 in suppressing AR expression differs between LNCaP and VCaP cells. Previously, we reported that CG-12 inhibited AR expression in LNCaP cells through β-TrCP-mediated Sp1 downregulation, leading to transcriptional repression of the *AR* gene. This mechanistic link was verified in CG-5-treated LNCaP cells as overexpression of Sp1 could protect LNCaP cells from CG-5-mediated AR downregulation (Fig. 6A). This protective effect, however, was not noted in VCaP cells (Fig. 6B), suggesting that a distinct mechanism was involved in the drug effect on AR expression. It is noteworthy that CG-5-mediated inhibition of Sp1 expression was accompanied by parallel decreases in the level of c-Myc in both cell lines (Fig. 6A and B) (as well as CG-12, data not shown). More important, enforced expression of c-Myc abolished the ability of CG-5 to suppress AR expression in VCaP, but not LNCaP cells. This finding is of clinical implications as it suggests that involvement of multiple mechanisms in the regulation of AR expression in prostate cancer cells.

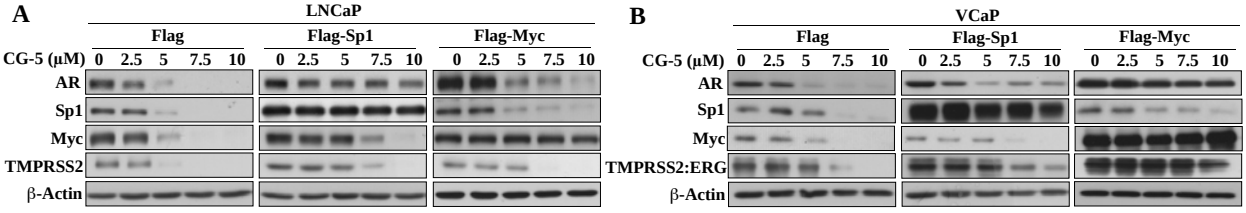

Fig. 6. Effects of the ectopic expression of Sp1 versus c-Myc on CG-5-mediated suppression of AR expression in (A) LNCaP versus (B) VCaP cells.

B.3. To assess the *in vivo* effect of CG-5 on blocking prostate tumor progression in the LNCaP-C4-2 and LNCaP-abl xenograft models (manuscript in preparation)

In this study, we aimed to determine CG-5's *in vivo* activity, namely whether CG-5 could suppress the growth of castration-resistant human prostate cancer cells in xenograft mice. First, we assessed the effect of daily oral CG-5 at 100 mg/kg on the growth of LNCaP-C4-2 xenograft tumors in nude mice. At day 7 of treatment, statistically significant tumor shrinkage was noted (Fig. 7). However, accurate measurements of tumor volume after day 7 of treatment could not be obtained because tumors developed multiple expansile hematomas (data not shown) that obscured the tumor borders. These hematomas persisted through day 28 of the treatment, and undermined the ability to accurately measure the tumors using calipers.

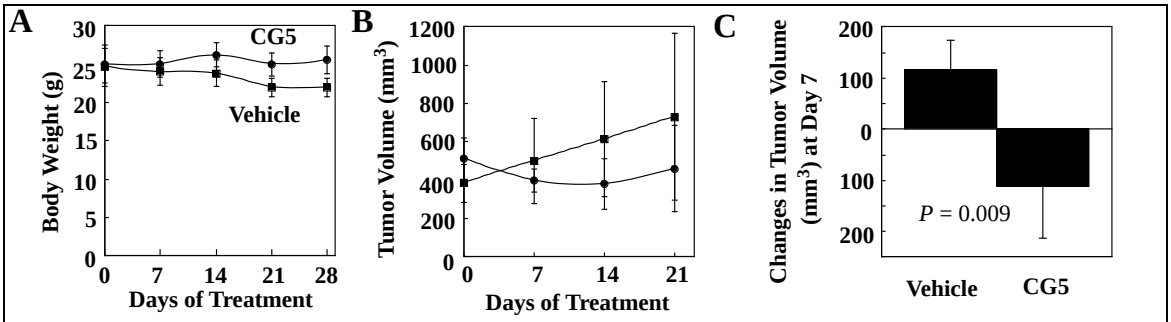

Fig. 7. ***A and B***, Time-dependent effects of daily oral CG5 at 100 mg/kg versus vehicle control on the body weight and xenograft tumor volume of C4-2 xenograft tumor-bearing mice (n = 4). ***C***, Changes in the volume of C4-2 xenograft tumor volume at day 7 of CG5 versus vehicle treatment.

Given the encouraging results regarding CG-5's effect on the growth of LNCaP-C4-2 tumors, we decided to investigate the effect of CG-5 treatment on the *in vivo* growth of another castration-resistant LNCaP derivative, the LNCaP-abl line. Treatment of LNCaP-abl xenograft tumor baring mice resulted in statistically significant suppression of tumor growth starting at day 7 of treatment (Fig. 8). At day 59, the study end point, the average tumor volume for the vehicle-treated mice was 115.3±56.7 mm^3 and the average tumor volume for the CG-5-treated mice was 58.5±26 mm^3 (*P*=0.033). The average change in tumor volume over the course of the study was +68.6±51.2 mm^3 and +13.3±26.2 mm^3 (*P*=0.026) for the vehicle-treated and CG-5 treated mice, respectively. This translates to an approximately 81% suppression of tumor growth by CG-5.

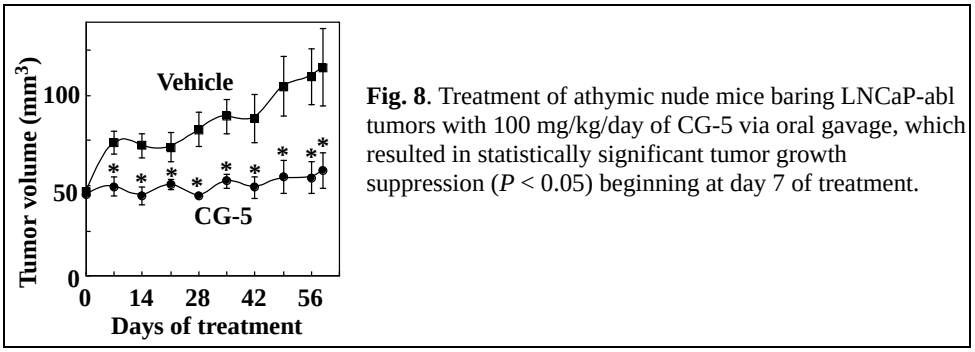

Fig. 8. Treatment of athymic nude mice baring LNCaP-abl tumors with 100 mg/kg/day of CG-5 via oral gavage, which resulted in statistically significant tumor growth suppression ($P < 0.05$) beginning at day 7 of treatment.

Suppression of LNCaP-abl xenograft tumor growth by CG-5 was not associated with any evidence of systemic toxicity. There was no statistically significant difference between the amount of weight mice in the two groups gained over the 4-week course of the study (*P*=0.233). On average, the CG-5-treated mice gained 1.44±0.75g (n=7). For comparison, the vehicle-treated mice gained 1.93±0.71g (n=7). Additionally, histological evaluation of H&E-stained sections of

heart, lung, liver, spleen, kidney, small intestine, brain, eye, and bone marrow from 5 mice per group did not reveal any lesions compatible with systemic or organ specific toxicity. Complete blood counts did not reveal any significant hematologic abnormalities, and serum chemistry for evaluation of renal and hepatic parameters was not consistent with hepatic or renal dysfunction (n=3 mice/group).

The suppression of tumor growth associated with CG-5 treatment was due to decreased intratumoral cell proliferation. Western blots for PCNA demonstrated that CG-5 treatment reduced intratumoral PCNA expression by 57% (*P*=0.030) (Fig. 9). Given that CG-5 was able to invoke the starvation-associated response in LNCaP cells *in vitro*, Western blotting for selected biomarkers was performed to determine if induction of a similar response occurred *in vivo*. Western blotting for the downstream targets of β-TRCP, namely Sp1, AR, cyclin D1, and cyclin E, was performed (Fig. 9A). Western blots from LNCaP-abl tumor homogenates revealed that CG-5 treatment resulted in statistically significant decreases in Sp1, AR, cyclin D1, and cyclin E with reductions in protein levels by 54% (*P*=0.017), 67% (*P*=0.010), 60% (*P*=0.014), and 54% (*P*=0.015), respectively (Fig. 9B).

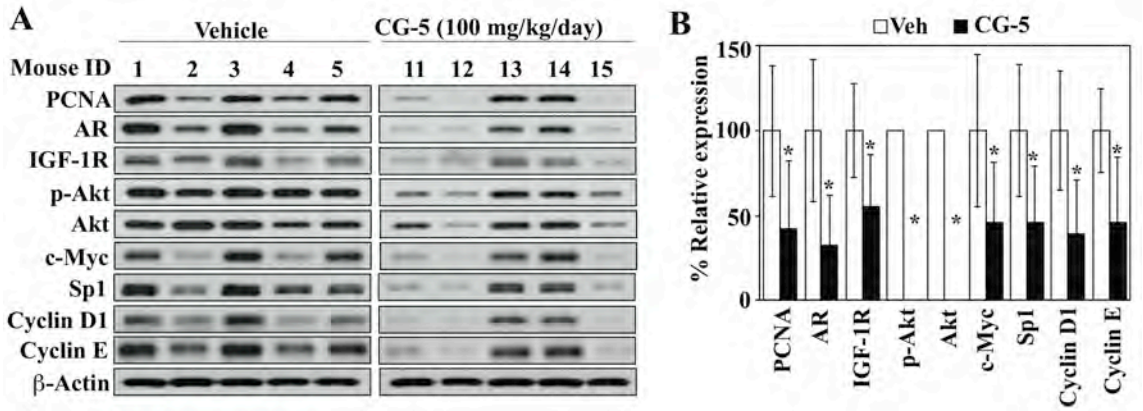

Fig. 9. 100 mg/kg/day of oral CG-5 reduced LNCaP-abl xenograft intratumoral proliferation, as evidenced by the 57% decrease (*P*=0.030) in PCNA compared to the vehicle-treated control mice, and biomarkers downstream of β-TRCP, namely Sp1 (54%, *P*=0.017), AR (67%, *P*=0.010), cyclin D1 (60%, *P*=0.014), and cyclin E (54%, *P*=0.015) compared to the vehicle-treated control.

B.4. Suppression of Prostate Epithelial Proliferation and Intraprostatic Pro-Growth and Survival Signaling in Transgenic Mice by a Novel Energy Restriction-Mimetic Agent

L. D. Berman-Booty, P.-C. Chu, J. M. Thomas-Ahner, D. Wang, T. Yang, S. K. Clinton, S. K. Kulp, **C.-S. Chen** (2013) "Suppression of Prostate Epithelial Proliferation and Intraprostatic Pro-Growth and Survival Signaling in Transgenic Mice by a Novel Energy Restriction-Mimetic Agent" ***Cancer Prev. Res.*** 6, 232-241

In this study, we examined the effect of OSU-CG5 on the severity of pre-neoplastic lesions in male transgenic adenocarcinoma of the mouse prostate (TRAMP) mice. Daily oral treatment with OSU-CG5 at 100 mg/kg from six to ten weeks of age resulted in a statistically significant decrease in the weight of urogenital tract and microdissected dorsal, lateral, and anterior prostatic lobes relative to vehicle controls (Fig. 10).

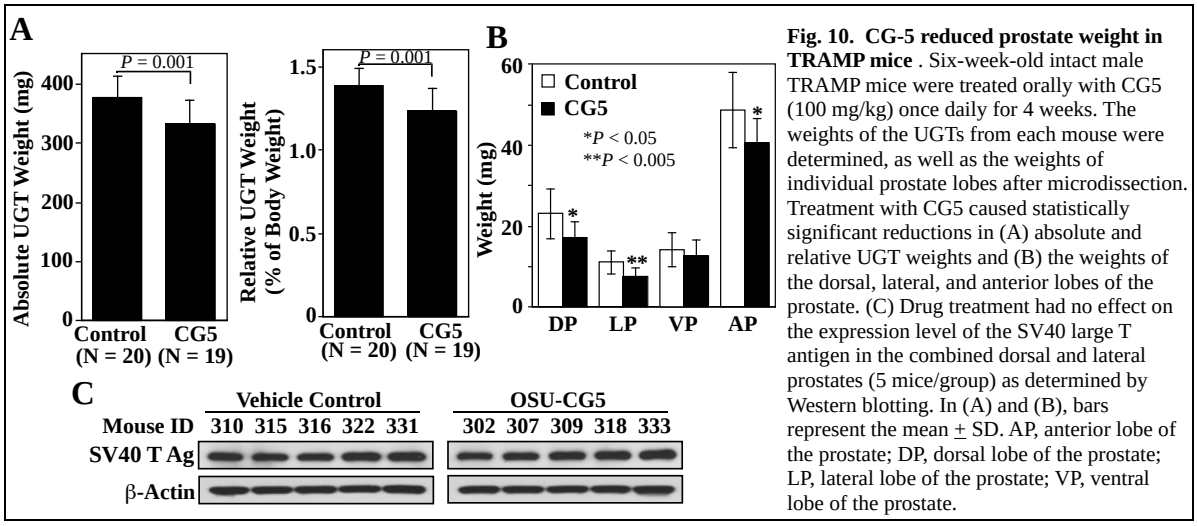

Fig. 10. CG-5 reduced prostate weight in TRAMP mice . Six-week-old intact male TRAMP mice were treated orally with CG5 (100 mg/kg) once daily for 4 weeks. The weights of the UGTs from each mouse were determined, as well as the weights of individual prostate lobes after microdissection. Treatment with CG5 caused statistically significant reductions in (A) absolute and relative UGT weights and (B) the weights of the dorsal, lateral, and anterior lobes of the prostate. (C) Drug treatment had no effect on the expression level of the SV40 large T antigen in the combined dorsal and lateral prostates (5 mice/group) as determined by Western blotting. In (A) and (B), bars represent the mean ± SD. AP, anterior lobe of the prostate; DP, dorsal lobe of the prostate; LP, lateral lobe of the prostate; VP, ventral lobe of the prostate.

The suppressive effect of OSU-CG5 was evidenced by marked decreases in Ki-67 immunostaining and proliferating cell nuclear antigen expression in the prostate, as well as a reduction in the disease index, a reflection of prostate pathology across all lobes (Fig. 11).

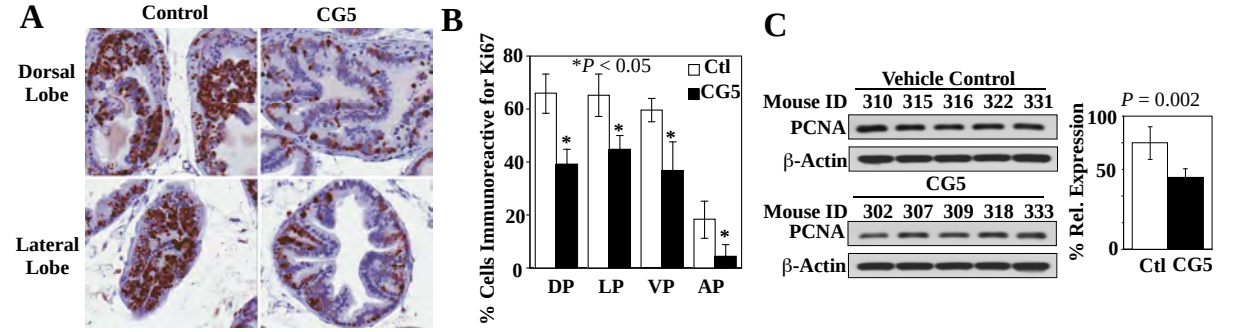

Fig. 11. CG5 reduced prostate epithelial proliferation in TRAMP mice. Proliferation within the prostates of TRAMP mice treated with CG5 (100 mg/kg/d) or vehicle for 4 weeks was assessed by immune-histochemistry for Ki67 (A and B) and Western blotting for PCNA (C). A, photomicrographs showing Ki67 immunoreactivity in the dorsal and lateral lobes of representative vehicle- and OSU-CG5–treated TRAMP mice (x400). B, the percentages of cells that were immunopositive for Ki67 in each prostate lobe were reduced in CG5-treated TRAMP mice relative to vehicle-treated controls (n = 5 mice/group). C, Western blot analysis shows that CG5 treatment reduced the expression levels of PCNA in the combined dorsal and lateral lobes prostates of TRAMP mice relative to vehicle-treated controls (5 mice/group). In (B) and (C), bars represent the mean ± SD.

CG5 treatment was not associated with evidence of systemic toxicity. Microarray analysis indicated a central role for Akt, and Western blot analysis showed reduced phosphorylation and/or expression levels of Akt, Src, androgen receptor, and insulin-like growth factor-1 receptor in prostate lobes (Fig. 12).

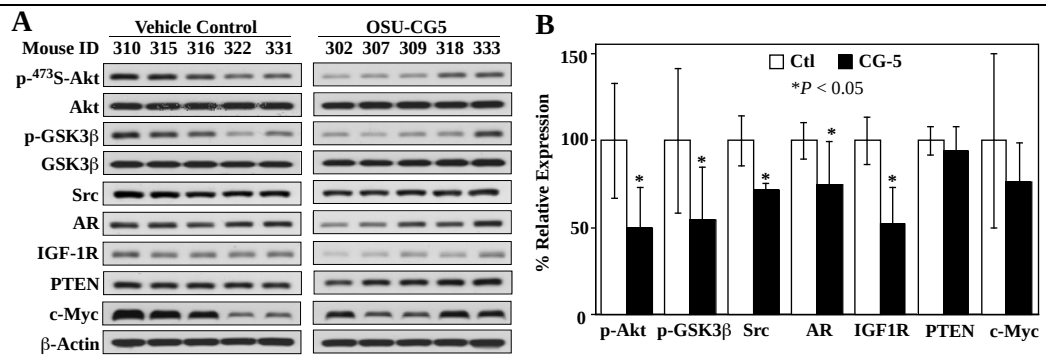

Fig. 12. (A) Western blot analysis of the effects of CG5 on the phosphorylation of Akt-^{473}Ser and GSK3β and the expression of several prosurvival factors (Src, AR, IGF-1R, c-Myc) and a tumor suppressor (PTEN) in the combined dorsal and lateral lobes of prostates in TRAMP mice treated with CG5 (100 mg/kg/d) or vehicle for 4 weeks. (B) Densitometric analysis of protein bands was conducted to calculate relative phosphorylation/expression levels of individual proteins. Bars represent the mean ± SD.

Together, these findings support further investigation of CG5 as a potential chemopreventive agent.

C. KEY RESEARCH ACCOMPLIAHMENTS

The accomplishment of this project is multifold.

1. Cells undergoing malignant transformation often exhibit a shift in cellular metabolism from oxidative phosphorylation to glycolysis. This glycolytic shift, called the Warburg effect, provides a mechanistic basis for targeting glycolysis to suppress prostate carcinogenesis. By using a novel glucose transporter inhibitor, CG-5, the present study demonstrates the clinical utility of this strategy in prostate cancer therapy, in part, through the blockade of AR signaling.
2. Oral CG-5 exhibits *in vivo* efficacy in suppressing LNCaP-abl xenograft tumor growth in nude mice, and in suppressing the progression of pre-neoplastic PIN progression in TRAMP mice, which correlated with the drug's ability to modulate biomarkers associated with β-TrCP-mediated protein degradation and AR downregulation. These data provides a rationale to continue the lead optimization of CG-5 to develop potent glucose transporter inhibitors for prostate cancer prevention/therapy, which is currently undergoing in the PI's laboratory.
3. We obtained evidence that AR expression is regulated by distinct mechanisms in different cell lines, i.e., Sp1 and c-Myc in LNCaP and VCaP, respectively. This discrepancy underlies heterogeneity in the regulation of AR signaling in prostate cancer, which warrants further investigation.

D. REPORTABLE OUTCOMES

1. C.H. Chen, P.-H. Huang, P.-C. Chu, M.-C. Chen, C.-C. Chou, D.-S. Wang, S. K. Kulp, C.-M. Teng, and **C.-S. Chen** (2010) "Epigenetic activation of KLF6 tumor suppressor gene expression by energy restriction in prostate cancer cells, in part, through histone modifications" ***J. Biol. Chem***. 286, 9968-9976

2. H.-Y. Lin, Y.-C. Kuo, Y.-I. Weng, T. H.-M. Huang, S.-P. Lin, D.-M. Niu, and **C.-S. Chen** (2012) "Activation of silenced tumor suppressor genes in prostate cancer cells by a novel glucose transporter inhibitor" ***Prostate*** 72, 1767-78

3. D. Wang, P.-C. Chu, C.N. Yang, R. Yan, Y.-C. Chung, S. K. Kulp, and **C.-S. Chen** (2012) "Development of a Novel Class of Glucose Transporter Inhibitors" *J. Med. Chem.* 55, 3827-3836

4. L. D. Berman-Booty, P.-C. Chu, J. M. Thomas-Ahner, D. Wang, T. Yang, S. K. Clinton, S. K. Kulp, **C.-S. Chen** (2013) "Suppression of Prostate Epithelial Proliferation and Intraprostatic Pro-Growth and Survival Signaling in Transgenic Mice by a Novel Energy Restriction-Mimetic Agent" ***Cancer Prev. Res.*** 6, 232-241

E. Conclusion

By using a novel glucose transporter inhibitor, CG-5, the present study demonstrates the clinical utility of targeting the Warburg effect in prostate cancer therapy, in part, through the blockade of AR signaling. Oral CG-5 exhibits *in vivo* efficacy in suppressing LNCaP-abl xenograft tumor growth in nude mice, and in suppressing the progression of pre-neoplastic PIN progression in TRAMP mice, which correlated with the drug's ability to modulate biomarkers associated with β-TrCP-mediated protein degradation and AR downregulation. These data provides a rationale to continue the lead optimization of CG-5 to develop potent glucose transporter inhibitors for prostate cancer prevention/therapy, which is currently undergoing in the PI's laboratory. Moreover, we obtained evidence that AR expression is regulated by distinct mechanisms in different cell lines, i.e., Sp1 and c-Myc in LNCaP and VCaP, respectively. This discrepancy underlies heterogeneity in the regulation of AR signaling in prostate cancer, which warrants further investigation.

Appendix

1. C.H. Chen, P.-H. Huang, P.-C. Chu, M.-C. Chen, C.-C. Chou, D.-S. Wang, S. K. Kulp, C.-M. Teng, and **C.-S. Chen** (2011) "Epigenetic activation of KLF6 tumor suppressor gene expression by energy restriction in prostate cancer cells, in part, through histone modifications" ***J. Biol. Chem***. 286, 9968-9976
2. H.-Y. Lin, Y.-C. Kuo, Y.-I. Weng, T. H.-M. Huang, S.-P. Lin, D.-M. Niu, and **C.-S. Chen** (2012) "Activation of silenced tumor suppressor genes in prostate cancer cells by a novel glucose transporter inhibitor" ***Prostate*** 72, 1767-78
3. D. Wang, P.-C. Chu, C.N. Yang, R. Yan, Y.-C. Chung, S. K. Kulp, and **C.-S. Chen** (2012) "Development of a Novel Class of Glucose Transporter Inhibitors" *J. Med. Chem.* 55, 3827-3836
4. L. D. Berman-Booty, P.-C. Chu, J. M. Thomas-Ahner, D. Wang, T. Yang, S. K. Clinton, S. K. Kulp, **C.-S. Chen** (2013) "Suppression of Prostate Epithelial Proliferation and Intraprostatic Pro-Growth and Survival Signaling in Transgenic Mice by a Novel Energy Restriction-Mimetic Agent" ***Cancer Prev. Res.*** 6, 232-241

THE JOURNAL OF BIOLOGICAL CHEMISTRY VOL. 286, NO. 12, pp. 9968–9976, March 25, 2011

Energy Restriction-mimetic Agents Induce Apoptosis in Prostate Cancer Cells in Part through Epigenetic Activation of KLF6 Tumor Suppressor Gene Expression*[S]

Received for publication, November 14, 2010, and in revised form, January 27, 2011 Published, JBC Papers in Press, January 31, 2011, DOI 10.1074/jbc.M110.203240

Chun-Han Chen[‡§], Po-Hsien Huang[‡], Po-Chen Chu[‡], Mei-Chuan Chen[‡§], Chih-Chien Chou[‡], Dasheng Wang[‡], Samuel K. Kulp[‡], Che-Ming Teng[§], Qianben Wang[¶], and Ching-Shih Chen[‡1]

From the [‡]Division of Medicinal Chemistry, College of Pharmacy, and the [¶]Department of Molecular and Cellular Biochemistry, The Ohio State University, Columbus, Ohio 43210 and the [§]Department of Pharmacology, College of Medicine, National Taiwan University, Taipei 10051, Taiwan

Although energy restriction has been recognized as an important target for cancer prevention, the mechanism by which energy restriction-mimetic agents (ERMAs) mediate apoptosis remains unclear. By using a novel thiazolidinedione-derived ERMA, CG-12 (Wei, S., Kulp, S. K., and Chen, C. S. (2010) *J. Biol. Chem.* 285, 9780–9791), *vis-à-vis* 2-deoxyglucose and glucose deprivation, we obtain evidence that epigenetic activation of the tumor suppressor gene Kruppel-like factor 6 (*KLF6*) plays a role in ERMA-induced apoptosis in LNCaP prostate cancer cells. KLF6 regulates the expression of many proapoptotic genes, and shRNA-mediated KLF6 knockdown abrogated the ability of ERMAs to induce apoptosis. Chromatin immunoprecipitation analysis indicates that this *KLF6* transcriptional activation was associated with increased histone H3 acetylation and histone H3 lysine 4 trimethylation occupancy at the promoter region. Several lines of evidence demonstrate that the enhancing effect of ERMAs on these active histone marks was mediated through transcriptional repression of histone deacetylases and H3 lysine 4 demethylases by down-regulating Sp1 expression. First, putative Sp1-binding elements are present in the promoters of the affected histone-modifying enzymes, and luciferase reporter assays indicate that site-directed mutagenesis of these Sp1 binding sites significantly diminished the promoter activities. Second, shRNA-mediated knockdown of Sp1 mimicked the repressive effect of energy restriction on these histone-modifying enzymes. Third, ectopic Sp1 expression protected cells from the repressive effect of CG-12 on these histone-modifying enzymes, thereby abolishing the activation of KLF6 expression. Together, these findings underscore the intricate relationship between energy restriction and epigenetic regulation of tumor suppressor gene expression, which has therapeutic relevance to foster novel strategies for prostate cancer therapy.

A hallmark feature of tumorigenesis is the shift of cellular metabolism from oxidative phosphorylation to aerobic glycolysis, the so-called Warburg effect, which provides a growth advantage to cancer cells in the microenvironment (1, 2). Recent evidence indicates that the high rate of glycolysis in tumor cells is attributable to the dysregulation of multiple oncogenic signaling pathways (1), including those mediated by hypoxia-inducible factor 1 (3), Akt (4), c-Myc (5), and p53 (6). This glycolytic shift is considered to be a fundamental property of neoplasia, and the high rate of glucose uptake in glycolytic tumor cells, including those of lung, breast, liver, and colon, is the basis for imaging tumors by [^{18}F]2-fluoro-2-deoxyglucose positron emission tomography (7). Moreover, in light of the *in vivo* efficacy of dietary caloric restriction and natural product-based energy restriction-mimetic agents (ERMAs)[2] such as 2-deoxyglucose (2-DG) and resveratrol in suppressing carcinogenesis in various animal models, targeting aerobic glycolysis represents a therapeutically relevant strategy for cancer prevention and treatment.

Previously, we obtained evidence that the antitumor effects of the thiazolidinedione peroxisome proliferator-activated receptor γ agonists troglitazone and ciglitazone were, in part, attributable to their ability to mimic glucose starvation to elicit cellular responses characteristic of energy restriction independent of peroxisome proliferator-activated receptor γ (8). These starvation-like responses include reduced glycolytic rates and intracellular levels of NADH and lactate, transient induction of the silent information regulator 1 gene, activation of the intracellular fuel sensor AMP-activated protein kinase, and endoplasmic reticulum stress, the interplay among which culminates in autophagy and apoptosis. On the basis of this finding, we used ciglitazone as a scaffold to develop a novel ERMA, CG-12, whose translational potential is manifested by an antiproliferative potency that is 3 orders of magnitude higher relative to 2-DG. Equally important, CG-12 provides a unique pharmacological tool to study the complex signaling

* This work is supported, in whole or in part, by National Institutes of Health Grant CA112250 and Department of Defense Prostate Cancer Research Program Grant W81XWH-09-0198.

[S] The on-line version of this article (available at http://www.jbc.org) contains supplemental Table 1.

[1] To whom correspondence should be addressed: College of Pharmacy, 336 Parks Hall, The Ohio State University, 500 West 12th Ave., Columbus, OH 43210-1291. Tel.: 614-688-4008; Fax: 614-688-8556; E-mail: chen.844@osu.edu.

[2] The abbreviations used are: ERMA, energy restriction-mimetic agent; 2-DG, 2-deoxyglucose; qRT-PCR, quantitative RT-PCR; DMSO, dimethyl sulfoxide; Ac-H3, histone H3 acetylation; HDAC, histone deacetylase; DM, demethylase; HAT, H3 acetyl; H3K4MT, H3 lysine 4 methyltransferase; H3K4DM, H3 lysine 4 demethylase; H3K4Me3, H3 lysine 4 trimethylation; H3K4Me2, H3 lysine 4 dimethylation; H3K4, H3 lysine 4; H3K27Me3, H3 lysine 27 trimethylation.

network underlying the suppressive effect of energy restriction on cancer cell proliferation. For example, we demonstrated that exposure of cancer cells to CG-12, 2-DG, or glucose-depleted medium triggered an intricate cascade of signaling pathways, leading to autophagic and apoptotic cell death (8).

In this study, we report the first evidence of the epigenetic effect of glucose starvation and ERMAs on the transcriptional activation of the tumor suppressor gene Kruppel-like factor 6 (*KLF6*) through histone modifications. KLF6 plays an important role in suppressing oncogenesis and tumor progression by regulating the transcription of a broad range of genes governing cell cycle progression, apoptosis, and invasive phenotype (9) and is frequently inactivated in many cancer types, including those of the prostate (10, 11), liver (12), lung (13), colon (14), ovary (15), brain (16), stomach (17), and head and neck (18). From a mechanistic perspective, this epigenetic activation of *KLF6* gene expression accounts at least in part for the ability of energy restriction to suppress cancer cell proliferation and may foster novel strategies for cancer prevention and therapy.

EXPERIMENTAL PROCEDURES

Cell Culture and Reagents—Androgen-responsive LNCaP and androgen-insensitive DU-145 prostate cancer cells were obtained from the ATCC. Cells were maintained in 10% FBS-supplemented RPMI 1640 medium (Invitrogen). CG-12 was synthesized in our laboratory as described previously (19). Glucose-free RPMI 1640 medium was purchased from Invitrogen. 2-DG and actinomycin D were purchased from Sigma. Antibodies used and their sources are as follows: H3K4Me2, H3K27Me3, PLU-1, RBP2, p-Ser 5 RNA polymerase II (Abcam, Inc., Cambridge, MA); ATF-3 (Abnova, Taipei, Taiwan); HDAC4, HDAC5, HDAC7, histone H3, LSD1, and PARP (Cell Signaling Technology, Inc., Beverly, MA); Noxa and DAPK2 (Imgenex, San Diego, CA); β-actin (MP Biomedicals, Irvine, CA); acetyl-histone H3, H3K4Me3, HDAC1, HDAC2, HDAC3, and HDAC8, (Millipore, Billerica, MA); HDAC6, KLF6, Sp1 (Santa Cruz Biotechnology, Santa Cruz, CA); Flag (Sigma-Aldrich); goat anti-rabbit IgG-HRP conjugates, rabbit anti-mouse IgG-HRP conjugates (Jackson ImmunoResearch Laboratories, West Grove, PA). The sequences of all primers used are listed in supplemental Table 1.

Apoptosis Assay—Apoptotic cell death was assessed with the Cell Death Detection ELISA kit (Roche Applied Science), which quantitates cytoplasmic histone-associated DNA fragments in the form of mono-/oligonucleosomes. Cells were treated with CG-12 for 48 h in 10% FBS-supplemented RPMI 1640 medium and then analyzed according to the manufacturer's instructions.

Transient Transfection and Luciferase Assay—LNCaP cells were transfected by electroporation using Nucleofector kit R (Lonza, Walkersville, MD) according to the manufacturer's protocol and then cultured in 6-well plates in 10% FBS-supplemented RPMI 1640 medium. Plasmids expressing shRNA for KLF6 and Sp1 were obtained from Origene Technologies (Rockville, MD) and Sigma-Aldrich, respectively. FLAG-Sp1 plasmid was prepared as described previously (20). HDAC1-FLAG (13820) and HDAC4-Flag (13821) plasmids were purchased from Addgene (Cambridge, MA). For the luciferase assay, transfected LNCaP cells were cultured in 6-well plates for 48 h. Luciferase activities were determined with the dual-luciferase system (Promega, Madison, WI), which uses co-transfected herpes simplex virus thymidine kinase promoter-driven *Renilla reniformis* luciferase as an internal control.

RT-PCR—Total RNA was isolated and reverse-transcribed to cDNA using TRIzol reagent (Invitrogen) and the iScript cDNA synthesis kit (Bio-Rad), respectively. For semi-quantitative PCR, products were resolved by 1.2% agarose gel electrophoresis and visualized with ethidium bromide. For real-time PCR, cDNAs were amplified in iQ SYBR Green Supermix (Bio-Rad) and detected with the Bio-Rad CFX96 real-time PCR detection system. Relative gene expression was normalized to GAPDH and calculated by using the 2(-Delta Delta C(T)) method (21).

ChIP Assay—ChIP was performed as reported previously, with modifications (22). After cross-linking and cell lysis, the cross-linked chromatin was sonicated, diluted, precleaned by incubation with protein A/G-agarose beads and normal mouse/rabbit IgG, and then immunoprecipitated with 4 μg of specific antibodies at 4 °C overnight. Protein A/G-agarose beads and yeast tRNA (Invitrogen) were then added and incubated for 1 h at 4 °C. Beads were then washed sequentially with the reported low-salt, high-salt, LiCl, and TE buffers (10 mM Tris, pH 8.0, containing 1 mM EDTA). After elution of the protein-DNA complexes and reversal of cross-linking, DNA fragments were isolated and analyzed by real-time PCR.

Plasmid Construction and Site-directed Mutagenesis—The genomic sequences of RBP2 (uc001qie. at chr12:chr12:389223–499220), PLU-1 (uc001gyf.2 at chr1:202696533–202778149), LSD1 (uc001bgj.2 at chr1:23345341–23410184), HDAC1 (uc010ohd.1 at chr1:32757108–32793590), HDAC2 (uc003pwd.1 at 114257327–114292954), HDAC3 (uc003llf.2 at chr5:141000443–141017023), and HDAC4 (uc002vyk.3 at chr2:239969865–240323243) were obtained from the University of California Santa Cruz genome browser. The primer pairs specific to the promoter fragments containing putative Sp1 consensus sequences of RBP2 (-460 to +60), PLU-1 (-228 to +21), LSD1 (-195 to +167), HDAC1(-310 to +10), HDAC2 (-440 to +10), HDAC3 (-180 to +80), and HDAC4 (-320 to +10) were PCR-amplified from whole genomic DNA isolated from LNCaP cells. The amplified fragments were cloned into KpnI/BglII sites of the pGL3-Basic vector (Promega) to generate the following constructs: pGL3-RBP2-Luc, pGL3-PLU1-Luc, pGL3-LSD1-Luc, pGL3-HDAC1-Luc, pGL3-HDAC2-Luc, pGL3-HDAC3-Luc, and pGL3-HDAC4-Luc. Reporter plasmids containing mutated Sp1 binding sites (GGGCGG to GTTCGG) were generated by site-directed mutagenesis using the QuikChange site-directed mutagenesis kit (Stratagene, La Jolla, CA).

Western Blotting—Western blotting was performed as described previously (8). Densitometric analysis of protein bands was performed by using Gel-Pro Analyzer (V3.1, Media Cybernetics, Bethesda, MD) to determine the relative intensities of drug-treated samples *versus* those of vehicle-treated controls after normalization to the internal reference protein β-actin.

Statistical Analysis—Data from quantitative qRT-PCR, ChIP-qPCR, cell death ELISA, Western blotting, and luciferase

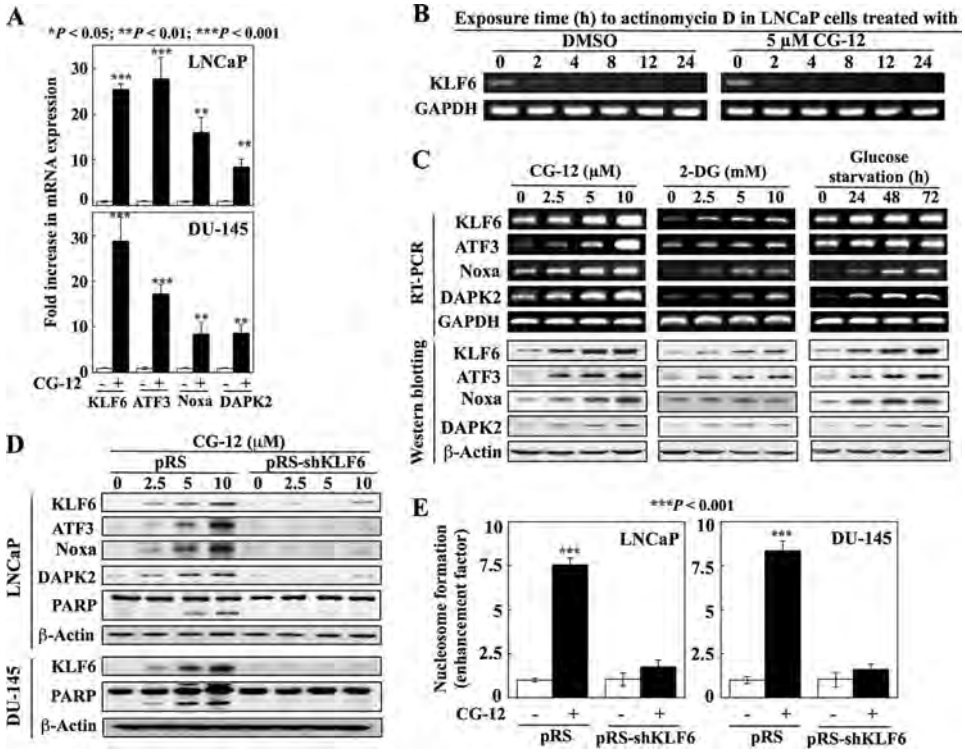

FIGURE 1. **Energy restriction-mimetic agents up-regulate the expression of the *KLF6* gene, its downstream targets, and subsequent apoptosis in cancer cells.** *A*, effect of CG-12 on the gene expression of *KLF6* and its proapoptotic downstream targets ATF3, Noxa, and DAPK. LNCaP cells (*upper panel*) and DU-145 cells (*lower panel*) were treated with CG-12 (10 μM, 48 h), and gene expression was analyzed by qRT-PCR. *Column*, mean ($n = 3$); *error bars*, mean ± S. D. *B*, evidence that CG-12 does not affect KLF6 mRNA stability. LNCaP cells were treated with actinomycin D (10 μM), an RNA polymerase II inhibitor, with CG-12 (5 μM), or with DMSO vehicle for the indicated times, and changes in KLF6 mRNA levels were assessed by semi-quantitative RT-PCR. *C*, RT-PCR (*upper panel*) and Western blot analysis (*lower panel*) of the effects of CG-12, 2-DG, and glucose starvation on the expression of KLF6 and its downstream targets. LNCaP cells were treated with CG-12 or 2-DG for 48 h or with glucose-depleted RPMI 1640 medium for the indicated times. *D*, Western blot analysis of the effect of shRNA-mediated repression of KLF6 on CG-12-induced expression of ATF3, Noxa, DAPK2, and PARP cleavage in LNCaP cells, and on CG-12-induced PARP cleavage in DU-145 cells. Cells were transfected with control vector (*pRS*) or KLF6 shRNA (*pRS-shKLF6*) for 24 h and then treated with CG-12 for 48 h. *E*, protective effect of shRNA-mediated knockdown of KLF6 against apoptosis as indicated by nucleosome formation in LNCaP (*left*) and DU-145 (*right*) cells treated with CG-12 (10 μM, 48 h). *Column*, mean ($n = 3$); *error bars*, mean ± S.D.

reporter assays were analyzed using Student's *t* test. Differences between group means were considered significant at $p < 0.05$.

RESULTS

Transcriptional Activation of the Tumor Suppressor Gene KLF6 Represents a Cellular Death Response to Energy Restriction—As part of our effort to understand the complex signaling network by which ERMAs suppress cancer cell proliferation, we examined the effect of CG-12 on tumor suppressor gene expression in androgen-responsive LNCaP cells. Among various tumor suppressor genes examined, the ability of CG-12 to up-regulate the expression of KLF6, a zinc finger transcription factor involved in prostate tumorigenesis (10), is especially noteworthy. Quantitative real-time reverse-transcription polymerase chain reaction (qRT-PCR) analysis indicates that 48-h exposure of LNCaP cells to 10 μM CG-12 boosted *KLF6* mRNA levels by 25-fold, accompanied by increases in its proapoptotic target genes, including activating transcription factor (ATF) 3 (28-fold), Noxa (16-fold), and death-associated protein kinase (DAPK) 2 (8-fold) (Fig. 1*A*, *upper panel*). These changes were also noted in androgen-nonresponsive DU-145 cells (Fig. 1*A*, *lower panel*), indicating that the drug effect on KLF6 mRNA expression was not a cell line-specific event and that it was independent of the functional status of androgen receptor in prostate cancer cells. To address the possibility that CG-12-mediated up-regulation of KLF6 mRNA levels was a result of enhanced mRNA stability, we assessed the effect of 5 μM CG-12 *versus* dimethyl sulfoxide (DMSO) vehicle on KLF6 mRNA turnover by co-treatment with 10 μM actinomycin D, a transcriptional inhibitor, in LNCaP cells (Fig. 1*B*). As shown, the disappearance of KLF6 mRNA was nearly completed by 2 h in vehicle-treated cells, whereas CG-12 had no appreciable effect on prolonging its half-life. Together, these findings indicate that CG-12 mediated the up-regulation of KLF6 mRNA expression through transcriptional activation. Moreover, the ability of CG-12 to increase the expression of KLF6 and its target genes at both mRNA and protein levels was shared by 2-DG and glucose deprivation (Fig. 1*C*) in LNCaP cells, suggesting that transcriptional activation of the *KLF6* gene represents an energy restriction-elicited signaling event.

As ATF3, Noxa, and DAPK2 have proapoptotic activities (10, 23, 24), we assessed the role of *KLF6* gene activation in CG-12-induced apoptosis in LNCaP cells via shRNA-mediated knockdown of KLF6. Ablation of KLF6 abolished the ability of CG-12 to up-regulate the expression of these three proapoptotic proteins and protected cells from CG-12-induced apoptosis as evidenced by lack of poly(ADP-ribose) polymerase cleavage and nucleosome formation (Fig. 1, *D* and *E*). This protective effect was also observed in DU-145 cells, suggesting the

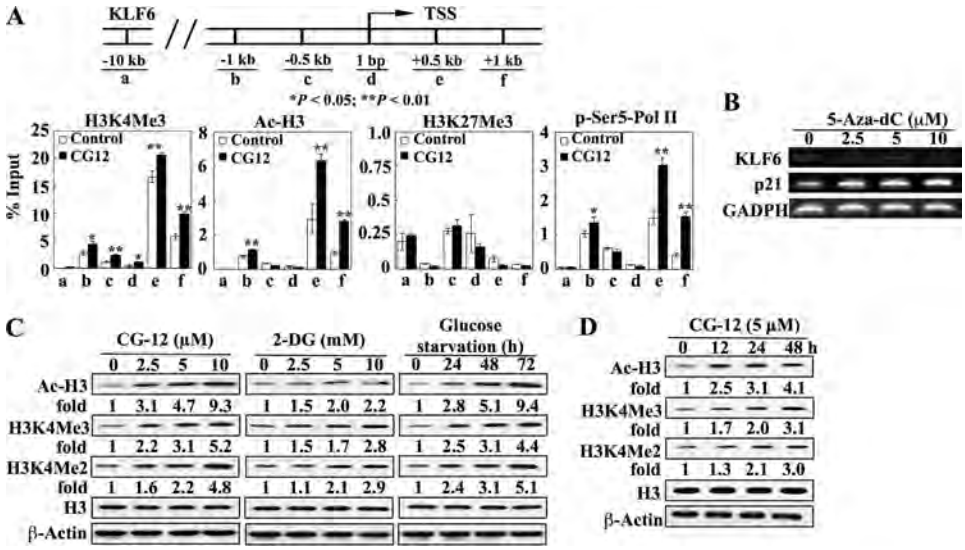

FIGURE 2. **CG-12 increases the genomic occupancy of active histone marks at the promoter region of the *KLF6* gene in LNCaP cells.** *A*, effect of CG-12 on the distribution of various histone marks. *Upper panel*, diagram depicting the locations in the *KLF6* gene of amplicons used in the ChIP-qPCR assay. *TSS*, transcriptional start site. *Lower panel*, ChIP-qPCR analysis of the effects of CG-12 (10 μM, 24 h) on *KLF6* gene occupancy by H3K4Me3, Ac-H3, H3K27Me3, and phospho-Ser-5-Pol II in LNCaP cells. *Column*, mean ($n = 3$); *error bars*, mean ± S.D. *B*, the DNA demethylating agent 5-aza-2′-deoxycytidine (*5-aza-dC*) has no effect on *KLF6* gene expression as determined by RT-PCR. LNCaP cells were treated with 5-aza-dC for 72 h. Expression of p21 served as a positive control. *C* and *D*, global changes in histone H3 acetylation and H3K4 methylation status in energy-restricted LNCaP cells. Cells were treated with CG-12 or 2-DG at the indicated concentrations for 48 h or glucose-deprived medium for the indicated times (*C*) and 5 μM CG-12 for the indicated times (*D*). The respective effects on histone acetylation and H3K4 tri- and dimethylation were evaluated by Western blot analysis. The values denote fold changes as determined by the relative intensity of protein bands of treated samples to that of the respective DMSO vehicle-treated control after normalization to the respective internal reference β-actin. Each value represents the average of three independent experiments.

involvement of KLF6 in CG-12-mediated apoptotic death in prostate cancer cells irrespective of the androgen receptor functional status.

CG-12 Activates KLF6 Gene Expression by the Enrichment of Histone H3 Acetylation (Ac-H3) and Histone H3 Lysine 4 Trimethylation (H3K4Me3) in the Promoter Region—The *KLF6* gene can be inactivated in tumor cells through loss of heterozygosity, somatic mutation, or epigenetic silencing (11). As LNCaP cells do not harbor mutations in the *KLF6* gene (11), we rationalized that the up-regulation of *KLF6* gene expression might be attributable to epigenetic activation. Recent evidence indicates that H3K4Me3 and histone H3 lysine 27 trimethylation (H3K27Me3) act as transcriptional activating and repressive marks, respectively, in regulating the expression of oncogenes and tumor suppressor genes in prostate carcinogenesis (25) and that histone acetylation and histone methylation function cooperatively to prepare chromatin for transcriptional activation (26). Thus, we assessed the effects of CG-12 on the levels of H3K4Me3, H3K27Me3, Ac-H3, and phospho-Ser-5 RNA polymerase II, a key enzyme involved in transcription initiation (27), occupancy at the promoter region of the *KFL6* gene in LNCaP cells (Fig. 2*A*, *upper panel*, *a–f*) by ChIP-qPCR analysis. As shown, CG-12 significantly enriched H3K4Me3 and Ac-H3, accompanied by parallel increases in the presence of phospho-Ser-5-Pol II, upstream of the transcription start site, as well as in the downstream transcribed region (Fig. 2*A*, *lower panel*). In contrast, no significant changes in H3K27Me3 were noted in response to CG-12, refuting the role of this repressive mark in regulating the transcriptional activation of the *KLF6* gene. As promoter hypermethylation has been implicated in the suppression of KLF6 expression in esophageal cancer cell lines (28), we examined whether a change in DNA methylation status played a role in regulating *KLF6* gene expression in LNCaP cells. Treatment of LNCaP cells with the DNA demethylating agent 5-aza-2′-deoxycytidine had no effect on KLF6 mRNA expression, whereas p21, a tumor suppressor gene known to be regulated by promoter methylation in LNCaP cells (29), showed a dose-dependent increase in its mRNA level (Fig. 2*B*). Together, these data suggest that the activation of *KLF6* gene expression in CG-12-treated LNCaP cells resulted at least in part from the enrichment for positive histone marks in the promoter region.

Western blot analysis indicates that this enrichment in active histone marks resulted from the ability of CG-12 to enhance global histone H3 acetylation and Lys-4 methylation. CG-12, glucose-depleted medium, and, to a lesser extent, 2-DG substantially increased the levels of Ac-H3 and H3K4Me3 and H3K4Me2 in a dose- and/or time-dependent manner (Fig. 2, *C* and *D*). Reminiscent of the time course observed after glucose starvation, these changes occurred as soon as 12 h after CG-12 treatment (Fig. 2*D*).

Increased Positive Histone Marks Are Attributable to the Transcriptional Repression of Histone Deacetylases (HDACs) and H3K4 Demethylases (DMs) in Response to Energy Restriction—Histone modifications like those described above result from a reversible process that is regulated by a dynamic balance between histone acetyl-/methyltransferase and histone deacetylase/demethylase activities. Aside from the complexity of histone-modifying enzymes involved in H3 acetylation, at least ten methyltransferases and five demethylases have been implicated in H3K4 methylation, each of which displays distinct substrate specificity and biological function in chromatin regulation. From a mechanistic perspective, increases in Ac-H3 and H3K4Me3 might arise from the up-regulation of

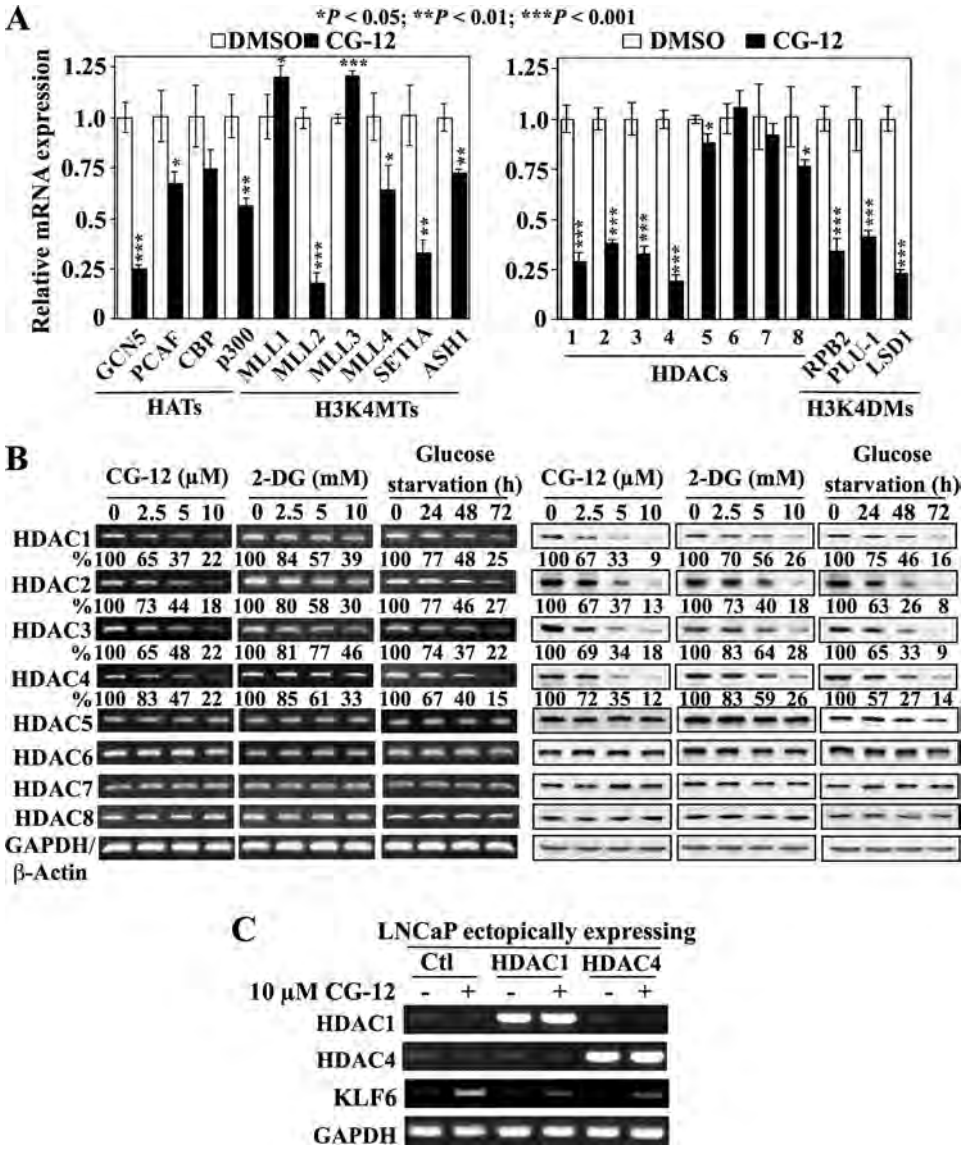

FIGURE 3. **Transcriptional repression of HDACs in response to ERMAs and glucose deprivation.** *A*, effects of CG-12 on the expression of histone-modifying enzymes involved in H3 acetylation and H3K4 methylation. *Left*, HATs and H3K4MTs. *Right*, HDACs and H3K4DMs. LNCaP cells were treated with 10 μM CG-12 for 48h, followed by qRT-PCR analysis. *Column*, mean ($n = 3$); *error bars*, mean ± S.D. *B*, parallel analyses of the effect of energy restriction on mRNA (*left*) and protein (*right*) expression levels of HDAC isozymes. LNCaP cells were treated with CG-12 and 2-DG for 48 h or glucose-free medium for the indicated times. The expression levels of various HDACs were examined by RT-PCR and Western blotting. The percentages denote the relative intensity of mRNA or protein bands of treated samples to that of the respective DMSO vehicle-treated control after normalization to the respective internal reference GADPH or β-actin. Each value represents the average of three independent experiments. *C*, effect of the ectopic expression of HDAC1 or HDAC4 *versus* pCMV control on CG-12-induced *KLF6* gene expression. Cells were transiently transfected with plasmids encoding HDAC1 or 4 or pCMV for 24 h and then treated with DMSO control (-) or 10 μM CG-12 (+) for 48 h, followed by RT-PCR analysis of mRNA levels of HDAC1, HDAC4, and KLF6.

histone H3 acetyl-/Lys-4 methyltransferases (HATs/H3K4MTs) and/or the down-regulation of histone deacetylases/H3K4 demethylases (HDACs/H3K4DMs).

To discern these two possibilities, we used qRT-PCR to assess the effect of CG-12 on the mRNA expression of various histone-modifying enzymes involved in the regulation of H3 acetylation and H3K4 methylation in LNCaP cells, which included HATs (GCN5, PCAF, CBP, p300), H3K4MTs (MLL1, MLL2, MLL3, MLL4, SET1A, ASH1), HDACs (HDAC1–8), and demethylases for H3K4Me3 (RBP-2/JARID1a, PLU-1/JARID1b), and H3K4Me1/2 (LSD1/KDM1). Relative to vehicle control, the mRNA levels of most of the HATs and H3K4MTs examined were significantly decreased after 24-h treatment with 10 μM CG-12, with the exception of the modest (≤20%) but statistically significant increases in the mRNA levels of MLL1 and 3 (Fig. 3*A*). In contrast, CG-12 suppressed the mRNA levels of HDAC1–4, RBP2, PLU-1, and LSD1 (≥60%), whereas those of HDAC5–8 remained largely unaltered. These findings suggest that the selective repression of HDACs and H3K4DMs played a major role in the observed energy restriction-associated increases in histone H3 acetylation and H3K4 methylation.

Pursuant to these findings, we examined the suppressive effects of CG-12, 2-DG, and glucose starvation on the expression of HDAC isozymes and H3K4DMs by RT-PCR and Western blot analysis. As shown in Fig. 3*B*, CG-12, 2-DG, and glu-

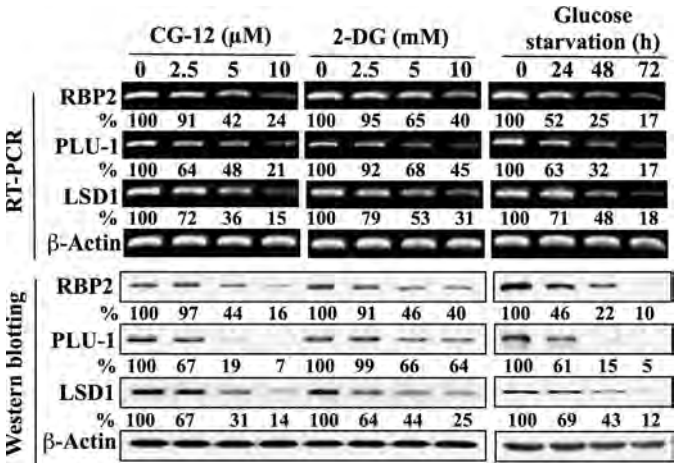

FIGURE 4. **Transcriptional repression of H3K4DMs in response to ERMAs and glucose deprivation.** LNCaP cells were treated with CG-12 and 2-DG for 48 h or glucose-free medium for the indicated times. The mRNA and protein expression levels of various H3K4DMs were examined by RT-PCR and Western blotting, respectively. The percentages denote the relative intensity of mRNA or protein bands of treated samples to that of the respective DMSO vehicle-treated control after normalization to the respective internal reference β-actin. Each value represents the average of three independent experiments.

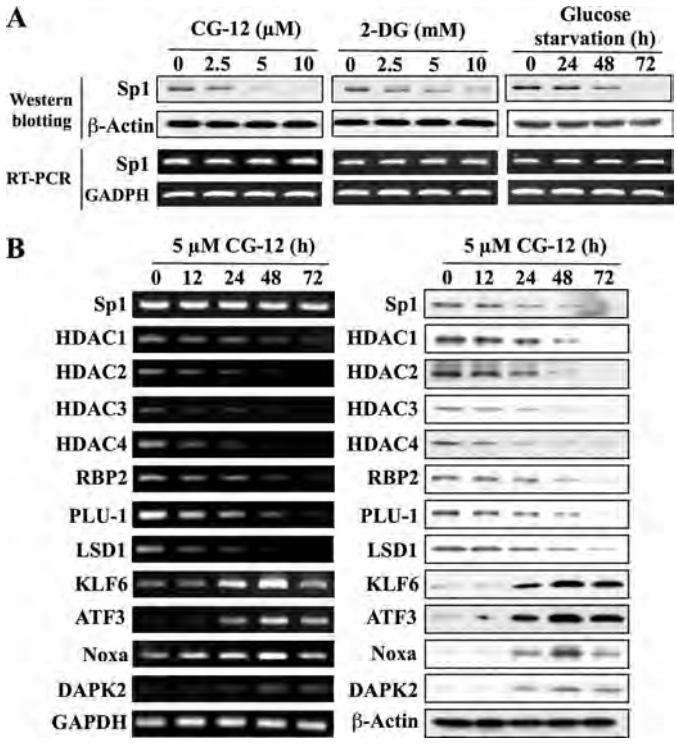

FIGURE 5. **Evidence that Sp1 regulates the expression of histone-modifying enzymes.** *A*, effect of energy restriction on the expression of Sp1. LNCaP cells were treated with CG-12 or 2-DG for 48 h or glucose-free medium for the indicated times. Protein and mRNA levels of Sp1 were assessed by Western blot (*upper panel*) and RT-PCR (*lower panel*) analyses, respectively. *B*, time-dependent effects of CG-12 on the mRNA and protein expression of Sp1, HDAC1–4, H3K4DMs RBP2, PLU-1, and LSD1, and KLF6 and its targets ATF3, Noxa, and DAPK2. LNCaP cells were exposed to 5 μM CG-12 for different time periods followed by Western blot analysis and RT-PCR for the aforementioned proteins.

cose starvation suppressed the mRNA and protein levels of HDAC1–4 in a dose- or time-dependent manner without disturbing those of HDAC5–8. From a mechanistic perspective, the concomitant reduction in the expression of HDAC1–4 would lead to increases in H3 acetylation in energy-restricted LNCaP cells. Furthermore, we examined the effect of the transient transfection of LNCaP cells with plasmids encoding HDAC1 and 4 *versus* pCMV on CG-12-induced *KLF6* gene expression. As shown, ectopic expression of either HDAC1 or 4 abrogated the ability of CG-12 to increase KLF6 mRNA expression levels (Fig. 3*C*), confirming the involvement of these HDAC isozymes in regulating KLF6 mRNA levels in response to CG-12.

These energy-restricted conditions also suppressed the expression of RBP2, PLU-1, and LSD1 at both mRNA and protein levels, in a dose and/or time-dependent fashion (Fig. 4), thereby providing a plausible molecular basis for the accumulation of H3K4Me3 and H3K4Me2 in drug-treated cells. It is interesting to note that, in response to each of these treatments, the extent of down-regulation of these three H3K4DMs paralleled that of HDAC1–4, suggesting that the energy restriction-induced transcriptional repression of these histone-modifying enzymes might share a similar mechanism.

Together, these data suggest that the epigenetic activation of *KLF6* gene expression by CG-12 was, in part, attributable to its ability to enhance positive histone marks by suppressing the expression of target HDACs and H3K4DMs.

Sp1 Degradation Underlies the Repressive Effects of CG-12 on Histone-modifying Enzymes—To understand the mechanistic link between energy restriction and histone modifications, we investigated the involvement of the transcription factor Sp1 in CG-12-mediated repression of histone-modifying enzymes, of which the rationale is 2-fold. First, our previous study demonstrated that β-transducin repeat-containing protein (β-TrCP)-dependent proteasomal degradation of Sp1 represents an energy restriction-elicited signaling response (8), which was manifested by the suppressive effect of CG-12, 2-DG, and glucose starvation on the level of Sp1 protein, but not mRNA expression (Fig. 5*A*). Moreover, the time course of Sp1 protein repression over a 72-h period of treatment with 5 μM CG-12 paralleled that of HDAC1–4, RBP2, PLU-1, and LSD1 at both mRNA and protein levels and showed an inverse relationship with the mRNA and protein expression of KLF6 and its targets ATF3, Noxa, and DAPK2 (Fig. 5*B*). It is noteworthy that changes in the expression levels of Sp1 and most histone-modifying enzymes preceded that of KLF6 and its target genes, *i.e.* 12 h *versus* 24 h, suggesting a causal relationship.

Second, Sp1 has been shown to regulate the expression of HDAC1 (30), HDAC4 (31), and PLU-1 (32), and analysis of the promoter sequences of genes encoding HDAC2–4, RBP2, and LSD1 revealed the presence of one or more putative Sp1 binding elements (GGGCGG) in each promoter (Fig. 6, *A* and *B*, *left panels*).

To establish the functional role of Sp1 in regulating the transcription of these HDAC isozymes and H3K4DMs, we constructed luciferase reporter plasmids harboring the RBP2, PLU-1, LSD1, and HDAC1–4 promoter regions and their respective counterparts containing mutated Sp1 binding sites in which the GGGCGG sequence was replaced with GTTCGG (Fig. 6, *A* and *B*, *left panels*). LNCaP cells were transiently transfected with individual wild-type or mutant reporter plasmids. Relative to the wild-type control, mutation of the Sp1 binding

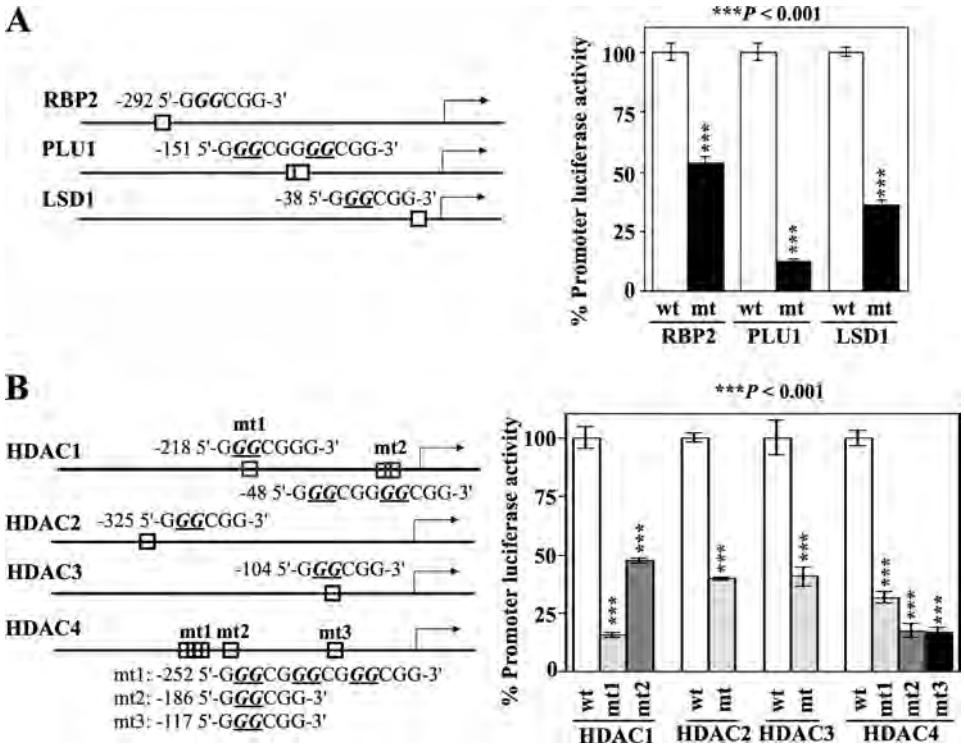

FIGURE 6. **Involvement of Sp1 in the expression of H3K4DMs and HDACs.** *A* and *B*, *left panels*, diagrams indicating the putative Sp1 binding sites on the proximal promoter regions of RBP2, PLU-1, LSD1, and HDAC1–4. Putative Sp1 binding sites are boxed and their nucleotide positions relative to the transcription start site are labeled. The bases altered by site-directed mutagenesis are underlined. *Right panels*, relative differences in luciferase-reporter activities with mutated *versus* wild-type H3K4DM and HDAC promoters. LNCaP cells were transiently transfected with plasmids expressing wild-type (*wt*) and mutant (*mt*) promoters for 48 h. *Column*, mean ($n = 3$); *error bars*, mean ± S.D.

site significantly diminished the promoter activities of these genes (Fig. 6, *A* and *B*, *right panels*).

Pursuant to this finding, we tested the ability of shRNA-mediated silencing of Sp1 expression to mimic energy restriction-mediated repression of HDAC1–4, RBP2, PLU-1, and LSD1 and the consequent epigenetic changes in LNCaP cells. Western blot analysis indicates that, relative to control shRNA, transfection with Sp1 shRNA reduced the levels of these histone-modifying enzymes in a dose-dependent manner (Fig. 7*A*). These decreases were accompanied by increases in histone H3 acetylation and H3K4 methylation, and parallel increases in the expression of KLF6 and its target gene products ATF3, Noxa, and DAPK2.

To further validate the role of Sp1 in energy restriction-induced transcriptional activation of *KLF6* gene expression, we examined the effect of ectopic Sp1 expression on CG-12-induced epigenetic changes. Overexpression of Sp1 blocked the dose-dependent repressive effects of CG-12 on HDAC1–4, RBP2, PLU-1, and LSD1 expression, thereby abolishing its ability to enhance histone H3 acetylation, H3K4 methylation, and the expression of KLF6 and its target gene products (Fig. 7*B*).

Together, these findings underscore the important role of Sp1 down-regulation in mediating the epigenetic activation of the *KLF6* gene by ERMAs and glucose starvation through the repression of histone-modifying enzymes.

DISCUSSION

In light of the metabolic adaptation of cancer cells to anaerobic glycolysis to gain growth advantages (1), there is increasing interest in targeting tumor metabolism for cancer therapy. Because chronic energy restriction proves to be difficult to implement as an antitumor strategy, ERMAs have received wide attention as they can mimic the beneficial effects of energy restriction through the inhibition of glucose utilization. Previously, we developed CG-12, a thiazolidinedione-based ERMA that exhibits potency 3 orders of magnitude higher than 2-DG in inhibiting cancer cell proliferation through autophagy and apoptosis (8). Although it is well understood that AMPK activation plays a crucial role in ERMA-induced autophagy in cancer cells (33), the underlying mechanism of apoptosis remains unclear. Thus, CG-12 provides a useful pharmacological probe to understand the underlying signaling pathways.

Here, we report evidence that the epigenetic up-regulation of tumor suppressor gene *KLF6* expression represents a key signaling mechanism by which energy restriction mediates apoptosis (Fig. 8). Previously, we reported that CG-12, 2-DG, and glucose starvation facilitated β-TrCP-mediated proteasomal degradation of Sp1 and other target proteins via a Sirt1-dependent mechanism in LNCaP cells (8, 20), and that this β-TrCP-dependent proteolysis plays an integral role in ERMA-induced apoptosis since dominant-negative inhibition of β-TrCP protected cells against apoptosis (8). In this study, we extended our understanding of the cellular response to energy restriction by defining the epigenetic activation of *KLF6* gene expression as a key mediator of energy restriction-induced apoptosis.

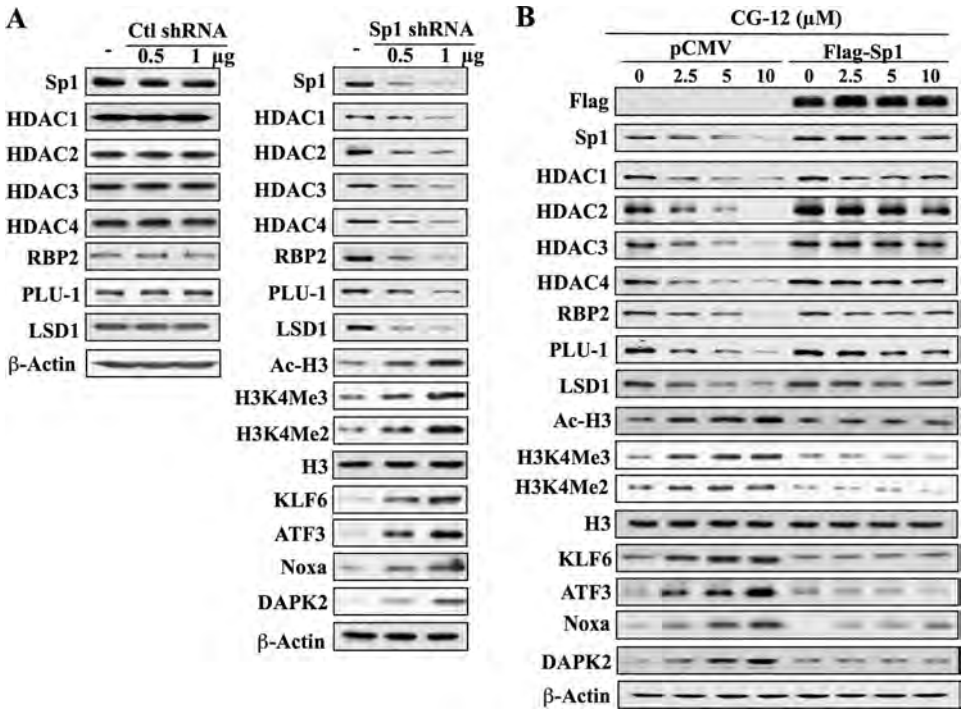

FIGURE 7. **Sp1 degradation underlies the repressive effects of CG-12 on histone-modifying enzymes and consequent up-regulation of *KLF6* gene expression.** *A*, effects of the knockdown of Sp1 expression on the expression of HDACs and H3K4DMs, histone H3 acetylation and methylation status, and the expression of KLF6 and the products of its target genes. 48 h after transfection of LNCaP cells with control (*left panel*) or Sp1-specific (*right panel*) shRNA (0, 0.5, and 1 μg), Western blot analysis of the indicated proteins was performed. Western blot data representative of three independent experiments are shown. *B*, effect of ectopic Sp1 expression on CG-12-induced epigenetic changes. LNCaP cells were transfected with FLAG-tagged Sp1 for 24 h and then treated with CG-12 for 48 h. Western blot data representative of three independent experiments are shown.

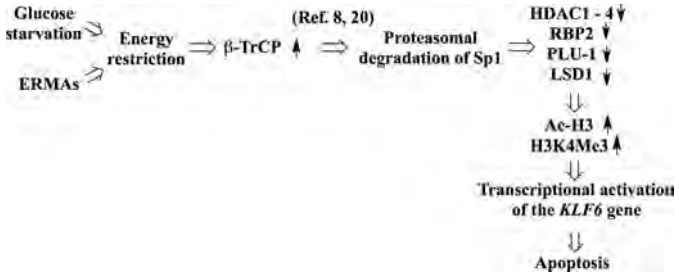

FIGURE 8. **Diagram depicting the mode of action by which energy restriction activates *KLF6* tumor suppressor gene expression.** Previously, we reported the mechanistic link between energy restriction and β-TrCP-mediated proteasomal degradation of Sp1 (8, 20). Here, we extend our understanding that ERMA-mediated Sp1 down-regulation facilitates the transcriptional repression of HDAC1–4 and H3K4DMs (RBP2, PLU-1, and LSD1), resulting in increased histone H3 acetylation and H3K4 methylation. Evidence suggests that enhanced occupancy of the active histone marks Ac-H3 and H3K4Me3 in the promoter region of the *KLF6* gene gives rise to *KLF6* transcriptional activation. As KLF6 regulates the expression of many proapoptotic genes, this epigenetic activation plays a role in ERMA-induced apoptosis.

KLF6 plays a crucial role in tumor suppression by modulating the expression of a broad range of genes governing biological functions associated with cell growth, cell differentiation, cell adhesion, and endothelial motility (9), among which ATF3 has been shown to represent a major mediator of KLF6-induced apoptosis in prostate cancer cells (24). In this study, we demonstrated the concomitant up-regulation of ATF3, Noxa, and DAPK2 with KLF6 in LNCaP and DU-145 cells treated with ERMAs or glucose-depleted medium (Fig. 1). Conceivably, the concerted effort of these proapoptotic proteins underlies the key role of KLF6 in mediating energy restriction-induced apoptosis.

Evidence suggests that the transcriptional activation of *KLF6* gene expression resulted from enhanced active histone marks, *i.e.* H3K4Me3 and Ac-H3, in the promoter region (Fig. 2). Our data also indicate that increased H3 acetylation and H3K4 methylation were attributable to transcriptional repression of HDACs (Fig. 3) and H3K4DMs (Fig. 4) because of reduced Sp1 expression (Fig. 5). Pursuant to previous findings that Sp1 regulates the transcription of HDAC1 and 4 and PLU-1 (30–32), we identified HDAC2 and 3, RPB2, and LSD1 as additional Sp1 target genes through mutational analysis (Fig. 6). The functional role of Sp1 in mediating these epigenetic changes leading to *KLF6* gene activation was further confirmed by using shRNA-mediated knockdown and ectopic expression to observe the consequent effects on relevant biomarkers (Fig. 7).

Substantial evidence points to Sp1 as a relevant target for cancer therapy in light of its pivotal role in regulating the gene expression of a host of key effectors of signaling pathways governing cell cycle progression, cell proliferation, angiogenesis, apoptosis, and metastasis (34–36). In this study, we demonstrated the ability of Sp1 to modulate the expression of multiple histone-modifying enzymes, leading to the transcriptional activation of the *KLF6* gene by increasing active histone marks. From a mechanistic perspective, the ability of Sp1 to effect epigenetic changes by modifying histones adds a layer of complexity to its functional role in regulating gene expression, which warrants further investigations.

It is noteworthy that CG-12 also significantly down-regulated (>50%) the mRNA expression of a number of the HATs

and H3K4MTs examined, including GCN5, MLL2, and SET1A (Fig. 3). As none of these three genes contains any Sp1-binding site in their promoters, other mechanisms are involved in the transcriptional regulation of these genes. For example, GCN5 is known to be a direct target gene of Myc (37), of which the mRNA expression was also significantly reduced by CG-12[3]. However, the transcription factors that regulate the gene expression of MLL2 and SET1A remain to be investigated.

In summary, our data identify the epigenetic activation of *KLF6* tumor suppressor gene expression as a critical event leading to apoptosis in energy-restricted cancer cells. This causal relationship between energy restriction and the epigenetic modulation of *KLF6* gene expression underscores the complexity of the signaling network involved in the apoptotic response to energy restriction. As KLF6 represents a new molecular marker candidate for tumor prognosis and a potential target for cancer therapy (38), our findings are of potential translational value for the development of therapeutic strategies involving new-generation ERMAs such as CG-12.

REFERENCES

1. Kroemer, G., and Pouyssegur, J. (2008) *Cancer Cell* **13,** 472–482
2. Kim, J. W., and Dang, C. V. (2006) *Cancer Res.* **66,** 8927–8930
3. Denko, N. C. (2008) *Nat. Rev. Cancer* **8,** 705–713
4. Elstrom, R. L., Bauer, D. E., Buzzai, M., Karnauskas, R., Harris, M. H., Plas, D. R., Zhuang, H., Cinalli, R. M., Alavi, A., Rudin, C. M., and Thompson, C. B. (2004) *Cancer Res.* **64,** 3892–3899
5. Osthus, R. C., Shim, H., Kim, S., Li, Q., Reddy, R., Mukherjee, M., Xu, Y., Wonsey, D., Lee, L. A., and Dang, C. V. (2000) *J. Biol. Chem.* **275,** 21797–21800
6. Matoba, S., Kang, J. G., Patino, W. D., Wragg, A., Boehm, M., Gavrilova, O., Hurley, P. J., Bunz, F., and Hwang, P. M. (2006) *Science* **312,** 1650–1653
7. Kelloff, G. J., Hoffman, J. M., Johnson, B., Scher, H. I., Siegel, B. A., Cheng, E. Y., Cheson, B. D., O'Shaughnessy, J., Guyton, K. Z., Mankoff, D. A., Shankar, L., Larson, S. M., Sigman, C. C., Schilsky, R. L., and Sullivan, D. C. (2005) *Clin. Cancer Res.* **11,** 2785–2808
8. Wei, S., Kulp, S. K., and Chen, C. S. (2010) *J. Biol. Chem.* **285,** 9780–9791
9. DiFeo, A., Martignetti, J. A., and Narla, G. (2009) *Drug Resist. Updates* **12,** 1–7
10. Narla, G., Heath, K. E., Reeves, H. L., Li, D., Giono, L. E., Kimmelman, A. C., Glucksman, M. J., Narla, J., Eng, F. J., Chan, A. M., Ferrari, A. C., Martignetti, J. A., and Friedman, S. L. (2001) *Science* **294,** 2563–2566
11. Chen, C., Hyytinen, E. R., Sun, X., Helin, H. J., Koivisto, P. A., Frierson, H. F., Jr., Vessella, R. L., and Dong, J. T. (2003) *Am. J. Pathol.* **162,** 1349–1354
12. Kremer-Tal, S., Narla, G., Chen, Y., Hod, E., DiFeo, A., Yea, S., Lee, J. S., Schwartz, M., Thung, S. N., Fiel, I. M., Banck, M., Zimran, E., Thorgeirsson, S. S., Mazzaferro, V., Bruix, J., Martignetti, J. A., Llovet, J. M., and Friedman, S. L. (2007) *J. Hepatol.* **46,** 645–654
13. Ito, G., Uchiyama, M., Kondo, M., Mori, S., Usami, N., Maeda, O., Kawabe, T., Hasegawa, Y., Shimokata, K., and Sekido, Y. (2004) *Cancer Res.* **64,** 3838–3843
14. Reeves, H. L., Narla, G., Ogunbiyi, O., Haq, A. I., Katz, A., Benzeno, S., Hod, E., Harpaz, N., Goldberg, S., Tal-Kremer, S., Eng, F. J., Arthur, M. J., Martignetti, J. A., and Friedman, S. L. (2004) *Gastroenterology* **126,** 1090–1103
15. DiFeo, A., Narla, G., Camacho-Vanegas, O., Nishio, H., Rose, S. L., Buller, R. E., Friedman, S. L., Walsh, M. J., and Martignetti, J. A. (2006) *Oncogene* **25,** 6026–6031
16. Camacho-Vanegas, O., Narla, G., Teixeira, M. S., DiFeo, A., Misra, A., Singh, G., Chan, A. M., Friedman, S. L., Feuerstein, B. G., and Martignetti, J. A. (2007) *Int. J. Cancer* **121,** 1390–1395
17. Sangodkar, J., Shi, J., DiFeo, A., Schwartz, R., Bromberg, R., Choudhri, A., McClinch, K., Hatami, R., Scheer, E., Kremer-Tal, S., Martignetti, J. A., Hui, A., Leung, W. K., Friedman, S. L., and Narla, G. (2009) *Eur. J. Cancer* **45,** 666–676
18. Teixeira, M. S., Camacho-Vanegas, O., Fernandez, Y., Narla, G., DiFeo, A., Lee, B., Kalir, T., Friedman, S. L., Schlecht, N. F., Genden, E. M., Urken, M., Brandwein-Gensler, M., and Martignetti, J. A. (2007) *Int. J. Cancer* **121,** 1976–1983
19. Yang, J., Wei, S., Wang, D. S., Wang, Y. C., Kulp, S. K., and Chen, C. S. (2008) *J. Med. Chem.* **51,** 2100–2107
20. Wei, S., Chuang, H. C., Tsai, W. C., Yang, H. C., Ho, S. R., Paterson, A. J., Kulp, S. K., and Chen, C. S. (2009) *Mol. Pharmacol.* **76,** 47–57
21. Livak, K. J., and Schmittgen, T. D. (2001) *Methods* **25,** 402–408
22. Wang, Q., Carroll, J. S., and Brown, M. (2005) *Mol. Cell* **19,** 631–642
23. Britschgi, A., Trinh, E., Rizzi, M., Jenal, M., Ress, A., Tobler, A., Fey, M. F., Helin, K., and Tschan, M. P. (2008) *Oncogene* **27,** 5706–5716
24. Huang, X., Li, X., and Guo, B. (2008) *J. Biol. Chem.* **283,** 29795–29801
25. Ke, X. S., Qu, Y., Rostad, K., Li, W. C., Lin, B., Halvorsen, O. J., Haukaas, S. A., Jonassen, I., Petersen, K., Goldfinger, N., Rotter, V., Akslen, L. A., Oyan, A. M., and Kalland, K. H. (2009) *PLoS ONE* **4,** e4687
26. Wang, Z., Zang, C., Rosenfeld, J. A., Schones, D. E., Barski, A., Cuddapah, S., Cui, K., Roh, T. Y., Peng, W., Zhang, M. Q., and Zhao, K. (2008) *Nat. Genet.* **40,** 897–903
27. Weake, V. M., and Workman, J. L. (2010) *Nat. Rev. Genet.* **11,** 426–437
28. Yamashita, K., Upadhyay, S., Osada, M., Hoque, M. O., Xiao, Y., Mori, M., Sato, F., Meltzer, S. J., and Sidransky, D. (2002) *Cancer Cell* **2,** 485–495
29. Bott, S. R., Arya, M., Kirby, R. S., and Williamson, M. (2005) *Prostate Cancer Prostatic Dis.* **8,** 321–326
30. Schuettengruber, B., Simboeck, E., Khier, H., and Seiser, C. (2003) *Mol. Cell. Biol.* **23,** 6993–7004
31. Liu, F., Pore, N., Kim, M., Voong, K. R., Dowling, M., Maity, A., and Kao, G. D. (2006) *Mol. Biol. Cell* **17,** 585–597
32. Catteau, A., Rosewell, I., Solomon, E., and Taylor-Papadimitriou, J. (2004) *Int. J. Oncol.* **25,** 5–16
33. Singletary, K., and Milner, J. (2008) *Cancer Epidemiol. Biomark. Prev.* **17,** 1596–1610
34. Safe, S., and Abdelrahim, M. (2005) *Eur. J. Cancer* **41,** 2438–2448
35. Solomon, S. S., Majumdar, G., Martinez-Hernandez, A., and Raghow, R. (2008) *Life Sci.* **83,** 305–312
36. Wierstra, I. (2008) *Biochem. Biophys. Res. Commun.* **372,** 1–13
37. Knoepfler, P. S., Zhang, X. Y., Cheng, P. F., Gafken, P. R., McMahon, S. B., and Eisenman, R. N. (2006) *EMBO J.* **25,** 2723–2734
38. Gehrau, R. C., D'Astolfo, D. S., Dumur, C. I., Bocco, J. L., and Koritschoner, N. P. (2010) *PLoS ONE* **5,** e8929

[3] C. Chen, unpublished data.

The Prostate 72:1767–1778 (2012)

Activation of Silenced Tumor Suppressor Genes in Prostate Cancer Cells by a Novel Energy Restriction-Mimetic Agent

Hsiang-Yu Lin,[1,2,3] Yi-Chiu Kuo,[1] Yu-I Weng,[4] I-Lu Lai,[1] Tim H.-M. Huang,[4] Shuan-Pei Lin,[3] Dau-Ming Niu,[2,5]** and Ching-Shih Chen[1]*

[1]*Division of Medicinal Chemistry, College of Pharmacy, The Ohio State University, Columbus, Ohio*
[2]*Institute of Clinical Medicine, National Yang-Ming University, Taipei, Taiwan*
[3]*Department of Pediatrics, Mackay Memorial Hospital and Mackay Medicine, Nursing and Management College, Taipei, Taiwan*
[4]*Human Cancer Genetics Program, The Ohio State University, Columbus, Ohio*
[5]*Department of Pediatrics, Taipei Veterans General Hospital, Taipei, Taiwan*

BACKGROUND. Targeting tumor metabolism by energy restriction-mimetic agents (ERMAs) has emerged as a strategy for cancer therapy/prevention. Evidence suggests a mechanistic link between ERMA-mediated antitumor effects and epigenetic gene regulation.
METHODS. Microarray analysis showed that a novel thiazolidinedione-derived ERMA, CG-12, and glucose deprivation could suppress DNA methyltransferase (DNMT)1 expression and reactivate DNA methylation-silenced tumor suppressor genes in LNCaP prostate cancer cells. Thus, we investigated the effects of a potent CG-12 derivative, CG-5, vis-à-vis 2-deoxy-glucose, glucose deprivation and/or 5-aza-deoxycytidine, on DNMT isoform expression (Western blotting, RT-PCR), DNMT1 transcriptional activation (luciferase reporter assay), and expression of genes frequently hypermethylated in prostate cancer (quantitative real-time PCR). Promoter methylation was assessed by pyrosequencing analysis. SiRNA-mediated knockdown and ectopic expression of DNMT1 were used to validate DNMT1 as a target of CG-5.
RESULTS. CG-5 and glucose deprivation upregulated the expression of DNA methylation-silenced tumor suppressor genes, including *GADD45a*, *GADD45b*, *IGFBP3*, *LAMB3*, *BASP1*, *GPX3*, and *GSTP1*, but also downregulated methylated tumor/invasion-promoting genes, including *CD44*, *S100A4*, and *TACSTD2*. In contrast, 5-aza-deoxycytidine induced global reactivation of these genes. CG-5 mediated these epigenetic effects by transcriptional repression of DNMT1, which was associated with reduced expression of Sp1 and E2F1. SiRNA-mediated knockdown and ectopic expression of DNMT1 corroborated DNMT1's role in the modulation of gene expression by CG-5. Pyrosequencing revealed differential effects of CG-5 versus 5-aza-deoxycytidine on promoter methylation in these genes.

Additional supporting information may be found in the online version of this article.

Grant sponsor: National Institutes of Health; Grant number: CA112250; Grant sponsor: Department of Defense Prostate Cancer Research Program; Grant number: W81XWH-09-0198; Grant sponsor: National Science Council, Taiwan.

The authors declare no conflicts of interest.

*Correspondence to: Dr. Ching-Shih Chen, College of Pharmacy, The Ohio State University, 500 West 12th Avenue, Columbus, OH 43210. E-mail: chen.844@osu.edu

**Correspondence to: Dau-Ming Niu, Department of Pediatrics, Taipei Veterans General Hospital, No. 201, Section 2, Shih-Pai Road, Taipei 112, Taiwan. E-mail: dmniu1111@yahoo.com.tw
Received 2 December 2011; Accepted 30 March 2012
DOI 10.1002/pros.22530
Published online 26 April 2012 in Wiley Online Library (wileyonlinelibrary.com).

CONCLUSIONS. These findings reveal a previously uncharacterized epigenetic effect of ERMAs on DNA methylation-silenced tumor suppressor genes, which may foster novel strategies for prostate cancer therapy. *Prostate 72: 1767–1778, 2012.* © 2012 Wiley Periodicals, Inc.

KEY WORDS: **energy restriction-mimetic agent; prostate cancer; energy restriction; DNA methyltransferases; epigenetics**

INTRODUCTION

Cells undergoing malignant transformation often exhibit a shift in cellular metabolism from oxidative phosphorylation to glycolysis, known as the Warburg effect, to gain growth advantage in the microenvironment [1,2]. This enhanced glycolysis appears to be attributable to the dysregulation of multiple oncogenic signaling pathways [1], including those mediated by hypoxia-inducible factor 1 [3], Akt [4], c-Myc [5], and p53 [6], and enables cancer cells to adapt to low-oxygen environments, to produce biosynthetic building blocks needed for cell proliferation, to acidify the local environment to facilitate tumor invasion, and to generate NADPH and glutathione through the pentose phosphate shunt to increase resistance to oxidative stress [1,2]. The Warburg effect is considered to be a fundamental property of neoplasia, and constitutes the basis for tumor imaging by [^{18}F]2-fluoro-2-deoxyglucose positron emission tomography [7]. From a therapeutic perspective, targeting glycolysis represents a relevant strategy for cancer prevention and treatment [2], of which the proof-of-concept is provided by the effective suppression of carcinogenesis in various animal models by dietary caloric restriction and natural product-based energy restriction-mimetic agents (ERMAs), such as 2-deoxyglucose (2-DG) and resveratrol.

Previously, based on the scaffold of thiazolidinediones, we developed a novel class of ERMAs, as represented by CG-12, that mimic the ability of 2-DG and glucose deprivation to elicit starvation-like cellular responses with high potency in cancer cells through the inhibition of glucose uptake [8]. The suppression of energy metabolism by CG-12 leads to an intricate signaling network mediated by silent information regulator 1, AMP-activated protein kinase, and oxidative stress, the interplay among which culminates in autophagy and apoptosis in cancer cells. More recently, we demonstrated an epigenetic effect of CG-12 in cancer cells involving histone acetylation and H3 lysine 4 methylation, leading to the transcriptional activation of Kruppel-like factor 6 (*KLF6*) and a series of proapoptotic genes [9]. In this study, we report the unique ability of CG-5, a structurally optimized CG-12 derivative (Fig. 1A) to suppress the expression of DNA methyltransferase (DNMT)1 and DNMT3A in prostate cancer cells, resulting in the reactivation of a series of DNA methylation-silenced tumor suppressor genes. Pyrosequencing analysis indicates that this effect was attributable to hypomethylation in the promoter regions of these tumor suppressor genes. In light of the important role of aberrant DNA methylation in carcinogenesis [10], our findings underscore the translational potential of this novel class of glucose uptake inhibitors in prostate cancer prevention and therapy.

MATERIALS AND METHODS

Detailed information on materials, reagents, their commercial sources, and experimental procedures are available in Supplementary Information.

Microarray Analysis

Total RNA isolated from LNCaP cells exposed to 10 μM CG-12 or glucose-depleted medium for 48 hr was submitted to the Microarray Shared Resource at The Ohio State University Comprehensive Cancer Center for microarray analysis of gene expression.

Glucose Uptake Assay

This assay was performed as we described previously [8] with modifications. Specifically, LNCaP cells were treated with test agents for 1.5 hr, followed by exposure to [^{3}H]2-DG in the presence of excess non-radioactive 2-DG for 30 min.

Cell Viability Assay

Cell viability was determined using the 3-(4,5-dimethylthiazol-2-yl)-2,5-diphenyltetrazolium bromide (MTT) assay as we described previously [8].

RNA Interference and Luciferase Reporter Assay

For siRNA experiments, cells were transfected with scrambled or DNMT1-specific siRNA. Knockdown of DNMT1 was confirmed by immunoblotting. For the DNMT1 promoter-luciferase reporter assay, luciferase activities were determined with the dual-luciferase system, which uses co-transfected herpes simplex virus thymidine kinase promoter-driven *Renilla reniformis* luciferase as an internal control.

Western Blotting

Western blotting was performed as described previously [8]. Relative differences in protein levels

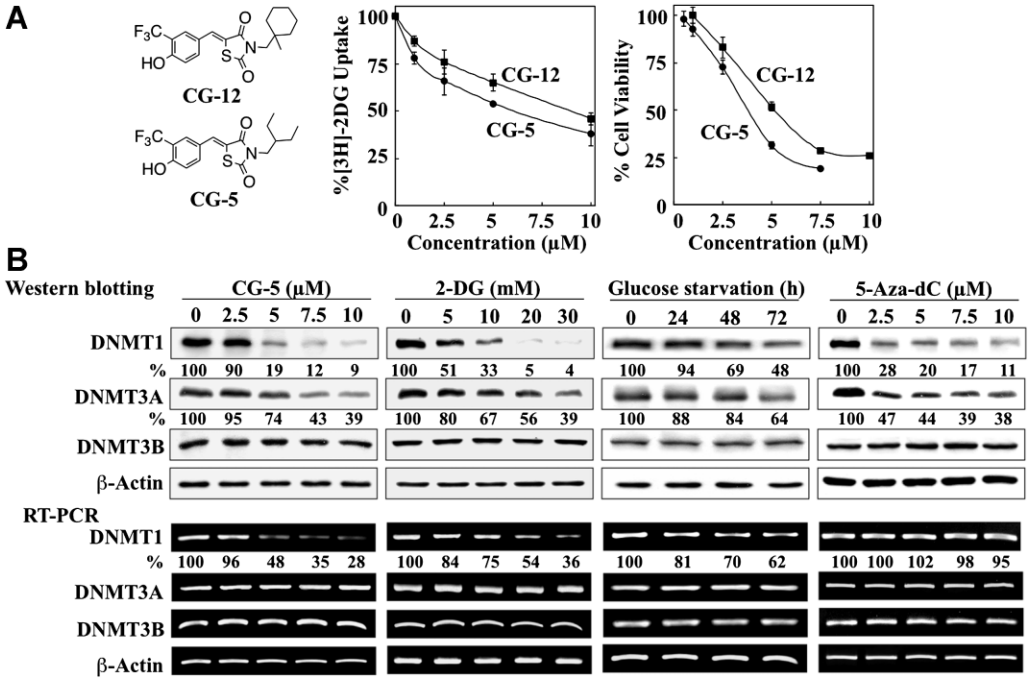

Fig. 1. CG-5, 2-DG, glucose starvation and 5-aza-dC differentially affect the expression levels of DNMT isoforms. **A**: **Left**, structures of CG-12 and CG-5. Center, dose-dependent inhibitory effects of CG-5 versus CG-12 on the uptake of [^{3}H]-2DG into LNCaP cells after 30 min of treatment. Point, mean; bars, SD (n = 3). **Right**, dose-dependent inhibitory effects of CG-5 versus CG-12 on the viability of LNCaP cells by MTT assays after 72 hr of treatment. Point, mean; bars, SD (n = 6). **B**: LNCaP cells were treated with CG-5, 2-DG, and 5-aza-dC at the indicated concentrations in 10% FBS-supplemented medium for 48 hr or glucose-free medium for various time intervals. The expression levels of DNMT1, DNMT3A and DNMT3B were determined by Western blotting (**upper**) and RT-PCR (**lower**). The percentages denote the relative intensities of mRNA and protein bands of treated samples to those of the respective DMSO vehicle-treated controls after normalization to the respective internal reference β-actin. Each value represents the average of three independent experiments.

among experimental groups were determined by densitometry.

DNA Methylation Analysis by Pyrosequencing

To determine methylation levels of candidate genes in response to drug treatment or glucose deprivation, the Pyrosequencing System (Qiagen) was used to detect methylated CpG sites in sequencing reactions [11].

Statistical Analysis

Data from quantitative real time (qRT)-PCR, luciferase reporter assays and pyrosequencing were analyzed using Student's *t*-test. Differences between group means were considered significant at $P < 0.05$.

RESULTS

Microarray Analysis Reveals the Suppression of *DNMT1* and *DNMT3A* Expression and the Upregulation of Methylation-Silenced Genes by Energy Restriction in Prostate Cancer Cells

Pursuant to our hypothesis that energy restriction mediates antitumor effects, in part, through epigenetic gene regulation, we examined the effect of 10 μM CG-12 versus glucose depletion on global gene expression in LNCaP cells via cDNA microarray analysis after 48 hr of treatment. This microarray analysis showed that both treatments significantly reduced the gene expression of *DNMT1*, accompanied by a modest, but statistically significant, decrease in *DNMT3B* expression and no change in *DNMT3A* levels (Table I).

The ability of CG-12 and glucose starvation to downregulate DNMT expression suggests a mechanistic link between energy restriction and epigenetic regulation of gene expression through changes in DNA methylation. Previously, a global survey of DNA methylation patterns in prostate cancer cell lines identified a number of cancer-related genes that were transcriptionally silenced due to aberrant promoter hypermethylation [12]. Based on this report, we examined the microarray data for the effect of CG-12 versus glucose depletion on the expression of 13 genes reported to be silenced by DNA methylation (Table II). Among these, *BASP1*, *GADD45a*, *GADD45b*, *GPX3*, *GSTP1*, *IGFBP3*, *KRT7*, *LAMB3*, *PDLIM4*, and *THBS1* are tumor-suppressive genes, whereas *CD44*, *S100A4*, and *TACSTD2* have been

TABLE I. Microarray Analyses of the Effects of 10 μM CG-12 Versus Glucose Depletion on the Expression of DNMTs in LNCaP Cells After 48 hr of Treatment

	10 μM CG-12		Glucose depletion	
Gene name	Fold change	*P*-value	Fold change	*P*-value
DNMT1	−2.208398	5.32E−06	−2.1143294	6.45E−07
DNMT3A	−1.023485	0.690570233	−1.0391039	0.404186671
DNMT3B	−1.468048	0.001498209	−1.3947437	2.82E−04

associated with tumorigenesis or aggressive phenotype of prostate cancer [13–15]. It is noteworthy that CG-12 mimicked the ability of glucose starvation to activate the expression of *GADD45a*, *GADD45b*, and *IGFBP3*, while many other genes examined were not affected by either treatment, with the exception of *THBS1*, which was upregulated by CG-12.

Energy Restriction Suppresses the Expression of DNMT1 and DNMT3A Through Transcriptional Repression and Proteasomal Degradation, Respectively

Our efforts to structurally optimize CG-12 led to the identification of CG-5, an active derivative in which the terminal methylcyclohexyl ring was replaced by a 3-pentyl moiety. This simple modification improved the potency of CG-5 relative to CG-12 in suppressing [^{3}H]-2DG uptake (IC_{50}, 6 μM vs. 9 μM) and cell viability (IC_{50}, 4.5 μM vs. 6 μM) in LNCaP cells (Fig. 1A). Consequently, we used CG-5 to validate our microarray data by examining the dose-dependent suppressive effects of CG-5 and 2-DG vis-à-vis glucose starvation on the expression of DNMT1, DNMT3A, and DNMT3B, at both protein and mRNA levels, in LNCaP cells. In addition, the DNMT inhibitor 5-aza-dC was used as a control in light of its reported activity in suppressing DNMT1 expression via proteasomal degradation [27,28], and, to a lesser extent, DNMT3A through a yet unidentified mechanism [29].

Western blot analysis indicated that CG-5, 2-DG, and glucose depletion shared with 5-aza-dC the ability to decrease the expression levels of DNMT1 and, to a lesser extent, DNMT3A in a dose- or time-dependent manner (Fig. 1B, upper panel). Nevertheless, the mechanism underlying energy restriction-facilitated downregulation of DNMT1 was different from that of 5-aza-dC as CG-5, 2-DG, and glucose starvation decreased DNMT1 mRNA levels, while no significant changes were noted in response to 5-aza-dC (Fig. 1B, lower panel). In addition, consistent with the microarray findings, no changes in the mRNA level of DNMT3A were noted in response to any of these treatments, suggestive of a posttranslational effect on protein levels. As for DNMT3B, neither the protein nor mRNA expression level was affected by any of the treatments, which contrasted with the microarray data that showed a modest decrease in DNMT3B gene expression in response to energy restriction (Table I). This discrepancy might have arisen from inherent systematic errors associated with microarrays [30].

To examine the mechanism by which CG-5 suppressed the mRNA expression of DNMT1, we assessed its effect on the promoter activity of DNMT1 by using a DNMT1 promoter-luciferase reporter construct. As shown, CG-5 diminished the luciferase activity in a dose-dependent manner (Fig. 2A), suggesting that CG-5 suppressed DNMT1 expression through transcriptional repression. As the core promoter region of *DNMT1* contains three Sp1 [31] and four E2F [32] binding sites, we examined the effect of CG-5 on the expression of these transcription factors and their target genes, androgen receptor (AR) for Sp1 [33], and cyclins E and D3 for E2F1 [34,35].

In line with our previous findings with CG-12 [8,9], CG-5 facilitated a dose-dependent decrease in Sp1 protein level without affecting mRNA expression, suggestive of proteasomal degradation (Fig. 2B). It is noteworthy that the expression of E2F1, at both protein and mRNA levels, was also reduced suggesting a different mode of regulation from that of Sp1. Moreover, decreases in the expression of Sp1 and E2F1 were accompanied by parallel decreases in the expression of their respective targets, namely AR and cyclins D3 and E (Fig. 2B).

As for the CG-5-mediated inhibition of DNMT3A protein expression, a role for proteasomal degradation was supported by the ability of the proteasome inhibitor MG-132 to rescue DNMT3A protein expression from drug-induced suppression in LNCaP cells (Fig. 2C).

Similar findings regarding the ability of CG-5 to suppress the expression of DNMT1 and DNMT3A without disturbing that of DNMT3B was also noted

TABLE II. Microarray Analyses of the Effects of 10 μM CG-12 Versus Glucose Depletion on the Expression of 13 DNA Methylation-Silenced Genes in LNCaP Cells After 48 hr of Treatment

Gene name	Gene description	Molecular function	CG-12	Glucose depletion
			Fold change (*P*-value)	
BASP1 (NM_006317_1)	Brain acid soluble protein 1	Inhibition of Myc-induced cell transformation; a potential tumor suppressor [16]	1.182303151 (0.027893026)	0.920825697 (0.307789115)
CD44 (NM_000610_1)	Receptor for hyaluronic acid	Cell adhesion; markers for breast and prostate cancer stem cells [15]	n/a	n/a
GADD45a (NM_001924-1)	Growth arrest and DNA-damage-inducible protein 45a	Apoptosis, cell cycle arrest, and DNA repair; tumor suppressive [17]	5.838104359 (3.73E−10)	3.11320375 (1.21E−08)
GADD45b (AL050044_1)	Growth arrest and DNA-damage-inducible protein 45b	Apoptosis, cell cycle arrest, and DNA repair; reported tumor suppressor in hepatocellular carcinoma [18]	5.333934097 (2.01E−08)	4.483731849 (5.37E−09)
GPX3 (NM_002084)	Glutathione peroxidase 3	Maintaining genomic integrity via the detoxification of reactive oxygen species; tumor suppressive [19]	1.089147993 (0.370942845)	0.946090435 (0.352881698)
GSTP1 (NM_000852_1)	Glutathione *S*-transferase pi	Conjunction and detoxification of carcinogens; tumor suppressive [20]	1.192508872 (0.028969162)	0.952208888 (0.362806007)
IGFBP3 (NM_000598_1)	Insulin-like growth factor binding protein 3	Inhibiting cancer cell proliferation, adhesion, motility, and metastasis; tumor suppressive [21,22]	5.195274579 (4.89E−08)	2.137167525 (4.50E−07)
KRT7 (NM_005556_1)	Keratin 7	Cytoskeletal organization and biogenesis [12]	1.241685666 (0.018831416)	1.04298615 (0.622715314)
LAMB3 (NM_000228_1)	Laminin, b3	A component of the extracellular matrix involved in cell adhesion, growth, migration, proliferation, and differentiation; tumor suppressive [23]	n/a	1.22357285 (0.031432552)
PDLIM4 (NM_003687_1)	PDZ and LIM domain 3	An actin-binding protein; tumor suppressive [24]	0.993684661 (0.94564817)	0.981663174 (0.801008691)
S100A4 (NM_019554_1)	S100 calcium-binding protein A4	A Ca^{2+}-binding protein; promoting metastasis [25]	0.900563555 (0.217905821)	0.933789972 (0.206088795)
TACSTD2 (NM_002353_1)	Tumor-associated calcium signal transducer 2	A marker of human prostate basal cells with stem cell characteristics; promoting tumorigenesis and invasion [13]	n/a	0.907644973 (0.10922003)
THBS1 (NM_003246_1)	Thrombo-spondin-1	Cell adhesion and motility; a p53 and Rb regulated angiogenesis inhibitor; tumor suppressive [26]	2.609367236 (8.89E−08)	0.986198525 (0.755628795)

n/a: Gene was not listed in the array results.

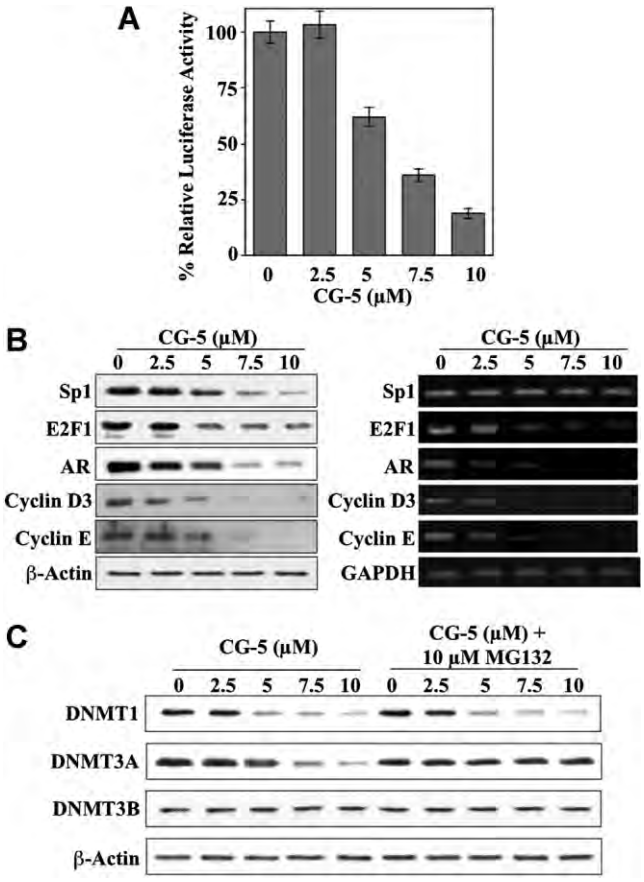

Fig. 2. CG-5 suppresses the expression of DNMT1 and DNMT3A through transcriptional repression and proteasomal degradation, respectively. **A**: Dose-dependent, suppressive effect of CG-5 on DNMT1 promoter activity. LNCaP cells were transiently transfected with the DNMT1 promoter-luciferase reporter plasmid pGL3-DNMT1-Luc, and exposed to CG-5 at the indicated concentrations or DMSO vehicle control in 10% FBS-containing medium for 48 hr. Column, mean (n = 3); error bars, SD. **B**: Parallel Western blot and RT-PCR analyses of the dose-dependent suppressive effect of CG-5 on the expression levels of Sp1, E2F1, AR, and cyclins D3 and E. **C**: The proteasome inhibitor MG132 protected cells from CG-5-induced ablation of DNMT3A, but not DNMT1. LNCaP cells were treated with CG-5 at the indicated concentrations for 36 hr, followed by co-treatment with 10 μM MG132 for an additional 12 hr. Cell lysates were analyzed by immunoblotting for DNMT1 and -3A.

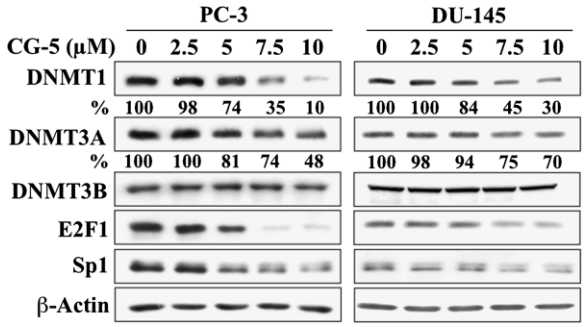

Fig. 3. Western blot analysis of the dose-dependent effects of CG-5 on the expression of DNMT1, DNMT3A, DNMT3B, E2F1, and Sp1 in PC-3 and DU-145 cells. Cells were treated with CG-5 at the indicated concentrations for 48 hr. The percentages denote the relative intensities of protein bands of treated samples to those of the respective DMSO vehicle-treated controls after normalization to the respective internal reference β-actin. Each value represents the average of three independent experiments.

in PC-3 and DU-145 cells (Fig. 3), indicating that this was not a cell line-specific effect. Moreover, the drug's effect on DNMT1 expression correlated with that on E2F1 and Sp1 expression in a dose-dependent manner, suggestive of a causal relationship.

Differential Effects of Energy Restriction on the Activation of DNA Methylation-Silenced Genes

The 13 DNA methylation-silenced genes previously evaluated by microarray analysis (Table II) were assessed by qRT-PCR for changes in expression in response to energy restriction. LNCaP cells were exposed to 5 μM CG-5 or 5 μM 5-aza-dC in 10% FBS-supplemented RPMI 1640 medium for 48 or 72 hr, or to 10% FBS-supplemented glucose-free medium for 72 hr. qRT-PCR analysis indicates that these treatments led to distinct patterns of activation of these epigenetically silenced genes (Fig. 4). 5-Aza-dC mediated varying degrees of activation of 12 of the 13 genes examined relative to the DMSO control (at 72 hr: *GSTP1*, 510-fold; *KRT7*, 295-fold; *CD44*, 26-fold; *TACSTD2*, 23-fold; *BASP1*, 12-fold; *LAMB3*, 10-fold; *IGFBP3*, 9-fold; *GPX3*, *S100A4*, and *THBS1*, 8-fold; *PDLIM4* and *GADD45a*, 3-fold), while no significant change in *GADD45b* mRNA expression was noted (Fig. 4A). In contrast, CG-5 activated 7 of the 13 genes with a distinct preference for the two DNA damage response genes *GADD45a* and *GADD45b* (81- and 31-fold, respectively), followed by *IGFBP3* (12-fold), *LAMB3* (11-fold), *BASP1* (9-fold), *GPX3* (5-fold), and *GSTP1* (2-fold) at 72 hr, while only modest increases (<2-fold) in the expression of *KRT7* and *THBS1* were noted (Fig. 4B). Moreover, CG-5 downregulated the mRNA levels of *PDLIM4*, *S100A4*, and *TACSTD2* by 97%, 56%, and 95%, respectively. Although CG-5 caused a modest, but statistically insignificant, increase in *CD44* mRNA expression at 48 hr (1.16-fold), the treatment led to a 54% decrease ($P < 0.05$) at 72 hr. It is noteworthy that two of these downregulated genes, *S100A4* and *TACSTD2*, are associated with the promotion of tumorigenesis, tumor invasion, and metastasis [13,25], and that CD44 represents a putative marker for prostate cancer stem cells [36].

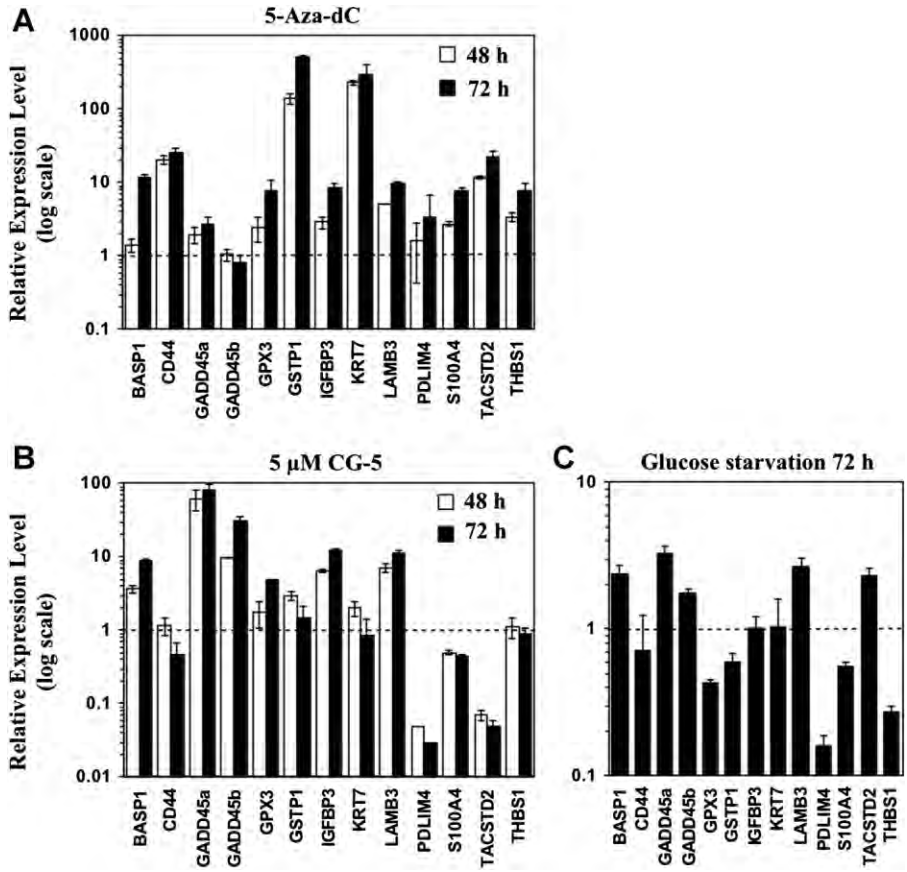

Fig. 4. Effects of 5-aza-dC, CG-5, and glucose deprivation on the expression levels of methylation-silenced cancer-related genes. LNCaP cells were treated with (**A**) 5 μM CG-5 or (**B**) 5 μM 5-aza-dC in 10% FBS-supplemented medium for 48 or 72 hr, or with (**C**) glucose-depleted medium for 72 hr. The expression levels of 13 target genes reported to be silenced by DNA hypermethylation in prostate cancer cells were quantitated by qRT-PCR. Column, mean (n = 3); error bars, SD.

As compared to CG-5-induced energy restriction, glucose deprivation showed a qualitatively similar, but muted effect on gene activation, which, in part, may be reflective of smaller decreases in the expression levels of DNMT1 and DNMT3A. Glucose-depleted medium shared the ability of CG-5 to activate *GADD45a* (3.3-fold), *LAMB3* (2.7-fold), *BASP1* (2.4-fold), and *GADD45b* (1.8-fold), as well as to downregulate the expression of *PDLIM4* and *S100A4*, while having no significant impact on the mRNA expression of *CD44* and *KRT7* (Fig. 4C). However, in contrast to CG-5, glucose deprivation diminished the mRNA expression of *GPX3*, *GSTP1*, and *THBS1*, and increased that of *TACSTD2*.

Role of DNMT1 Downregulation in CG-5-Facilitated Activation of Epigenetically Silenced Genes

Given the greater suppressive effect of CG-5 on DNMT1 expression than on that of DNMT3A (81% and 26%, respectively; Fig. 1B, upper panel), we rationalized that DNMT1 downregulation played a major role in the CG-5-mediated activation of these methylation-silenced genes. This premise was corroborated by two lines of evidence. First, qRT-PCR analysis indicated that siRNA-mediated knockdown of DNMT1 in LNCaP cells mimicked the effects of CG-5 by activating, by at least 2-fold, many of the same genes, including *IGFBP3* (7.5-fold), *BASP1* (3.8-fold), *LAMB3* (2.9-fold), and *GSTP1* (2.3-fold), as well as sharply reducing the expression of *PDLIM4* (Fig. 5A). Second, ectopic DNMT1 expression attenuated the effect of CG-5 on the expression of many of the 13 genes examined (Fig. 5B). With the exception of *IGFBP3*, DNMT1 overexpression diminished the extent of CG-5-mediated gene activation, returning the expression levels of many of these genes, such as *BASP1*, *GADD45b*, *GPX3*, and *GSTP1*, to the basal level or lower. DNMT1 overexpression also abrogated the suppressive effect of CG-5 on the expression of *PDLIM4* and *TACSTD2*. However, ectopic DNMT1 expression had no significant effect on *S100A4* expression.

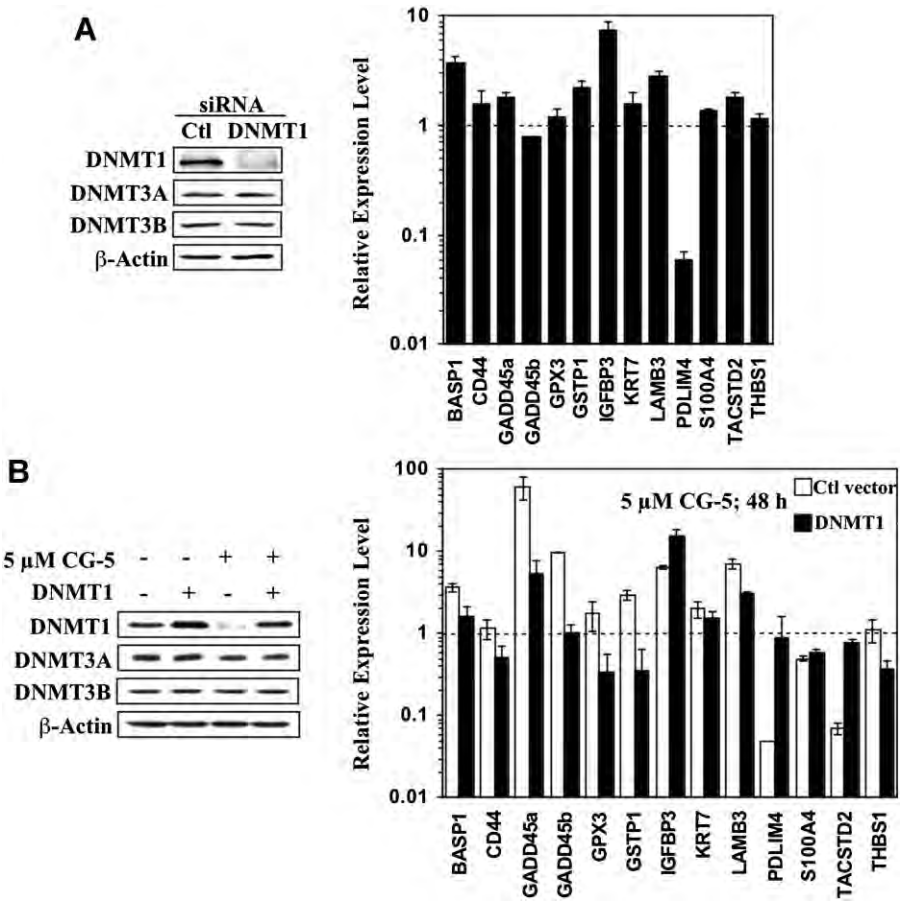

Fig. 5. Evidence that DNMTI plays a pivotal role in CG-5-mediated regulation of methylation-silenced cancer-related gene expression. **A**: siRNA-mediated knockdown of DNMTI mimics the effect of CG-5 on the expression of the selected I3 genes reported to be silenced by DNA hypermethylation in prostate cancer cells, as determined by qRT-PCR (**right**). LNCaP cells were transiently transfected with DNMTI or control (Ctl) siRNA, and then treated with 5 μM CG-5 for 72 hr. The expression levels of DNMT isoforms were analyzed by Western blotting to confirm the specificity of the knockdown (**left**). Column, mean (n = 3); error bars, SD. **B**: Ectopic expression of DNMTI protects cells from CG-5-mediated effects on the expression of the selected I3 methylation-silenced genes, as determined by qRT-PCR (**right**). LNCaP cells were transiently transfected with the flag-tagged DNMTI or control (Ctl) vector, and then treated with 5 μM CG-5 for 48 hr. The expression levels of DNMT isoforms following treatment with CG-5 or DMSO control were analyzed by Western blotting (**left**). Column, mean (n = 3); error bars, SD.

CG-5 Alters CpG methylation in the Promoter Region of the I3 Hypermethylated Genes in LNCaP Cells

To correlate the aforementioned changes in gene expression with the effects of 5-aza-dC, CG-5, and glucose deprivation on DNA methylation, we used pyrosequencing to analyze DNA methylation at CpG islands in the promoter regions of the aforementioned 13 genes in response to individual treatments (Fig. 6A–M). Pyrosequencing is the leading method for quantitative DNA methylation analysis, in part, due to its ability to identify differentially methylated positions in close proximity, thereby allowing concurrent quantification of multiple CpG sites in the promoter region [37]. As neighboring CpG sites within a single promoter showed different degrees of methylation (Fig. 6A–M, right panels; each color-coded circle represents a single CpG site and each designated row represents a treatment condition), the average of all sites was used to represent the level of methylation for each gene (left panels).

LNCaP cells were treated with DMSO (Fig. 6, control; a and b for 48 and 72 hr, respectively), 5 μM 5-aza-dC (c and d), 5 μM CG-5 (e and f), or glucose-depleted medium (g and h), after which genomic DNA was collected for pyrosequencing analysis. As noted, the promoter and/or the first exon of each of these 13 genes contain multiple CpG sites, ranging from 3 to 19 sites. Not only did the methylation level among these sites vary within a single promoter/exon region (Fig. 6A–M, right panels, a and b), but also the total methylation levels of the promoters/

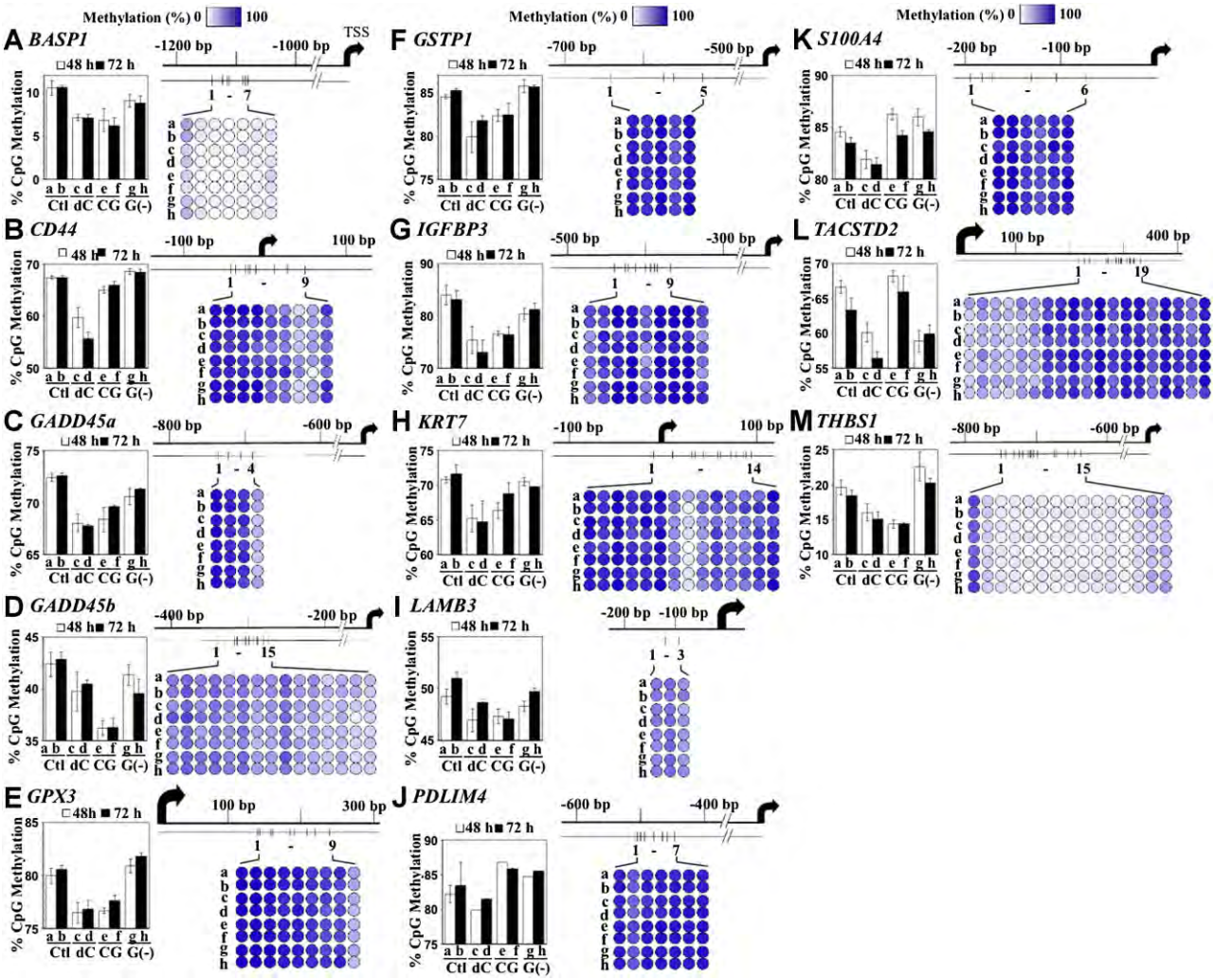

Fig. 6. Effects of CG-5, glucose deprivation, and 5-aza-dC on CpG island methylation in methylation-silenced cancer-related genes. LNCaP cells were treated with DMSO control (Ctl), 5 μM 5-aza-dC (dC), 5 μM CG-5 (CG), or glucose-depleted medium [G(−)] for 48 and 72 hr. Pyrosequencing analysis of CpG island methylation in the promoter/first exon regions of the selected 13 methylation-silenced genes was performed as described in Materials and Methods Section. **A**, *BASP1*; **B**, *CD44*; **C**, *GADD45a*; **D**, *GADD45b*; **E**, *GPX3*; **F**, *GSTP1*; **G**, *IGFBP3*; **H**, *KRT7*; **I**, *LAMB3*; **J**, *PDLIM4*; **K**, *SI00A4*; **L**, *TACSTD2*; **M**, *THBSI*. Average methylation levels of individual CpG sites in the promoter/first exon of each of the genes examined under each condition are represented by the color-coded circles (**right panels**; dark blue, 100%; white, 0%; scale at top of each column). The average methylation level of all CpG sites within each of the promoters/first exons was used to represent the level of methylation for each of the 13 genes under each treatment condition (**left panel**; column, mean (n = 3–19); error bars, SD). **a** and **b**: DMSO control for 48 and 72 hr, respectively; **c** and **d**: 5 μM 5-aza-dC for 48 and 72 hr, respectively; **e** and **f**: 5 μM CG-5 for 48 and 72 hr, respectively; **g** and **h**: glucose-depleted medium for 48 and 72 hr, respectively.

exons varied greatly among these genes (left panels, a and b). For example, while many of these genes were highly methylated, *BASP1* and *THBS1* showed only 10% and 20% CpG methylation, respectively, in control cells (Fig. 6A and M, respectively). Consistent with the qRT-PCR findings, 5-aza-dC, CG-5, and glucose-depleted medium exhibited differential effects on the DNA methylation patterns of these genes. 5-Aza-dC facilitated decreases in DNA methylation in all of the genes examined (all panels, c and d). These epigenetic changes correlated with activation of these genes in 5-aza-dC-treated LNCaP cells (Fig. 4A) with the exception of *GADD45b* (panel D), of which the mRNA levels remained unaltered after drug treatment. It is noteworthy that, while CG-5 mediated the hypomethylation and resulting activation of many tumor suppressor genes, it enhanced the DNA methylation of *PDLIM4* (panel J) and the tumor-promoting genes *S100A4* and *TACSTD2* (panels K and L, respectively), resulting in the downregulated expression of these genes (Fig. 4B). The effects of glucose-depleted medium on DNA methylation of many of

these genes paralleled those of CG-5, however, to a lesser extent. Nevertheless, glucose starvation contrasted with CG-5-induced energy restriction in its opposite effects on the DNA methylation pattern of *GPX3*, *GSTP1*, *TACSTD2*, and *THBS1* (panels E, F, L, and M, respectively), which underlies the observed differences in the effects of these two treatments on the activation of these DNA methylation-silenced genes (Fig. 4C).

DISCUSSION

Aberrant promoter hypermethylation of critical pathway genes plays an important role in prostate carcinogenesis and tumor progression [38,39], thereby representing a therapeutically relevant target for cancer treatment [40]. In this study, we demonstrated the high potency of the novel ERMA CG-5 relative to 2-DG in suppressing the expression of DNMT1 and, to a lesser extent, DNMT3A, which led to the reactivation of a series of DNA methylation-silenced tumor suppressor genes, including *GADD45a*, *GADD45b*, *IGFBP3*, *LAMB3*, *BASP1*, *GPX3*, and *GSTP1*, in prostate cancer cells through promoter hypomethylation.

The effect of CG-5 on DNA methylation profiles is largely associated with the reduction in the expression of DNMT1 as siRNA-mediated knockdown and ectopic expression of DNMT1 mimicked and diminished, respectively, the ability of CG-5 to modulate the expression of these silenced genes. Although CG-5 and 5-aza-dC share the ability to downregulate DNMT1 expression, the underlying mechanisms are distinctly different. Evidence suggests that CG-5 facilitated the downregulation of DNMT1 expression through transcriptional repression, which our data suggest is be associated with the reduced expression of Sp1 and E2F1. Our previous study demonstrated that β-transducin repeat-containing protein (β-TrCP)-dependent proteasomal degradation of Sp1 represents one of the energy restriction-associated cellular responses elicited by CG-12 [8], and is likely the mechanism by which Sp1 is suppressed in CG-5-treated cells. In contrast, CG-5-mediated suppression of E2F1 expression occurred at the transcriptional level.

The specificity with which CG-5 activates DNA methylation-silenced genes is noteworthy, and contrasts with the nonspecific reactivation of nearly of all the silenced genes examined by 5-aza-dC. For example, our data indicate that CG-5 reduced the basal expression levels of *PDLIM4* and the three tumor/invasion-promoting genes, namely *CD44*, *S100A4*, and *TACSTD2*, while 5-aza-dC increased the expression of these genes by 8- to 26-fold. This target specificity was further confirmed by pyrosequencing analysis, which showed the differential effect of CG-5 versus 5-aza-dC on DNA methylation in the promoter regions of the 13 genes examined. While 5-aza-dC caused universal hypomethylation of all of these 13 genes, CG-5 enhanced the DNA methylation of *PDLIM4* and the tumor-promoting genes *S100A4* and *TACSTD2*. However, the suppressive effect of CG-5 on CD44 promoter methylation relative to the control (65.9% vs. 67.42%; $P = 0.033$) represents an anomaly since CG-5 reduced *CD44* expression.

Mechanistically, this differential regulation of DNA methylation-silenced genes is attributed not just to CG-5's effect on DNA hypomethylation alone, but also to its ability to affect the expression of transcription factors, such as Sp1 and E2F1, and histone-modifying enzymes [9]. Together, these concerted actions underline a more complicated mode of epigenetic gene regulation than that of 5-aza-dC's inhibitory effect on DNMT activity alone.

CONCLUSIONS

It is well recognized that cancer cells undergo a metabolic shift to anaerobic glycolysis that provides growth advantages within the tumor microenvironment. Consequently, there is intense interest in targeting tumor metabolism as a therapeutic strategy, including small-molecule approaches. In this study, we demonstrate that epigenetic activation of DNA methylation-silenced tumor suppressor genes represents an important antitumor response to energy restriction. Moreover, our novel small-molecule ERMA, GC5, regulates the expression of these genes through modulation of DNA methylation and, perhaps by virtue of its concomitant effects on histone modifications, exhibits target gene specificity and a broader spectrum of antitumor gene activation that might offer therapeutic advantages over DNMT inhibitors.

ACKNOWLEDGMENTS

This work was supported by National Institutes of Health grant CA112250 and Department of Defense. Prostate Cancer Research Program grant W81XWH-09-0198 to C.S.C.; Predoctoral fellowship NSC98-2917-I-010-103 to H.Y.L. from the Graduate Student Study Abroad Program of the National Science Council, Taiwan.

REFERENCES

1. Kroemer G, Pouyssegur J. Tumor cell metabolism: Cancer's Achilles' heel. Cancer Cell 2008;13(6):472–482.
2. Vander Heiden MG. Targeting cancer metabolism: A therapeutic window opens. Nat Rev Drug Discov 2011;10(9):671–684.

3. Denko NC. Hypoxia, HIF1 and glucose metabolism in the solid tumour. Nat Rev Cancer 2008;8(9):705–713.
4. Elstrom RL, Bauer DE, Buzzai M, Karnauskas R, Harris MH, Plas DR, Zhuang H, Cinalli RM, Alavi A, Rudin CM, Thompson CB. Akt stimulates aerobic glycolysis in cancer cells. Cancer Res 2004;64(11):3892–3899.
5. Osthus RC, Shim H, Kim S, Li Q, Reddy R, Mukherjee M, Xu Y, Wonsey D, Lee LA, Dang CV. Deregulation of glucose transporter 1 and glycolytic gene expression by c-Myc. J Biol Chem 2000;275(29):21797–21800.
6. Matoba S, Kang JG, Patino WD, Wragg A, Boehm M, Gavrilova O, Hurley PJ, Bunz F, Hwang PM. p53 regulates mitochondrial respiration. Science 2006;312(5780):1650–1653.
7. Kelloff GJ, Hoffman JM, Johnson B, Scher HI, Siegel BA, Cheng EY, Cheson BD, O'Shaughnessy J, Guyton KZ, Mankoff DA, Shankar L, Larson SM, Sigman CC, Schilsky RL, Sullivan DC. Progress and promise of FDG-PET imaging for cancer patient management and oncologic drug development. Clin Cancer Res 2005;11(8):2785–2808.
8. Wei S, Kulp SK, Chen CS. Energy restriction as an antitumor target of thiazolidinediones. J Biol Chem 2010;285(13):9780–9791.
9. Chen CH, Huang PH, Chu PC, Chen MC, Chou CC, Wang D, Kulp SK, Teng CM, Wang Q, Chen CS. Energy restriction-mimetic agents induce apoptosis in prostate cancer cells in part through epigenetic activation of KLF6 tumor suppressor gene expression. J Biol Chem 2011;286(12):9968–9976.
10. Sharma S, Kelly TK, Jones PA. Epigenetics in cancer. Carcinogenesis 2010;31(1):27–36.
11. Tost J, Gut IG. DNA methylation analysis by pyrosequencing. Nat Protoc 2007;2(9):2265–2275.
12. Ibragimova I, Ibanez de Caceres I, Hoffman AM, Potapova A, Dulaimi E, Al-Saleem T, Hudes GR, Ochs MF, Cairns P. Global reactivation of epigenetically silenced genes in prostate cancer. Cancer Prev Res (Phila) 2010;3(9):1084–1092.
13. Goldstein AS, Lawson DA, Cheng D, Sun W, Garraway IP, Witte ON. Trop2 identifies a subpopulation of murine and human prostate basal cells with stem cell characteristics. Proc Natl Acad Sci USA 2008;105(52):20882–20887.
14. Herrlich P, Morrison H, Sleeman J, Orian-Rousseau V, Konig H, Weg-Remers S, Ponta H. CD44 acts both as a growth- and invasiveness-promoting molecule and as a tumor-suppressing cofactor. Ann NY Acad Sci 2000;910:106–118; discussion 118–120.
15. Li F, Tiede B, Massague J, Kang Y. Beyond tumorigenesis: Cancer stem cells in metastasis. Cell Res 2007;17(1):3–14.
16. Hartl M, Nist A, Khan MI, Valovka T, Bister K. Inhibition of Myc-induced cell transformation by brain acid-soluble protein 1 (BASP1). Proc Natl Acad Sci USA 2009;106(14):5604–5609.
17. Zerbini LF, Libermann TA. GADD45 deregulation in cancer: Frequently methylated tumor suppressors and potential therapeutic targets. Clin Cancer Res 2005;11(18):6409–6413.
18. Qiu W, David D, Zhou B, Chu PG, Zhang B, Wu M, Xiao J, Han T, Zhu Z, Wang T, Liu X, Lopez R, Frankel P, Jong A, Yen Y. Down-regulation of growth arrest DNA damage-inducible gene 45beta expression is associated with human hepatocellular carcinoma. Am J Pathol 2003;162(6):1961–1974.
19. Yu YP, Yu G, Tseng G, Cieply K, Nelson J, Defrances M, Zarnegar R, Michalopoulos G, Luo JH. Glutathione peroxidase 3, deleted or methylated in prostate cancer, suppresses prostate cancer growth and metastasis. Cancer Res 2007;67(17):8043–8050.
20. Cairns P, Esteller M, Herman JG, Schoenberg M, Jeronimo C, Sanchez-Cespedes M, Chow NH, Grasso M, Wu L, Westra WB, Sidransky D. Molecular detection of prostate cancer in urine by GSTP1 hypermethylation. Clin Cancer Res 2001;7(9):2727–2730.
21. Massoner P, Colleselli D, Matscheski A, Pircher H, Geley S, Jansen Durr P, Klocker H. Novel mechanism of IGF-binding protein-3 action on prostate cancer cells: Inhibition of proliferation, adhesion, and motility. Endocr Relat Cancer 2009;16(3):795–808.
22. Mehta H, Gao Q, Galet C, Paharkova V, Wan J, Said JW, Sohn J, Lawson G, Cohen P, Cobb L, Lee KW. IGFBP-3 is a metastasis suppression gene in prostate cancer. Cancer Res 2011;71(15):5154–5163.
23. Sathyanarayana UG, Padar A, Suzuki M, Maruyama R, Shigematsu H, Hsieh JT, Frenkel EP, Gazdar AF. Aberrant promoter methylation of laminin-5-encoding genes in prostate cancers and its relationship to clinicopathological features. Clin Cancer Res 2003;9(17):6395–6400.
24. Vanaja DK, Grossmann ME, Cheville JC, Gazi MH, Gong A, Zhang JS, Ajtai K, Burghardt TP, Young CY. PDLIM4, an actin binding protein, suppresses prostate cancer cell growth. Cancer Invest 2009;27(3):264–272.
25. Boye K, Maelandsmo GM. S100A4 and metastasis: A small actor playing many roles. Am J Pathol 2010;176(2):528–535.
26. Li Q, Ahuja N, Burger PC, Issa JP. Methylation and silencing of the thrombospondin-1 promoter in human cancer. Oncogene 1999;18(21):3284–3289.
27. Ghoshal K, Datta J, Majumder S, Bai S, Kutay H, Motiwala T, Jacob ST. 5-Aza-deoxycytidine induces selective degradation of DNA methyltransferase 1 by a proteasomal pathway that requires the KEN box, bromo-adjacent homology domain, and nuclear localization signal. Mol Cell Biol 2005;25(11):4727–4741.
28. Patel K, Dickson J, Din S, Macleod K, Jodrell D, Ramsahoye B. Targeting of 5-aza-2′-deoxycytidine residues by chromatin-associated DNMT1 induces proteasomal degradation of the free enzyme. Nucleic Acids Res 2010;38(13):4313–4324.
29. Palii SS, Van Emburgh BO, Sankpal UT, Brown KD, Robertson KD. DNA methylation inhibitor 5-Aza-2′-deoxycytidine induces reversible genome-wide DNA damage that is distinctly influenced by DNA methyltransferases 1 and 3B. Mol Cell Biol 2008;28(2):752–771.
30. Fang Y, Brass A, Hoyle DC, Hayes A, Bashein A, Oliver SG, Waddington D, Rattray M. A model-based analysis of microarray experimental error and normalisation. Nucleic Acids Res 2003;31(16):e96. http://www.ncbi.nlm.nih.gov/pubmed/12907748
31. Liu S, Liu Z, Xie Z, Pang J, Yu J, Lehmann E, Huynh L, Vukosavljevic T, Takeki M, Klisovic RB, Baiocchi RA, Blum W, Porcu P, Garzon R, Byrd JC, Perrotti D, Caligiuri MA, Chan KK, Wu LC, Marcucci G. Bortezomib induces DNA hypomethylation and silenced gene transcription by interfering with Sp1/NF-kappaB-dependent DNA methyltransferase activity in acute myeloid leukemia. Blood 2008;111(4):2364–2373.
32. Kimura H, Nakamura T, Ogawa T, Tanaka S, Shiota K. Transcription of mouse DNA methyltransferase 1 (Dnmt1) is regulated by both E2F-Rb-HDAC-dependent and -independent pathways. Nucleic Acids Res 2003;31(12):3101–3113.
33. Yang CC, Wang YC, Wei S, Lin LF, Chen CS, Lee CC, Lin CC. Peroxisome proliferator-activated receptor gamma-independent suppression of androgen receptor expression by troglitazone mechanism and pharmacologic exploitation. Cancer Res 2007;67(7):3229–3238.

34. Ohtani K, DeGregori J, Nevins JR. Regulation of the cyclin E gene by transcription factor E2F1. Proc Natl Acad Sci USA 1995;92(26):12146–12150.

35. Ma Y, Yuan J, Huang M, Jove R, Cress WD. Regulation of the cyclin D3 promoter by E2F1. J Biol Chem 2003;278(19):16770–16776.

36. Palapattu GS, Wu C, Silvers CR, Martin HB, Williams K, Salamone L, Bushnell T, Huang LS, Yang Q, Huang J. Selective expression of CD44, a putative prostate cancer stem cell marker, in neuroendocrine tumor cells of human prostate cancer. Prostate 2009;69(7):787–798.

37. Dejeux E, El abdalaoui H, Gut IG, Tost J. Identification and quantification of differentially methylated loci by the pyrosequencing technology. Methods Mol Biol 2009;507:189–205.

38. Li LC, Carroll PR, Dahiya R. Epigenetic changes in prostate cancer: Implication for diagnosis and treatment. J Natl Cancer Inst 2005;97(2):103–115.

39. Park JY. Promoter hypermethylation in prostate cancer. Cancer Control 2010;17(4):245–255.

40. Issa JP, Kantarjian HM. Targeting DNA methylation. Clin Cancer Res 2009;15(12):3938–3946.

Journal of Medicinal Chemistry

Article

pubs.acs.org/jmc

Development of a Novel Class of Glucose Transporter Inhibitors

Dasheng Wang,[†,‡] Po-Chen Chu,[†,‡] Chia-Ning Yang,[§] Ribai Yan,[†] Yu-Chung Chuang,[§] Samuel K. Kulp,[†] and Ching-Shih Chen*[,†,∥]

[†]Division of Medicinal Chemistry, College of Pharmacy, The Ohio State University, Columbus, Ohio 43210, United States

[§]Institute of Biotechnology, National Kaohsiung University, Kaohsiung, Taiwan 811

[∥]Institute of Basic Medical Sciences, National Cheng-Kung University, 1 Ta-Hsueh Road, Tainan, 70101, Taiwan

ABSTRACT: On the basis of our finding that the antitumor effect of 5-{4-[(1-methylcyclohexyl)methoxy]benzyl}thiazolidine-2,4-dione, a thiazolidinedione peroxisome proliferator-activated receptor (PPAR)γ agonist, was, in part, attributable to its ability to block glucose uptake independently of PPARγ, we used its PPARγ-inactive analogue to develop a novel class of glucose transporter (GLUT) inhibitors. This lead optimization led to compound **30** {5-(4-hydroxy-3-trifluoromethylbenzylidene)-3-[4,4,4-trifluoro-2-methyl-2-(2,2,2-trifluoroethyl)butyl]thiazolidine-2,4-dione} as the optimal agent, which exhibited high antitumor potency through the suppression of glucose uptake (IC_{50}, 2.5 μM), while not cytotoxic to prostate and mammary epithelial cells. This glucose uptake inhibition was associated with the inhibition of GLUT1 (IC_{50}, 2 μM). Moreover, the mechanism of antitumor action of compound **30** was validated by its effect on a series of energy restriction-associated cellular responses. Homology modeling analysis suggests that the inhibitory effect of compound **30** on glucose entry was attributable to its ability to bind to the GLUT1 channel at a site distinct from that of glucose.

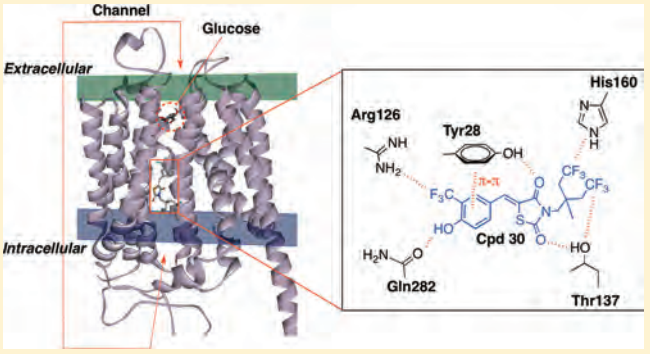

INTRODUCTION

Cancer cells gain growth advantages in the microenvironment by shifting cellular metabolism from oxidative phosphorylation to glycolysis, the so-called Warburg effect.[1−4] This glycolytic shift enables cancer cells to adapt to low-oxygen microenvironments, to generate biosynthetic building blocks for cell proliferation, to acidify the local environment to facilitate tumor invasion, and to generate NADPH and glutathione through the pentose phosphate shunt to increase resistance to oxidative stress.[2,5,6] Thus, the Warburg effect is considered as a fundamental property of neoplasia, thereby constituting the basis for tumor imaging by [^{18}F]2-fluoro-2-deoxyglucose positron emission tomography.[7] From a therapeutic perspective, targeting glycolysis by blocking glucose uptake represents a clinically relevant approach for cancer treatment, which has constituted the focus of many investigations.

Substantial evidence indicates that increased glucose uptake in malignant cells is associated with dysregulated expression of glucose transporter proteins, especially glucose transporter 1 (GLUT1).[8,9] GLUT1 is a class I facilitative sugar transporter responsible for basal glucose import required to maintain cellular respiration. GLUT1 overexpression has been reported in many types of human cancers, including those of brain,[10] breast,[11,12] cervix,[13] colon,[14] kidney,[15] lung,[16] ovary,[17] prostate,[18] thyroid,[19] and skin,[20] and is correlated with advanced cancer stages and poor clinical outcomes. This GLUT1 upregulation might be attributable to genetic alterations or environmental factors, including p53 mutations,[21] upregulated Akt signaling,[22] and hypoxia.[23] To date, a number of small-molecule agents capable of suppressing the activity/expression of GLUT1 and/or other GLUT members have been reported, including resveratrol,[24] naringenin,[25] phloretin,[26] fasentin,[27] 8-aminoadenosine,[28] and STF-31.[29] Exposure of cancer cells to these agents gave rise to reduced cell proliferation and/or chemosensitization, providing a proof-of-concept that targeting GLUT1 is a viable therapeutic strategy for cancer treatment.

Previously, we demonstrated that the suppressive effects of the peroxisome proliferator-activated receptor (PPAR)γ agonist 5-{4-[(1-methylcyclohexyl)methoxy]benzyl}thiazolidine-2,4-dione (**1**) on various signaling pathways, including those mediated by cyclin D1, Sp1, and androgen receptor (AR), in prostate cancer cells was attributable to its ability to block glucose entry independently of PPARγ.[30,31] This finding provides a mechanistic rationale for the present study of using the PPARγ-inactive analogues of **1** as a scaffold to develop a novel class of glucose transporter inhibitors. The proof-of-concept of this lead optimization was provided by compound **30**, which exhibited high potency in inducing apoptotic death in LNCaP cells through the suppression of glucose uptake (IC_{50}, 2.5 μM). Evidence suggests that this suppression of glucose entry was associated with the inhibition of GLUT1 (IC_{50}, 2 μM), the predominant

Received: January 4, 2012
Published: April 2, 2012

GLUT isoform expressed in LNCaP cells. Moreover, the mechanism of antitumor action of compound **30** was validated by its ability to elicit a series of energy restriction-associated cellular responses, reminiscent of that of its parent compound.[30,31]

CHEMISTRY

Previously, we reported the pharmacological exploitation of the PPARγ-inactive analogue of compound **1**, (*Z*)-5-{4-[(1-methylcyclohexyl)methoxy]benzylidene}thiazolidine-2,4-dione (Δ2CG, **2**), as a scaffold to develop AR-ablative agents via its permuted isomer **3**, which led to (*Z*)-5-[4-hydroxy-3-(trifluoromethyl)benzylidene]-3-[(1-methylcyclohexyl)methyl]-thiazolidine-2,4-dione (CG-12, **4**) as the optimal compound (Figure 1A).[32] Our recent studies demonstrated that the suppressive effect of compound **4** on AR expression was associated with its ability to mimic glucose starvation through the inhibition of glucose uptake and the subsequent increase in the expression level of the E3 ligase β-transducin repeat-containing protein (β-TrCP).[30,31,33] This upregulation facilitated the proteasomal degradation of the transcription factor Sp1, leading to the transcriptional repression of AR. Thus, compound **4** was used as a starting point to generate potent glucose uptake inhibitors.

On the structural modification of compound **4**, we hypothesized that there exists interplay between the polar substituents on the phenyl ring and the terminal hydrophobic moiety in regulating its glucose uptake inhibitory activity. Accordingly, the methylcyclohexyl moiety of compound **4** was replaced by a series of hydrophobic moieties with varying degrees of bulkiness, generating compounds **5**−**9**, among which compound **5** exhibited the most potent suppressive effect on the uptake of [^{3}H]-2-deoxyglucose (2-DG) into LNCaP cells (Figure 2A).

Compound **5** was subjected to further modifications via three different strategies: (i) replacement of the electronegative -CF_3 function with various substituents (compounds **11**−**14**) or rearrangement of the disubstituents on the phenyl ring (compounds **15** and **16**), (ii) substitution at the 5-position with various functional groups (compounds **17**−**22**) or rearrangement of the trisubstituents on the phenyl ring (compounds **23**−**27**), and (iii) replacement of the terminal -CH_3 functions of the hydrophobic side arm with -CF_3 to enhance electronegativity (compound **28**) in conjunction with substitution of the tertiary proton with a F atom or -CH_3 group (compounds **29** and **30**, respectively). General procedures for the synthesis of these compounds are depicted in Figure 1B.

RESULTS

Screening of the Focused Compound Library to Identify Lead Glucose Uptake Inhibitors. The aforementioned derivatives (**5**−**30**) along with the parent compounds (**1**−**4**), each at 5 μM, were assessed for their abilities to block the uptake of [^{3}H]-2-DG into LNCaP cells after 30 min of exposure, which revealed a subtle structure−activity correlation (Figure 2A).

The role of the hydrophobic side chain in regulating the glucose uptake-inhibitory potency was manifested by the differential activities among compounds **4**−**9**, which showed an inverse correlation with the bulkiness of the hydrophobic moiety. Especially, the large discrepancy in inhibitory potency between compounds **5**−**8** and **4**/**9** underscored the preferential recognition of ligands with smaller hydrophobic side chains by target proteins. On the basis of this consideration, compound **5** was selected as the lead agent for further modifications.

Evidence indicates that the ligand binding entailed hydrophilic interactions with the polar substituents on the terminal phenyl ring. For example, masking of the -OH substituent of the terminal phenyl ring of compound **5** with a methyl group (compound **10**) abrogated the inhibitory activity. Moreover, the adjacent -CF_3 function could only be replaced with -NO_2 (**13**), but not -OH (**11**), -CH_3 (**12**), or -NH_2 (**14**), without compromising the drug activity, suggesting the involvement of electronegative function in protein−ligand interactions. This premise was also supported by lack of inhibitory activity in compounds **15** and **16**, both of which lacked an electronegative substituent on the phenyl ring.

Introduction of an additional electron-withdrawing group, such as -F (**17**), -Br (**18**), or -NO_2 (**21**), or a -OH function (**19**) on the 5-position led to a modest decrease in the glucose uptake activity compared to the parent compound **5**. However, substitution with -OCH_3 (**20**) or -NH_2 (**22**) resulted in a complete loss of activity. Compound **19**'s regioisomers, **23** and **24**, showed similar potency as their parent molecule, indicating flexibility in ligand recognition. This premise was supported by replacement of the -CF_3 of compound **23** with a -Br atom (**25**) which substantially reduced the inhibitory activity, but was contradicted by the similarity in the potencies of **24** and **26**. This discrepancy suggested the role of the catechol moiety of **26** in interacting with target protein(s), which was corroborated by the ability of its regioisomer **27** to block glucose uptake with similar potency. These catechols, however, were not amenable to drug development due to intrinsic chemical/metabolic instability.

Furthermore, compounds **18** and **21** are more acidic than the other derivatives examined, including **5**, **17**, **19**, **20**, and **22**, due to the inductive effect of the Br and NO_2 substituents ortho to the -OH group. By using a computational protocol in Discovery Studio 3.1, the pK_a values of these derivatives were calculated as follows: **5**, 8.0; **17**, 6.0; **18**, 6.6; **19**, 11.5; **20**, 9.6; **21**, 8.8; and **22**, 8.9. These pK_a values, however, did not show a correlation with the respective potencies of these compounds in suppressing glucose uptake, that is, **5** > **19** > **17**, **18** > **21** > **22**. This finding suggests that acidity of the phenolic moiety was not a primary determinant of the ligand binding.

Considering the enhancing effect of the CF_3 moiety on the activity and metabolic stability of drug candidates in the course of lead optimization,[34−36] we replaced the two terminal methyl functions at the hydrophobic side chain of compound **5** with CF_3 groups with or without substitution at the tertiary carbon, leading to **28**−**30**. All of these derivatives showed substantially improved potency relative to compound **5**, in the relative order **30** > **28** > **29**.

Furthermore, MTT assays indicated that the abilities of these thiazolidinedione derivatives to suppress the viability of LNCaP cells paralleled their respective inhibitory activities on glucose uptake (Figure 2B), suggesting a potential causal relationship between these two cellular events.

Suppression of Glucose Uptake through the Inhibition of Glucose Transporters. Dose−response analysis confirmed the high potency of compound **30** in blocking [^{3}H]-2-DG uptake into LNCaP cells with IC_{50} of 2.5 μM, while the IC_{50} values of other compounds examined were as follows: **28**, 3.5 μM; **5**, 6 μM; **4**, 9 μM; **2**, 52 μM; and **1**, 78 μM (Figure 3A). Glucose transport across the cytoplasmic membrane is mediated by members of the facilitative glucose transporter/solute carrier

dx.doi.org/10.1021/jm300015m | J. Med. Chem. 2012, 55, 3827−3836

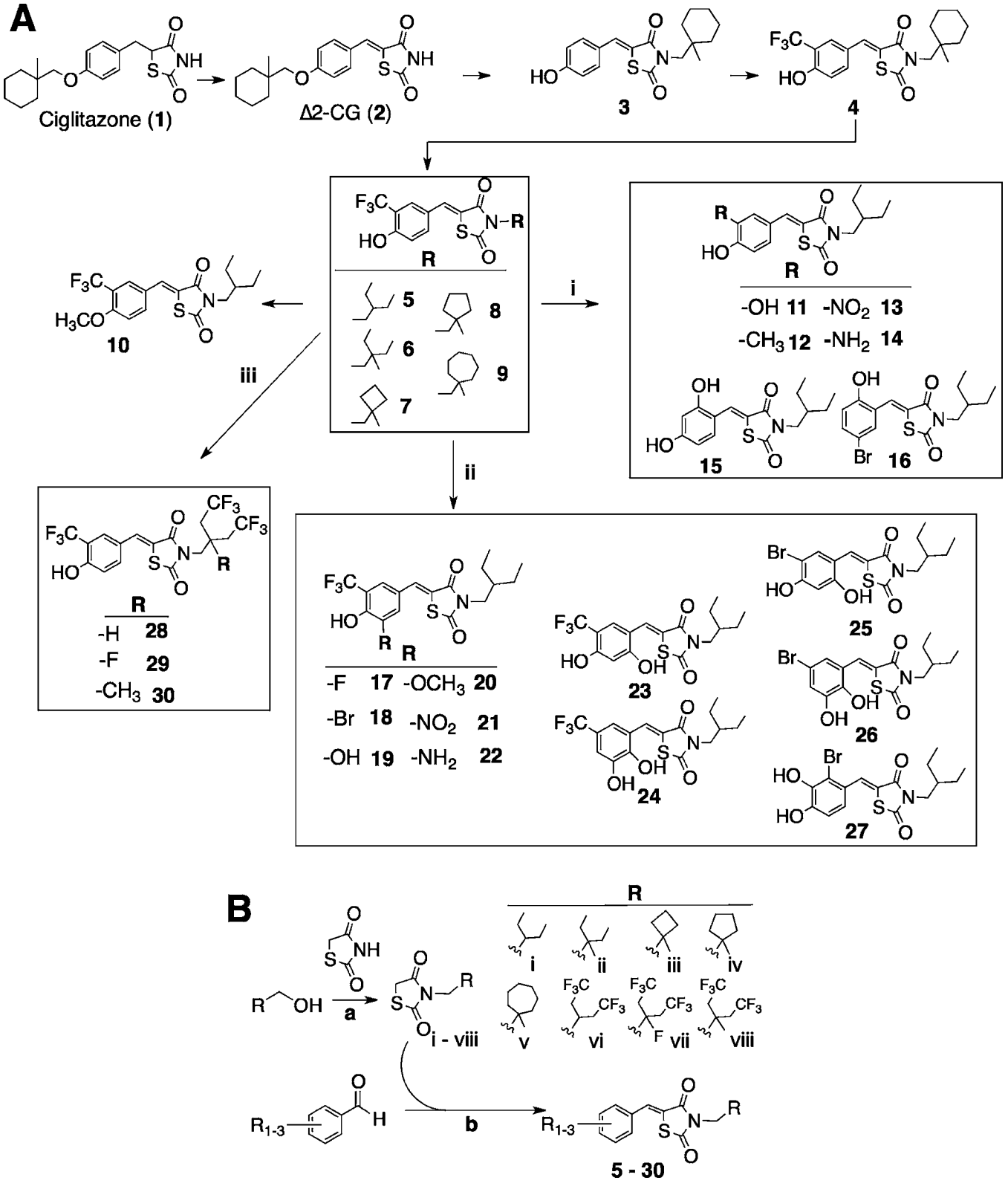

Figure 1. (A) Chemical structures of compounds **1**−**30** in the 5-{4-[(1-methylcyclohexyl)methoxy]benzyl}thiazolidine-2,4-dione-based focused compound library. (B) General synthetic procedure for compounds **5**−**30**. Reaction conditions: (a) DIPAD, TPP/dry THF; (b) piperidine, ethanol/reflux.

(GLUT/SLC2A) family.[37] To date, a total of 14 members have been identified, which are divided into three classes: class I, GLUT1−4 and GLUT14; class II, GLUT5, GLUT7, GLUT9, and GLUT11; class III, GLUT6, GLUT8, GLUT10, GLUT12, and H^+-coupled *myo*-inositol transporter.[37] As information regarding the expression patterns of individual GLUT members in LNCaP cells was lacking, we used quantitative real-time polymerase chain reaction to assess the mRNA levels of the

dx.doi.org/10.1021/jm300015m | *J. Med. Chem.* 2012, 55, 3827−3836

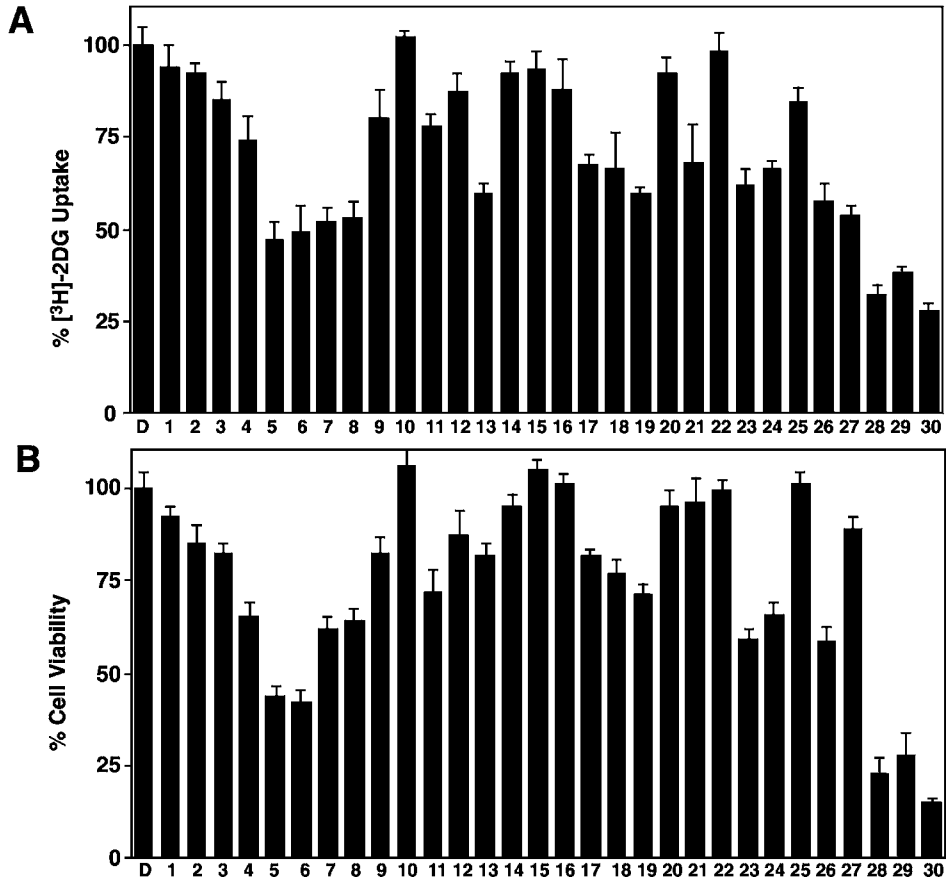

Figure 2. (A) Inhibitory effects of compounds **1**−**30**, each at 5 μM, on the uptake of [^{3}H]-2-DG into LNCaP cells in Krebs−Ringer phosphate buffer at 37 °C after 30 min of drug treatment. Column, mean; bars, SD (N = 3). (B) Corresponding effects of compounds **1**−**30** on the viability of LNCaP cells by MTT assays in 10% FBS-containing RPMI 1640 medium after 72 h of drug treatment. Column, mean; bars, SD (N = 6).

hypoxia-responsive GLUT1 and GLUT3 and three other representative GLUT members, including the class I GLUT2 and GLUT4 and the class II GLUT9. Among these five members, LNCaP cells expressed GLUT1 and, to a much lesser extent, GLUT9, while the mRNA levels of GLUT2−4 were negligible (Figure 3B).

To determine if the ability of compound **30** to inhibit glucose uptake in cancer cells could be attributed to the modulation of GLUT function, we examined the effects of **30** and its parent compound **5** on glucose uptake in LNCaP cells ectopically expressing GLUT isoforms. To assess the isoform specificities of the compounds, LNCaP cells were transfected with plasmids encoding GLUT1, GLUT3, GLUT4, or GLUT9 vis-à-vis the pCMV control vector so that the increased glucose uptake in GLUT-transfected cells relative to pCMV control cells was indicative of the activity of the ectopically expressed GLUT protein. Among the four GLUT members examined, GLUT1 was preferentially inhibited by compounds **5** and **30** at 5 μM (53% and 73%, respectively), followed by GLUT3 (41% and 48%, respectively), GLUT4 (32% and 42%, respectively), and GLUT9 (26% and 34%, respectively) (Figure 3C). The IC_{50} values for compounds **5** and **30** in inhibiting GLUT1-mediated [^{3}H]-2-DG uptake were 5 μM and 2 μM, respectively (Figure 3D), similar to those determined for suppression of glucose uptake in LNCaP cells (Figure 3A).

The high antiproliferative potency of compound **30** is associated with its ability to elicit energy restriction-associated cellular responses. Examinations of the dose-dependent suppressive effects of compounds **28** and **30** versus compounds **1**, **2**, **4**, and **5** on the viability of LNCaP cells revealed differential antiproliferative potencies that paralleled the respective inhibitory activities in glucose uptake (Figure 4A). After 72 h of exposure in 10% fetal bovine serum (FBS) -containing medium, the IC_{50} values for individual compounds were **30**, 1.5 μM; **28**, 2.2 μM; **5**, 4.2 μM; **4**, 6 μM; **2**, 28 μM; **1**, 60 μM. It is noteworthy that despite the high potency of the optimal agent compound **30** in suppressing the viability of LNCaP cells, normal human prostate epithelial cells (PrECs) and human mammary epithelial cells (HMECs) were resistant to the cytotoxic effect of compound **30** even at 10 μM (Figure 4B).

This drug-induced cell death was, at least in part, attributable to apoptosis, as evidenced by a dose-dependent increase in poly(ADP-ribose) polymerase (PARP) cleavage in response to compound **30** (Figure 4C). Equally important, compound **30** shared the reported activities of compound **4**, 2-DG, and glucose starvation in eliciting energy restriction-associated cellular responses in LNCaP cells, including β-TrCP-facilitated protein degradation, adenosine monophosphate-activated protein kinase (AMPK) activation, and endoplasmic reticulum (ER) stress.[30,38] Western blot analysis indicates that compound **30** dose-dependently increased β-TrCP expression, leading to the downregulated expression of its substrates cyclin D1 and Sp1, as well as the Sp1 target AR (Figure 4C). Furthermore, as AMPK negatively regulates the activation status of mammalian homologue of target of rapamycin (mTOR) and p70S6K signaling,[39] the drug-facilitated increases in AMPK phosphorylation

dx.doi.org/10.1021/jm300015m | J. Med. Chem. 2012, 55, 3827−3836

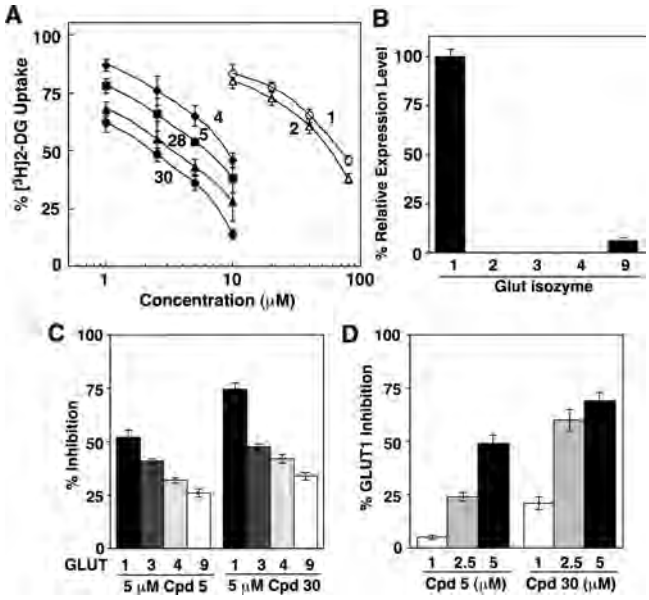

Figure 3. (A) Dose-dependent inhibitory effects of compounds **1**, **2**, **4**, **5**, **28**, and **30** on the uptake of [^{3}H]-2-DG into LNCaP cells in Krebs–Ringer phosphate buffer at 37 °C after 30 min of drug treatment. Points, mean; bars, SD (N = 3). (B) Quantitative real-time PCR analysis of the differential expression of GLUT1–4 and GLUT9 in LNCaP cells. Column, mean; bars, SD (N = 3). (C) Suppressive effects of compounds **5** and **30**, each at 5 μM, on [^{3}H]-2-DG uptake into LNCaP cells overexpressing GLUT1, GLUT3, GLUT4, or GLUT9. The analysis was carried out in Krebs–Ringer phosphate buffer at 37 °C after 30 min of drug treatment. Column, mean; bars, SD (N = 3). (D) Dose-dependent suppressive effects of compound **5** and **30** on [^{3}H]-2-DG uptake into LNCaP cells overexpressing GLUT1. Column, mean; bars, SD (N = 3).

was accompanied by concomitant decreases in the levels of p-mTOR and p-p70S6K. Compound **30**-induced ER stress was manifested by increased expression of two ER stress markers, glucose-regulated protein (GRP) 78 and growth arrest- and DNA damage-inducible gene (GADD) 153. Moreover, reminiscent of the demonstrated effect of compound **4** on the epigenetic activation of KLF6,[38] compound **30** increased the expression of this tumor suppressor protein in a dose-dependent manner.

Modeling Analysis of Ligand Binding. We also performed modeling analysis to envisage the mode of ligand binding using the homology-modeled structure of the human GLUT1 protein [Protein Data Bank (PDB) code 1SUK], which was developed by use of glycerol phosphate transporter as a template.[40] Blind docking simulations revealed that compound **30** and glucose bound to distinct sites in GLUT1's intermembrane channel for glucose passage (Figure 5A, left panel). While the glucose recognition site was located near the channel opening, compound **30** bound to the central segment of the channel. Docking analysis indicates that compound **30** interacted with the putative binding site through electrostatic and $\pi-\pi$ stacking interactions with Tyr^{28}, Arg^{126}, Thr^{137}, His^{160}, and Gln^{282}, as depicted in the close-up view (Figure 5A, right panel).

As compound **30** exhibits a calculated pK_a value of 8.0, the deprotonated form accounts for 13% of the total population of molecules in a physiological environment of pH 7.2. Therefore, we conducted another series of docking simulations to gain a better understanding of the interactions between the phenoxide and GLUT1's binding pocket. Compared to that shown in Figure 5A, the deprotonated form of compound **30** adopted a different mode of ligand binding such that the phenoxide moiety lay in close proximity to Arg^{126} to mediate ionic/hydrophilic interactions with its guanidine side chain (Figure 5B). Moreover, the amino hydrogen on the Trp^{412} side chain interacted with the sulfur atom and the carbonyl oxygen atom of the thiazolidinedione ring of compound **30**. In spite of the slightly upward shift in this binding mode, the $\pi-\pi$ interaction with Tyr^{28} and the electrostatic interaction of the terminal -CF_3 groups with His^{160} and Thr^{137} were maintained.

DISCUSSION

In the course of malignant transformation, tumor cells gain growth advantage by increasing glucose consumption through aerobic glycolysis.[1−4] This reprogramming of energy metabolism is manifested by increased glucose uptake through the upregulation of glucose transporters, especially GLUT1. In this study, we report the use of thiazolidinediones as a scaffold to develop a novel class of glucose transporter inhibitors. The optimal agent, compound **30**, exhibited high potency in suppressing the [^{3}H]-2-DG uptake and viability of LNCaP cells, with IC_{50} values of 2.5 μM and 1.5 μM, respectively, which represents a 40-fold improvement over that of compound **1**. Equally important, compound **30** exhibited no appreciable cytotoxicity in PrECs and HMECs, indicating the ability to discriminate between malignant and normal epithelial cells. Among the four GLUT isoforms examined, compound **30** preferentially inhibited GLUT1-mediated [^{3}H]-2-DG uptake with IC_{50} of 2 μM versus that of $\geq$5 μM for GLUT3, GLUT4, and GLUT9. The effectiveness of compound **30** in GLUT1 inhibition underlies its high potency in triggering energy restriction-associated cellular responses in LNCaP cells, leading to changes in the functional status of an array of signaling proteins governing cell cycle progression and apoptosis (Figure 6).

Docking modeling analysis suggests that the inhibitory effect of compound **30** on glucose entry is attributable to its ability to bind to the GLUT1 channel at a site distinct from that of glucose. This docking analysis provides a structural basis to account for the subtle structure–activity relationship among various derivatives of compound **5**. For example, compounds **28**–**30** exhibited higher potencies than compound **5** in GLUT1 inhibition, in part due to the additional electrostatic interactions of the two terminal -CF_3 functions with His^{160} and Thr^{137}. Similarly, relative to compounds **28** and **29**, the -CH_3 substituent on the tertiary carbon of compound **30** might have a steric effect on the configuration the two -CF_3 functions to allow closer interactions with His^{160} and Thr^{137} for tighter binding. Also noteworthy is the role of the -CF_3 function on the phenyl ring in mediating electrostatic interactions with Arg^{126}, which might account for the loss of glucose uptake inhibitory activity when this electronegative moiety in compound **5** was replaced by -CH_3 (compound **12**) or -NH_2 (compound **14**).

CONCLUSION

Data from this and other laboratories have demonstrated that targeting aerobic glycolysis via the inhibition of glucose transporters represents a therapeutically relevant strategy for cancer treatment. In light of the high potency of compound **30** in suppressing glucose uptake, it serves as a useful agent to shed light onto the signaling pathways, at both cellular and epigenetic levels, by which caloric restriction induces cancer cell

dx.doi.org/10.1021/jm300015m | J. Med. Chem. 2012, 55, 3827–3836

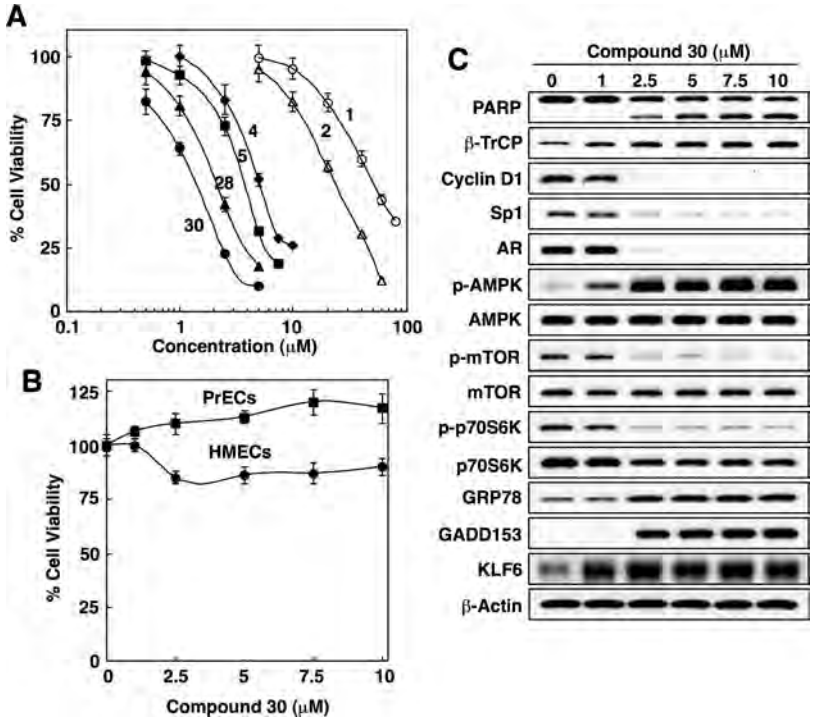

Figure 4. (A) Dose-dependent suppressive effects of compounds **1**, **2**, **4**, **5**, **28**, and **30** on the viability of LNCaP cells by MTT assays in 10% FBS-containing RPMI 1640 medium after 72 h of drug treatment. Points, mean; bars, SD ($N = 6$). (B) Dose-dependent effect of compound **30** on the viability of normal prostate epithelial cells (PrECs) and human mammary epithelial cells (HMECs) after 72 h of treatment. Points, mean; bars, SD ($N = 6$). (C) Western blot analysis of the dose-dependent effects of compound **30** on markers associated with apoptosis (PARP cleavage), β-TrCP-mediated protein degradation (β-TrCP, cyclin D1, Sp1, and AR), AMPK activation (p-AMPK, p-mTOR, and p-p706SK), ER stress (GRP78 and GADD153), and epigenetic activation of KLF6.

death through apoptosis and autophagy. From a translational perspective, research aimed at understanding these underlying mechanisms will help foster novel strategies for using this potent glucose transporter inhibitor, alone or in combination, in cancer therapy, which is currently underway.

EXPERIMENTAL SECTION

Unless otherwise indicated, all anhydrous solvents and chemical reagents were purchased at the highest grade available from Sigma–Aldrich (St. Louis, MO) and used without further purification. Flash column chromatography was performed with silica gel (230–400 mesh; Sorbent Technologies, Norcross, GA). Antibodies against various proteins were obtained from the following sources: Sp1, AR, cyclin D1, phospho-p70S6K (T389), p70S6K, GRP78, GADD153, and KLF6 were from Santa Cruz (Santa Cruz, CA); β-TrCP was from Invitrogen; phospho-Thr-172-AMPK, AMPK, phospho-Ser-2448-mTOR, mTOR, and PARP were from Cell Signaling Technology (Danvers, MA); and β-actin was from MP Biomedicals (Irvine, CA).

Nuclear magnetic resonance spectra (^{1}H NMR) were measured on a Bruker DPX 300 model spectrometer. Chemical shifts (δ) are reported in parts per million (ppm) relative to the tetramethylsilane (TMS) peak. Electrospray ionization mass spectrometric analyses were performed with a Micromass Q-Tof II high-resolution electrospray mass spectrometer. Melting points were determined by capillary melting point apparatus (Thomas-Hoover). The purity of all tested compounds was determined to be greater than 95% by elemental analyses, which were performed by Atlantic Microlab, Inc. (Norcross, GA) and were reported within 0.4% of calculated values. Compounds **2**–**4** were prepared as previously described.[32] General procedures for the synthesis of compounds **5**–**30** are depicted in Figure 1B.

Step a. To a mixture of individual alcohols (1.1 equiv), thiazolidine-2,4-dione (1.0 equiv), and triphenyl phosphine (3.5 equiv) in dry tetrahydrofuran (THF) was added diisopropyl azodicarboxylate (DIPAD; 3.3 equiv) dropwise at 0 °C. The reaction mixture was stirred at room temperature for 16 h, concentrated, dissolved in ethyl acetate, washed in tandem with water and brine, dried, and concentrated. The residue was purified by column chromatography (hexane/ethyl acetate) to afford N-substituted thiazolidine-2,4-diones (**i**–**viii**).

3-(2-Ethylbutyl)thiazolidine-2,4-dione ***(i)***. Light yellow oil; 81% yield. ^{1}H NMR ($CDCl_3$) δ 0.88 (t, J = 7.2 Hz, 6H), 1.28 (m, 4H), 1.70 (m, 1H), 3.51 (d, J = 7.2 Hz, 2H), 3.96 (s, 2H).

3-(2-Ethyl-2-methylbutyl)thiazolidine-2,4-dione ***(ii)***. Light yellow oil; 85% yield. ^{1}H NMR ($CDCl_3$) δ 0.81 (s, 3H), 0.86 (t, J = 7.2 Hz, 6H), 1.29 (m, 4H), 3.50 (s, 2H), 3.98 (s, 2H).

3-(1-Methylcyclobutylmethyl)thiazolidine-2,4-dione ***(iii)***. Light yellow oil; 80% yield. ^{1}H NMR ($CDCl_3$) δ 1.19 (s, 3H), 1.70 (m, 2H), 1.92 (m, 2H), 2.06 (m, 2H), 3.60 (s, 2H), 3.97 (s, 2H).

3-(1-Methylcyclopentylmethyl)thiazolidine-2,4-dione ***(iv)***. Light yellow oil; 81% yield. ^{1}H NMR ($CDCl_3$) δ 0.96 (s, 3H), 1.36 (m, 2H), 1.55 (m, 2H), 1.70 (m, 4H), 3.61 (s, 2H), 3.97 (s, 2H).

3-(1-Methylcycloheptylmethyl)thiazolidine-2,4-dione ***(v)***. Light yellow oil; 78% yield. ^{1}H NMR ($CDCl_3$) δ 0.93 (s, 3H), 1.36 (m, 2H), 1.54 (m, 10H), 3.60 (s, 2H), 3.97 (s, 2H).

3-[4,4,4-Trifluoro-2-(2,2,2-trifluoroethyl)butyl]thiazolidine-2,4-dione ***(vi)***. Light yellow oil; 82% yield. ^{1}H NMR ($CDCl_3$) δ 2.32 (m, 4H), 2.65 (m, 1H), 3.87 (d, J = 7.2 Hz, 2H), 4.05 (s, 2H).

3-[2,4,4,4-Tetrafluoro-2-(2,2,2-trifluoroethyl)butyl]thiazolidine-2,4-dione ***(vii)***. Light yellow oil; 81% yield. ^{1}H NMR ($CDCl_3$) δ 2.83–2.67 (m, 4H), 4.04 (d, J = 20.4 Hz, 2H), 4.07 (s, 2H).

3-[4,4,4-Trifluoro-2-methyl-2-(2,2,2-trifluoroethyl)butyl]-thiazolidine-2,4-dione ***(viii)***. Light yellow oil; 81% yield. ^{1}H NMR ($CDCl_3$) δ 1.19 (s, 3H), 2.47–2.25 (m, 4H), 3.77 (s, 2 H), 4.03 (s, 2H).

Step b. A mixture of individual di- and trisubstituted benzaldehydes (1.0 equiv), the corresponding N-substituted thiazolidine-2,4-dione (1.15 equiv), and a catalytic amount of piperidine in ethyl alcohol was refluxed until the reaction was completed, as monitored by thin-layer

dx.doi.org/10.1021/jm300015m | J. Med. Chem. 2012, 55, 3827–3836

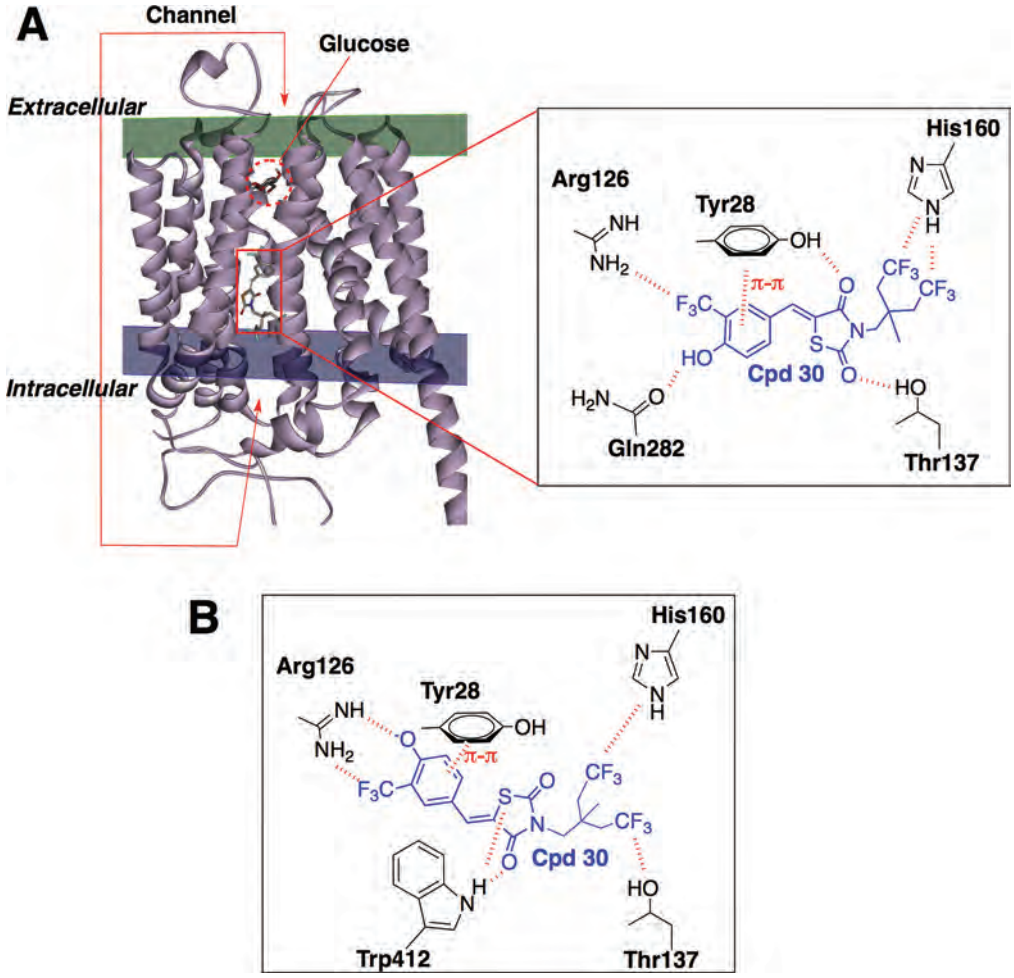

Figure 5. (A, left panel) Schematic representation of the predicted binding mode of compound **30** vis-à-vis that of glucose in the docking analysis of human GLUT1, showing that these two molecules bind to the transmembrane channel region at distinct sites. (A, right panel) Representation of the GLUT1 residues surrounding the docked compound **30**, showing the potential electrostatic and $\pi-\pi$ stacking interactions (dashed lines). (B) Representation of the GLUT1 residues surrounding the docked phenoxide species of compound **30**, showing the potential electrostatic and $\pi-\pi$ stacking interactions (dashed lines).

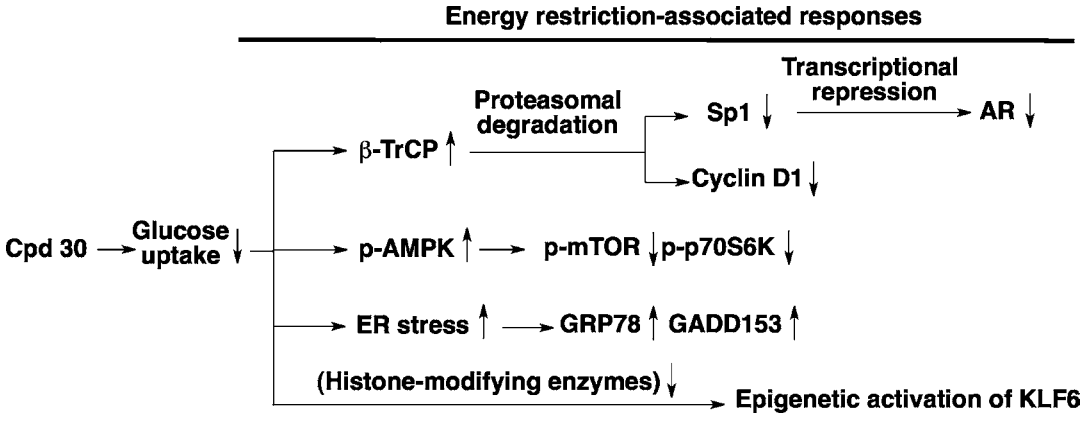

Figure 6. Schematic diagram depicting the mode of action of compound **30** in eliciting energy restriction-associated cellular responses.

chromatography (TLC), and concentrated. The residue was purified by column chromatography (hexane/ethyl acetate) to afford compounds **5**–**30**.

*3-(2-Ethylbutyl)-5-(4-hydroxy-3-trifluoromethylbenzylidene)-thiazolidine-2,4-dione (**5**).* White solid; 82% yield; mp 158–160 °C. ^{1}H NMR ($CDCl_3$) δ 0.92 (t, J = 7.2 Hz, 6H), 1.34 (m, 4H), 1.81 (m, 1H), 3.69 (d, J = 7.35 Hz, 2H), 6.19 (s, 1H), 7.10 (d, J = 8.58 Hz, 1H), 7.61 (d, J = 8.64 Hz, 1H), 7.70 (s, 1H), 7.83 (s, 1H). HRMS exact mass of $C_{17}H_{18}F_3NO_3S$ $(M + Na)^+$, 396.0857 amu; found, 396.0859 amu. Anal. Calcd, C 54.68, H 4.86, N 3.75; found, C 54.68, H 4.77, N 3.76.

*3-(2-Ethyl-2-methylbutyl)-5-(4-hydroxy-3-trifluoromethylbenzylidene)-thiazolidine-2,4-dione (**6**).* White solid; 78% yield. ^{1}H NMR ($CDCl_3$) δ 0.90 (m, 9H), 1.34 (m, 5H), 3.69 (s, 2H), 7.10 (d, J = 8.58 Hz, 1H), 7.55 (d, J = 8.64 Hz, 1H), 7.68 (s, 1H), 7.81 (s, 1H).

dx.doi.org/10.1021/jm300015m | J. Med. Chem. 2012, 55, 3827–3836

*5-(4-Hydroxy-3-trifluoromethylbenzylidene)-3-(1-methylcyclobutylmethyl)thiazolidine-2,4-dione (**7**).* White solid; 76% yield. ^{1}H NMR ($CDCl_3$) δ 1.19 (s, 3H), 1.86 (m, 4H), 2.08 (m, 2H), 3.78 (s, 2H), 6.21 (s, 1H), 7.11 (d, J = 6.6 Hz, 1H), 7.62 (d, *J* = 6.6 Hz, 1H), 7.71 (s, 1H), 7.85 (s, 1H).

*5-(4-Hydroxy-3-trifluoromethylbenzylidene)-3-(1-methylcyclopentylmethyl)thiazolidine-2,4-dione (**8**).* White solid; 80% yield. ^{1}H NMR ($CDCl_3$) δ 1.01 (s, 3H), 1.39 (m, 2H), 1.71 (m, 6H), 3.75 (s, 2H), 6.06 (s, 1H), 7.11 (d, *J* = 6.6 Hz, 1H), 7.62 (d, *J* = 6.0 Hz, 1H), 7.70 (s, 1H), 7.84 (s, 1H).

*5-(4-Hydroxy-3-trifluoromethylbenzylidene)-3-(1-methylcycloheptylmethyl)thiazolidine-2,4-dione (**9**).* White solid; 75% yield. ^{1}H NMR ($CDCl_3$) δ 0.93 (s, 3H), 1.38 (m, 2H), 1.54 (m, 10H), 3.75 (s, 2H), 6.08 (s, 1H), 7.11 (d, *J* = 6.6 Hz, 1H), 7.63 (d, *J* = 6.0 Hz, 1H), 7.70 (s, 1H), 7.86 (s, 1H).

*3-(2-Ethylbutyl)-5-(4-methoxy-3-trifluoromethylbenzylidene)-thiazolidine-2,4-dione (**10**).* White solid; 88% yield. ^{1}H NMR ($CDCl_3$) δ 0.92 (t, *J* = 7.2 Hz, 6H), 1.34 (m, 4H), 1.81 (m, 1H), 3.69 (d, *J* = 7.35 Hz, 2H), 4.02 (s, 3H), 7.10 (d, *J* = 8.58 Hz, 1H), 7.61 (d, *J* = 8.64 Hz, 1H), 7.70 (s, 1H), 7.83 (s, 1H).

*5-(3,4-Dihydroxybenzylidene)-3-(2-ethylbutyl)thiazolidine-2,4-dione (**11**).* Light brown solid; 80% yield. ^{1}H NMR ($CDCl_3$) δ 0.94 (t, *J* = 7.5 Hz, 6H), 1.34 (m, 4H), 1.81 (m, 1H), 3.68 (d, *J* = 7.2 Hz, 2H), 5.15 (s, 1H), 5.26 (s, 1H), 7.07 (d, *J* = 6.6 Hz, 1H), 7.10 (s, 1H), 7.18 (d, *J* = 8.58 Hz, 1H), 8.14 (s, 1H).

*3-(2-Ethylbutyl)-5-(4-hydroxy-3-methylbenzylidene)thiazolidine-2,4-dione (**12**).* White solid; 86% yield. ^{1}H NMR ($CDCl_3$) δ 0.92 (t, *J* = 7.2 Hz, 6H), 1.34 (m, 4H), 1.81 (m, 1H), 2.21 (s, 3H), 3.69 (d, *J* = 7.35 Hz, 2H), 6.19 (s, 1H), 7.10 (d, *J* = 8.58 Hz, 1H), 7.61 (d, *J* = 8.64 Hz, 1H), 7.70 (s, 1H), 7.83 (s, 1H).

*3-(2-Ethylbutyl)-5-(4-hydroxy-3-nitrobenzylidene)thiazolidine-2,4-dione (**13**).* Yellow solid; 73% yield. ^{1}H NMR ($CDCl_3$) δ 0.93 (t, *J* = 5.4 Hz, 6H), 1.35 (m, 4H), 1.80 (m, 1H), 3.67 (d, *J* = 5.4 Hz, 2H), 5.21 (s, 1H), 7.27 (d, *J* = 6.6 Hz, 1H), 7.32 (d, *J* = 6.8 Hz, 1H), 7.68 (s, 1H), 8.52 (s, 1H).

*5-(3-Amino-4-hydroxybenzylidene)-3-(2-ethylbutyl)thiazolidine-2,4-dione (**14**).* Brown solid; 68% yield. ^{1}H NMR ($CDCl_3$) δ 0.93 (t, *J* = 5.4 Hz, 6H), 1.35 (m, 4H), 1.80 (m, 1H), 2.26 (s, 2H), 3.67 (d, *J* = 5.4 Hz, 2H), 6.97 (d, *J* = 6.6 Hz, 1H), 7.22 (d, *J* = 6.8 Hz, 1H), 7.69 (br s, 1H), 7.87 (s, 1H), 8.76 (s, 1H).

*5-(2,4-Dihydroxybenzylidene)-3-(2-ethylbutyl)thiazolidine-2,4-dione (**15**).* Light yellow solid; 78% yield. ^{1}H NMR ($CDCl_3$) δ 0.93 (t, *J* = 7.5 Hz, 6H), 1.35 (m, 4H), 1.81 (m, 1H), 3.67 (d, *J* = 7.6 Hz, 2H), 6.52 (s, 1H), 6.60 (s, 1H), 6.76 (d, *J* = 6.6 Hz, 1H), 7.18 (d, *J* = 6.8 Hz, 1H), 7.54 (s, 1H), 8.14 (s, 1H).

*5-(5-Bromo-2-hydroxybenzylidene)-3-(2-ethylbutyl)thiazolidine-2,4-dione (**16**).* Light yellow solid; 84% yield. ^{1}H NMR ($CDCl_3$) δ 0.93 (t, *J* = 7.5 Hz, 6H), 1.35 (m, 4H), 1.81 (m, 1H), 3.67 (d, *J* = 7.6 Hz, 2H), 6.52 (s, 1H), 7.09 (d, *J* = 6.8 Hz, 1H), 7.21 (d, *J* = 6.6 Hz, 1H), 7.54 (s, 1H), 8.14 (s, 1H).

*3-(2-Ethylbutyl)-5-(3-fluoro-4-hydroxy-5-trifluoromethylbenzylidene)-thiazolidine-2,4-dione (**17**).* White solid; 81% yield. ^{1}H NMR ($CDCl_3$) δ 0.92 (t, *J* = 7.5 Hz, 6H), 1.34 (m, 4H), 1.80 (m, 1H), 3.68 (d, *J* = 7.2 Hz, 2H), 6.35 (br s, 1H), 7.46 (d, *J* = 10.8 Hz, 1H), 7.52 (s, 1H), 7.76 (s, 1H).

*3-(2-Ethylbutyl)-5-(3-bromo-4-hydroxy-5-trifluoromethylbenzylidene)-thiazolidine-2,4-dione (**18**).* Light yellow solid; 79% yield. ^{1}H NMR ($CDCl_3$) δ 0.91 (t, *J* = 7.5 Hz, 6H), 1.34 (m, 4H), 1.84 (m, 1H), 3.67 (d, *J* = 6.0 Hz, 2H), 6.05 (br s, 1H), 7.68 (d, *J* = 10.8 Hz, 1H), 7.76 (s, 1H), 7.82 (s, 1H).

*5-(3,4-Dihydroxy-5-trifluoromethylbenzylidene)-3-(2-ethylbutyl)-thiazolidine-2,4-dione (**19**).* Light brown solid; 76% yield. ^{1}H NMR ($CDCl_3$) δ 0.91 (t, *J* = 7.4 Hz, 6H), 1.34 (m, 4H), 1.84 (m, 1H), 3.67 (d, *J* = 8.4 Hz, 2H), 6.48 (br s, 1H), 6.53 (s, 1H), 7.18 (s, 1H), 7.35 (s, 1H), 7.81 (s, 1H).

*3-(2-Ethylbutyl)-5-(4-hydroxy-3-methoxy-5-trifluoromethylbenzylidene)-thiazolidine-2,4-dione (**20**).* White solid; 86% yield. ^{1}H NMR ($CDCl_3$) δ 0.91 (t, *J* = 7.4 Hz, 6H), 1.34 (m, 4H), 1.84 (m, 1H), 3.67 (d, *J* = 8.4 Hz, 2H), 4.05 (s, 3H), 6.48 (br s, 1H), 7.16 (s, 1H), 7.35 (s, 1H), 7.81 (s, 1H).

*3-(2-Ethylbutyl)-5-(4-hydroxy-3-nitro-5-trifluoromethylbenzylidene)-thiazolidine-2,4-dione (**21**).* Yellow solid; 75% yield. ^{1}H NMR ($CDCl_3$) δ0.91 (t, *J* = 7.4 Hz, 6H), 1.30 (m, 4H), 1.84 (m, 1H), 3.70 (d, *J* = 7.5 Hz, 2H), 5.69 (s, 1H), 7.81 (s, 1H), 8.05 (s, 1H), 8.48 (s, 1H).

*5-(3-Amino-4-hydroxy-5-trifluoromethylbenzylidene)-3-(2-ethylbutyl)thiazolidine-2,4-dione (**22**).* Brown solid; 70% yield. ^{1}H NMR ($CDCl_3$) δ 0.93 (t, *J* = 7.5 Hz, 6H), 1.35 (m, 4H), 1.81 (m, 1H), 2.36 (s, 2H), 3.67 (d, *J* = 7.2 Hz, 2H), 7.36 (s, 1H), 7.57 (s, 1H), 7.74 (s, 1H), 8.53 (s, 1H).

*5-(2,4-Dihydroxy-5-trifluoromethylbenzylidene)-3-(2-ethylbutyl)-thiazolidine-2,4-dione (**23**).* Off-white solid; 78% yield. ^{1}H NMR ($CDCl_3$) δ 0.93 (t, *J* = 7.5 Hz, 6H), 1.35 (m, 4H), 1.81 (m, 1H), 3.68 (d, *J* = 5.4 Hz, 2H), 6.32 (s, 1H), 6.56 (s, 1H), 7.20 (s, 1H), 7.68 (s, 1H), 8.26 (s, 1H).

*5-(2,3-Dihydroxy-5-trifluoromethylbenzylidene)-3-(2-ethylbutyl)-thiazolidine-2,4-dione (**24**).* Light brown solid; 74% yield. ^{1}H NMR ($CDCl_3$) δ 0.92 (t, *J* = 7.5 Hz, 6H), 1.33 (m, 4H), 1.79 (m, 1H), 3.67 (d, *J* = 7.2 Hz, 2H), 6.26 (br s, 2H), 7.21 (s, 1H), 7.30 (s, 1H), 8.12 (s, 1H).

*5-(5-Bromo-2,4-dihydroxybenzylidene)-3-(2-ethylbutyl)-thiazolidine-2,4-dione (**25**).* Off-white solid; 76% yield. ^{1}H NMR ($CDCl_3$) δ 0.93 (t, *J* = 7.5 Hz, 6H), 1.35 (m, 4H), 1.81 (m, 1H), 3.67 (d, *J* = 7.6 Hz, 2H), 6.52 (s, 1H), 6.66 (s, 1H), 6.76 (s, 1H), 7.54 (s, 1H), 8.14 (s, 1H).

*5-(5-Bromo-2,3-dihydroxybenzylidene)-3-(2-ethylbutyl)-thiazolidine-2,4-dione (**26**).* Light brown solid; 72% yield. ^{1}H NMR ($CDCl_3$) δ 0.94 (t, *J* = 7.5 Hz, 6H), 1.34 (m, 4H), 1.81 (m, 1H), 3.68 (d, *J* = 7.2 Hz, 2H), 5.55 (s, 1H), 5.90 (s, 1H), 7.07 (s, 1H), 7.17 (s, 1H), 8.14 (s, 1H).

*5-(2-Bromo-3,4-dihydroxybenzylidene)-3-(2-ethylbutyl)-thiazolidine-2,4-dione (**27**).* Light yellow solid; 83% yield. ^{1}H NMR ($CDCl_3$) δ 0.94 (t, *J* = 7.5 Hz, 6H), 1.34 (m, 4H), 1.81 (m, 1H), 3.68 (d, *J* = 7.5 Hz, 2H), 5.85 (s, 1H), 6.07 (s, 1H), 7.02 (d, *J* = 8.7 Hz, 1H), 7.11 (d, *J* = 8.4 Hz, 1H), 8.12 (s, 1H).

*5-(4-Hydroxy-3-trifluoromethylbenzylidene)-3-[4,4,4-trifluoro-2-(2,2,2-trifluoro-ethyl)butyl]thiazolidine-2,4-dione (**28**).* Off-white solid; 80% yield; mp 165−167 °C, ^{1}H NMR ($CDCl_3$) δ 2.31 (m, 4H), 2.68 (m, 1H), 3.86 (d, *J* = 7.4 Hz, 2H), 5.99 (br s, 1H), 7.10 (d, *J* = 8.1 Hz, 1H), 7.63 (d, *J* = 8.2 Hz, 1H), 7.72 (s, 1H), 7.89 (s, 1H). HRMS exact mass of $C_{17}H_{12}F_9NO_3S$ $(M + Na)^+$, 504.0292 amu; found, 504.0298 amu. Anal. Calcd, C 42.42, H 2.51, N 2.91; found, C 42.35, H 2.49, N 2.99.

*5-(4-Hydroxy-3-trifluoromethylbenzylidene)-3-[2,4,4,4-tetrafluoro-2-(2,2,2-trifluoroethyl)butyl]thiazolidine-2,4-dione (**29**).* White solid; 76% yield; mp 173−176 °C. ^{1}H NMR (DMSO-d_6) δ 3.00−2.82 (m, 2H), 3.30−3.10 (m, 2H), 4.09 (d, *J* = 21 Hz, 2H), 7.21 (d, *J* = 9 Hz, 1H), 7.73 (d, *J* = 9 Hz, 1H), 7.87 (s, 1H), 7.96 (s, 1H), 11.50 (br s, 1H). HRMS exact mass of $C_{17}H_{11}F_{10}NO_3S$ $(M + Na)^+$, 522.0198 amu; found, 522.0199 amu. Anal. Calcd, C 40.89, H 2.22, N 2.81; found, C 41.11, H 2.57, N 2.64.

*5-(4-Hydroxy-3-trifluoromethylbenzylidene)-3-[4,4,4-trifluoro-2-methyl-2-(2,2,2-trifluoroethyl)butyl]thiazolidine-2,4-dione (**30**).* Off-white solid; 86% yield; mp 164−166 °C. ^{1}H NMR (DMSO-d_6) δ 1.17 (s, 3H), 2.58−2.50 (m, 4H), 3.76 (s, 2H), 7.21 (d, *J* = 9 Hz, 1H), 7.74 (d, *J* = 9 Hz, 1H), 7.87 (s, 1H), 7.95 (s, 1H), 11.54 (br s, 1H). HRMS exact mass of $C_{18}H_{14}F_9NO_3S$ $(M + Na)^+$, 518.0448 amu; found, 518.0441 amu. Anal. Calcd, C 43.64, H 2.85, N 2.83; found, C 43.64, H 2.79, N 2.82.

Cells and Cell Culture. LNCaP prostate cancer cells were obtained from the American Type Culture Collection (Manassas, VA). Cells were maintained in 10% FBS-supplemented RPMI 1640 medium (Invitrogen). Normal HMECs and PrECs were obtained from Lonza (Walkersville, MD) and were maintained in mammary epithelial cell growth medium (MEGM) and prostate epithelial cell growth medium (PrEGM) (Lonza, Walkersville, MD), respectively.

Glucose Uptake Assay. LNCaP cells were seeded in six-well plates (3×10^5 cells/well) for 24 h. Cells were washed twice with Krebs−Ringer phosphate buffer (126 mM NaCl, 2.5 mM KCl, 25 mM $NaHCO_3$, 1.2 mM NaH_2PO_4, 1.2 mM $MgCl_2$, and 2.5 mM $CaCl_2$, pH 7.4) and were then treated with individual agents in Krebs−Ringer phosphate buffer. After 0.5 h, glucose uptake was initiated by adding

1 mL pf Krebs−Ringer buffer containing 1 mCi/mL [^{3}H]-2-DG (PerkinElmer Life Science) and 100 mM nonradioactive 2-DG and was terminated by washing with cold phosphate-buffered saline (PBS). The cells were lysed in 500 mL of lysis buffer (10 mM Tris-HCl, pH 8.0, and 0.1% sodium dodecyl sulfate, SDS) and aliquots were taken for measurement of radioactivity on a scintillation counter (Beckman LS6500).

Cell Viability Assay. Cell viability was determined by the 3-(4,5-dimethylthiazol-2-yl)-2,5-diphenyltetrazolium bromide (MTT) assay. Cancer cells were seeded at 5000 cells/well and normal cells were seeded at 8000 cells/well in 96-well plates, and the plates were incubated in 10% FBS-supplemented medium for 24 h. Cells were then treated with individual agents for 72 h. Drug-containing medium was replaced with medium containing MTT (0.5 mg/mL), followed by incubation at 37 °C for 1 h. After removal of medium, the reduced MTT dye in each well was solubilized in 100 μL of dimethyl sulfoxide (DMSO) and absorbance at 570 nm was measured.

Plasmid Construction, Transient Transfection, and Immunoblotting. The full-length GLUT1, GLUT4, and GLUT9 ORF cDNA clones were purchased from Addgene (Cambridge, MA) and GLUT3 ORF cDNA was purchased from Origene Technologies (Rockville, MD). GLUT1, GLUT3, and GLUT9 were subcloned into the *Hin*dIII/*Sal*I sites and GLUT4 was subcloned into the *Eco*RI/*Sal*I sites of the pEGFP-N2 expression vector (Clontech, Palo Alto, CA). Transfections were performed by electroporation with Nucleofector kit R of the Amaxa Nucleofector system (Lonza, Walkersville, MD) according to the manufacturer's protocol. Immunoblotting was performed with cell lysates harvested with SDS lysis buffer (1% SDS, 50 mM Tris-HCl, pH 8.0, and 10 mM ethylenediaminetetraacetic acid, EDTA) containing protease inhibitor cocktail (Sigma) and phosphatase inhibitor, electrophoresed in SDS−8−12% polyacrylamide gels, and then transferred onto nitrocellulose membranes. After being blotted in 5% nonfat dry milk, the membranes were incubated with primary antibodies at 1:1000 dilution in Tris-buffered saline (TBS)−Tween 20 overnight at 4 °C and then with secondary antibodies conjugated with horseradish peroxidase at 1:5000 dilution in TBS−Tween 20 for 1 h at room temperature. Protein bands were visualized on X-ray film via an enhanced chemiluminescence system.

Quantitative Real-Time Polymerase Chain Reaction (PCR). Total RNA was isolated and reversed-transcribed to cDNA by use of TRIzol reagent (Invitrogen) and the iScript cDNA synthesis kit (Bio-Rad Laboratories, Hercules, CA), respectively, according to the vendors' instructions. Real-time PCR was carried out in the Bio-Rad CFX96 real-time PCR detection system with iQ SYBR green supermix (Bio-Rad). The sequences of the primers used were as follows: GLUT1 forward, 5′-GCGGAATTCAATGCTGATGA-3′, GLUT1 reverse, 5′-CGAAGATGCTCGTGGAGTAA-3′; GLUT2 forward, 5′- ATGTCAGTGGGACTTGTGCTGC-3′, GLUT2 reverse, 5′- CACAGTCTCTGTAGCTCCTAG-3′; GLUT3 forward, 5′- TTAAAGGATAACTATAATGG-3′, GLUT3 reverse, 5′- GACATTGGTGGTGGTCTCCT-3′; GLUT4 forward, 5′- CAGAAGGTGATTGAACAGAG-3′, GLUT4 reverse, 5′- AGATGCTGGTCGAATAATAG-3′; GLUT9 forward, 5′-GC-TCTTGGAGAAGCACAACGAG-3′, GLUT9 reverse, 5′- AAAGTTGGAGAGCCAGTTGA-3′. Relative gene expression was normalized to that of 18s rRNA and calculated by using the published $2^{-\Delta\Delta Ct}$ method.[41]

Molecular Docking Experiment. Docking was carried out with AutoDock 4.2. The molecular structure of compound **30** was prepared by the SYBYL 8.1 program (Tripos International, St. Louis, MO) via MMFF94 molecular mechanics force-field calculation. The coordinates for GLUT1 (PDB code 1SUK) were obtained by homology modeling based on glycerol phosphate transporter as a template.[40] The initial blind docking used a grid box of 100 × 100 × 126 points in three dimensions with a spacing of 0.6 Å centered on the whole GLUT1 and indicated that the major interacting region was located in the channel. Accordingly, further docking simulations, centered at the channel with a grid box of 70 × 70 × 92 points in three dimensions with a spacing of 0.375 Å, were applied to explore the binding behavior.

Calculation of pK_a. Compounds **5**, **17**−**22**, and **28**−**30** were retrieved from those optimized for docking modeling and the respective pK_a values were calculated by the Molecular Properties protocol in Discovery Studio 3.1 (Accelrys, San Diego, CA).

AUTHOR INFORMATION

Corresponding Author

*Phone 614-688-4008; fax 614-688-8556; e-mail chen.844@osu.edu.

Author Contributions

‡These authors made equal contributions to this work.

Notes

The authors declare no competing financial interest.

ACKNOWLEDGMENTS

This work was supported by National Institutes of Health Grant CA112250 and Department of Defense Prostate Cancer Research Program Grant W81XWH-09-0198 (to C.-S.C.) and by Ministry of Economic Affairs (Taiwan) Grant 99-EC-17-A-17-S1-152 (to C.-N.Y.).

ABBREVIATIONS

PPARγ, peroxisome proliferator-activated receptor γ; GLUT, glucose transporter; AR, androgen receptor; β-TrCP, β-transducin repeat-containing protein; 2-DG, 2-deoxyglucose; PrECs, prostate epithelial cells; HMECs, human mammary epithelial cells; PARP, poly(ADP-ribose) polymerase; AMPK, adenosine monophosphate-activated protein kinase; ER, endoplasmic reticulum; mTOR, mammalian homologue of target of rapamycin; GRP78, glucose-regulated protein 78; GADD153, growth arrest- and DNA damage-inducible gene 153; PDB, Protein Data Bank

REFERENCES

(1) Warburg, O. On the origin of cancer cells. *Science* **1956**, *123*, 309−314.

(2) Kroemer, G.; Pouyssegur, J. Tumor cell metabolism: cancer's Achilles' heel. *Cancer Cell* **2008**, *13*, 472−482.

(3) Vander Heiden, M. G.; Cantley, L. C.; Thompson, C. B. Understanding the Warburg effect: the metabolic requirements of cell proliferation. *Science* **2009**, *324*, 1029−1033.

(4) Kim, J. W.; Dang, C. V. Cancer's molecular sweet tooth and the Warburg effect. *Cancer Res.* **2006**, *66*, 8927−8930.

(5) Vander Heiden, M. G. Targeting cancer metabolism: a therapeutic window opens. *Nat. Rev. Drug Discovery* **2011**, *10*, 671−684.

(6) Gatenby, R. A.; Gillies, R. J. Why do cancers have high aerobic glycolysis? *Nat. Rev. Cancer* **2004**, *4*, 891−899.

(7) Kelloff, G. J.; Hoffman, J. M.; Johnson, B.; Scher, H. I.; Siegel, B. A.; Cheng, E. Y.; Cheson, B. D.; O'Shaughnessy, J.; Guyton, K. Z.; Mankoff, D. A.; Shankar, L.; Larson, S. M.; Sigman, C. C.; Schilsky, R. L.; Sullivan, D. C. Progress and promise of FDG-PET imaging for cancer patient management and oncologic drug development. *Clin. Cancer Res.* **2005**, *11*, 2785−2808.

(8) Macheda, M. L.; Rogers, S.; Best, J. D. Molecular and cellular regulation of glucose transporter (GLUT) proteins in cancer. *J. Cell. Physiol.* **2005**, *202*, 654−662.

(9) Calvo, M. B.; Figueroa, A.; Pulido, E. G.; Campelo, R. G.; Aparicio, L. A. Potential role of sugar transporters in cancer and their relationship with anticancer therapy. *Int. J. Endocrinol.* **2010**, 2010.

(10) Nishioka, T.; Oda, Y.; Seino, Y.; Yamamoto, T.; Inagaki, N.; Yano, H.; Imura, H.; Shigemoto, R.; Kikuchi, H. Distribution of the glucose transporters in human brain tumors. *Cancer Res.* **1992**, *52*, 3972−3979.

(11) Brown, R. S.; Wahl, R. L. Overexpression of Glut-1 glucose transporter in human breast cancer. An immunohistochemical study. *Cancer* **1993**, *72*, 2979−2985.

(12) Younes, M.; Brown, R. W.; Mody, D. R.; Fernandez, L.; Laucirica, R. GLUT1 expression in human breast carcinoma: correlation with known prognostic markers. *Anticancer Res.* **1995**, *15*, 2895−2898.
(13) Rudlowski, C.; Becker, A. J.; Schroder, W.; Rath, W.; Buttner, R.; Moser, M. GLUT1 messenger RNA and protein induction relates to the malignant transformation of cervical cancer. *Am. J. Clin. Pathol.* **2003**, *120*, 691−698.
(14) Haber, R. S.; Rathan, A.; Weiser, K. R.; Pritsker, A.; Itzkowitz, S. H.; Bodian, C.; Slater, G.; Weiss, A.; Burstein, D. E. GLUT1 glucose transporter expression in colorectal carcinoma: a marker for poor prognosis. *Cancer* **1998**, *83*, 34−40.
(15) Nagase, Y.; Takata, K.; Moriyama, N.; Aso, Y.; Murakami, T.; Hirano, H. Immunohistochemical localization of glucose transporters in human renal cell carcinoma. *J. Urol.* **1995**, *153*, 798−801.
(16) Younes, M.; Brown, R. W.; Stephenson, M.; Gondo, M.; Cagle, P. T. Overexpression of Glut1 and Glut3 in stage I nonsmall cell lung carcinoma is associated with poor survival. *Cancer* **1997**, *80*, 1046−51.
(17) Cantuaria, G.; Fagotti, A.; Ferrandina, G.; Magalhaes, A.; Nadji, M.; Angioli, R.; Penalver, M.; Mancuso, S.; Scambia, G. GLUT-1 expression in ovarian carcinoma: association with survival and response to chemotherapy. *Cancer* **2001**, *92*, 1144−1150.
(18) Stewart, G. D.; Gray, K.; Pennington, C. J.; Edwards, D. R.; Riddick, A. C.; Ross, J. A.; Habib, F. K. Analysis of hypoxia-associated gene expression in prostate cancer: lysyl oxidase and glucose transporter-1 expression correlate with Gleason score. *Oncol. Rep.* **2008**, *20*, 1561−1567.
(19) Haber, R. S.; Weiser, K. R.; Pritsker, A.; Reder, I.; Burstein, D. E. GLUT1 glucose transporter expression in benign and malignant thyroid nodules. *Thyroid* **1997**, *7*, 363−367.
(20) Baer, S. C.; Casaubon, L.; Younes, M. Expression of the human erythrocyte glucose transporter Glut1 in cutaneous neoplasia. *J. Am. Acad. Dermatol.* **1997**, *37*, 575−577.
(21) Schwartzenberg-Bar-Yoseph, F.; Armoni, M.; Karnieli, E. The tumor suppressor p53 down-regulates glucose transporters GLUT1 and GLUT4 gene expression. *Cancer Res.* **2004**, *64*, 2627−2633.
(22) Young, C. D.; Anderson, S. M. Sugar and fat - that's where it's at: metabolic changes in tumors. *Breast Cancer Res.* **2008**, *10*, 202.
(23) Airley, R. E.; Mobasheri, A. Hypoxic regulation of glucose transport, anaerobic metabolism and angiogenesis in cancer: novel pathways and targets for anticancer therapeutics. *Chemotherapy* **2007**, *53*, 233−256.
(24) Park, J. B. Inhibition of glucose and dehydroascorbic acid uptakes by resveratrol in human transformed myelocytic cells. *J. Nat. Prod.* **2001**, *64*, 381−384.
(25) Harmon, A. W.; Patel, Y. M. Naringenin inhibits glucose uptake in MCF-7 breast cancer cells: a mechanism for impaired cellular proliferation. *Breast Cancer Res. Treat.* **2004**, *85*, 103−110.
(26) Cao, X.; Fang, L.; Gibbs, S.; Huang, Y.; Dai, Z.; Wen, P.; Zheng, X.; Sadee, W.; Sun, D. Glucose uptake inhibitor sensitizes cancer cells to daunorubicin and overcomes drug resistance in hypoxia. *Cancer Chemother. Pharmacol.* **2007**, *59*, 495−505.
(27) Wood, T. E.; Dalili, S.; Simpson, C. D.; Hurren, R.; Mao, X.; Saiz, F. S.; Gronda, M.; Eberhard, Y.; Minden, M. D.; Bilan, P. J.; Klip, A.; Batey, R. A.; Schimmer, A. D. A novel inhibitor of glucose uptake sensitizes cells to FAS-induced cell death. *Mol. Cancer Ther.* **2008**, *7*, 3546−3555.
(28) Shanmugam, M.; McBrayer, S. K.; Qian, J.; Raikoff, K.; Avram, M. J.; Singhal, S.; Gandhi, V.; Schumacker, P. T.; Krett, N. L.; Rosen, S. T. Targeting glucose consumption and autophagy in myeloma with the novel nucleoside analogue 8-aminoadenosine. *J. Biol. Chem.* **2009**, *284*, 26816−26830.
(29) Chan, D. A.; Sutphin, P. D.; Nguyen, P.; Turcotte, S.; Lai, E. W.; Banh, A.; Reynolds, G. E.; Chi, J. T.; Wu, J.; Solow-Cordero, D. E.; Bonnet, M.; Flanagan, J. U.; Bouley, D. M.; Graves, E. E.; Denny, W. A.; Hay, M. P.; Giaccia, A. J. Targeting GLUT1 and the Warburg effect in renal cell carcinoma by chemical synthetic lethality. *Sci. Transl. Med.* **2011**, *3*, 94ra70.
(30) Wei, S.; Kulp, S. K.; Chen, C. S. Energy restriction as an antitumor target of thiazolidinediones. *J. Biol. Chem.* **2010**, *285*, 9780−9791.
(31) Wei, S.; Chuang, H. C.; Tsai, W. C.; Yang, H. C.; Ho, S. R.; Paterson, A. J.; Kulp, S. K.; Chen, C. S. Thiazolidinediones mimic glucose starvation in facilitating Sp1 degradation through the up-regulation of beta-transducin repeat-containing protein. *Mol. Pharmacol.* **2009**, *76*, 47−57.
(32) Yang, J.; Wei, S.; Wang, D. S.; Wang, Y. C.; Kulp, S. K.; Chen, C. S. Pharmacological exploitation of the peroxisome proliferator-activated receptor gamma agonist ciglitazone to develop a novel class of androgen receptor-ablative agents. *J. Med. Chem.* **2008**, *51*, 2100−2107.
(33) Yang, C. C.; Wang, Y. C.; Wei, S.; Lin, L. F.; Chen, C. S.; Lee, C. C.; Lin, C. C. Peroxisome proliferator-activated receptor gamma-independent suppression of androgen receptor expression by troglitazone mechanism and pharmacologic exploitation. *Cancer Res.* **2007**, *67*, 3229−3238.
(34) Muller, K.; Faeh, C.; Diederich, F. Fluorine in pharmaceuticals: looking beyond intuition. *Science* **2007**, *317*, 1881−1886.
(35) Hagmann, W. K. The many roles for fluorine in medicinal chemistry. *J. Med. Chem.* **2008**, *51*, 4359−4369.
(36) Purser, S.; Moore, P. R.; Swallow, S.; Gouverneur, V. Fluorine in medicinal chemistry. *Chem. Soc. Rev.* **2008**, *37*, 320−330.
(37) Joost, H. G.; Thorens, B. The extended GLUT-family of sugar/polyol transport facilitators: nomenclature, sequence characteristics, and potential function of its novel members (review). *Mol. Membr. Biol.* **2001**, *18*, 247−256.
(38) Chen, C. H.; Huang, P. H.; Chu, P. C.; Chen, M. C.; Chou, C. C.; Wang, D.; Kulp, S. K.; Teng, C. M.; Wang, Q.; Chen, C. S. Energy restriction-mimetic agents induce apoptosis in prostate cancer cells in part through epigenetic activation of KLF6 tumor suppressor gene expression. *J. Biol. Chem.* **2011**, *286*, 9968−9976.
(39) Inoki, K.; Zhu, T.; Guan, K. L. TSC2 mediates cellular energy response to control cell growth and survival. *Cell* **2003**, *115*, 577−590.
(40) Salas-Burgos, A.; Iserovich, P.; Zuniga, F.; Vera, J. C.; Fischbarg, J. Predicting the three-dimensional structure of the human facilitative glucose transporter GLUT1 by a novel evolutionary homology strategy: insights on the molecular mechanism of substrate migration, and binding sites for glucose and inhibitory molecules. *Biophys. J.* **2004**, *87*, 2990−2999.
(41) Livak, K. J.; Schmittgen, T. D. Analysis of relative gene expression data using real-time quantitative PCR and the 2(-ΔΔC(T)) method. *Methods* **2001**, *25*, 402−408.

Cancer Prevention Research

Suppression of Prostate Epithelial Proliferation and Intraprostatic Progrowth Signaling in Transgenic Mice by a New Energy Restriction-Mimetic Agent

Lisa D. Berman-Booty, Po-Chen Chu, Jennifer M. Thomas-Ahner, et al.

Cancer Prev Res 2013;6:232-241. Published OnlineFirst December 28, 2012.

Published OnlineFirst December 28, 2012; DOI:10.1158/1940-6207.CAPR-12-0057

Research Article

Cancer Prevention Research

Suppression of Prostate Epithelial Proliferation and Intraprostatic Progrowth Signaling in Transgenic Mice by a New Energy Restriction-Mimetic Agent

Lisa D. Berman-Booty[1,2], Po-Chen Chu[1], Jennifer M. Thomas-Ahner[3], Brad Bolon[2,4], Dasheng Wang[1], Tiffany Yang[1], Steven K. Clinton[3], Samuel K. Kulp[1], and Ching-Shih Chen[1,5]

Abstract

Cells undergoing malignant transformation often exhibit a shift in cellular metabolism from oxidative phosphorylation to glycolysis. This glycolytic shift, called the Warburg effect, provides a mechanistic basis for targeting glycolysis to suppress carcinogenesis through the use of dietary caloric restriction and energy restriction-mimetic agents (ERMA). We recently reported the development of a novel class of ERMAs that exhibits high potency in eliciting starvation-associated cellular responses and epigenetic changes in cancer cells though glucose uptake inhibition. The lead ERMA in this class, OSU-CG5, decreases the production of ATP and NADH in LNCaP prostate cancer cells. In this study, we examined the effect of OSU-CG5 on the severity of preneoplastic lesions in male transgenic adenocarcinoma of the mouse prostate (TRAMP) mice. Daily oral treatment with OSU-CG5 at 100 mg/kg from 6 to 10 weeks of age resulted in a statistically significant decrease in the weight of urogenital tract and microdissected dorsal, lateral, and anterior prostatic lobes relative to vehicle controls. The suppressive effect of OSU-CG5 was evidenced by marked decreases in Ki67 immunostaining and proliferating cell nuclear antigen (PCNA) expression in the prostate. OSU-CG5 treatment was not associated with evidence of systemic toxicity. Microarray analysis indicated a central role for Akt, and Western blot analysis showed reduced phosphorylation and/or expression levels of Akt, Src, androgen receptor, and insulin-like growth factor-1 receptor in prostate lobes. These findings support further investigation of OSU-CG5 as a potential chemopreventive agent. *Cancer Prev Res; 6(3); 232–41. ©2012 AACR.*

Introduction

In 1924, Otto Warburg reported that cancer cells preferentially metabolize glucose via glycolysis to lactate, even in the presence of adequate oxygen. This phenomenon, termed "aerobic glycolysis," results in the net production of 2 adenosine triphosphate (ATP) molecules per molecule of glucose, in contrast to the approximately 36 molecules produced per molecule of glucose directed into the tricarboxylic acid cycle and used for oxidative phosphorylation (1–7). The metabolic shift toward aerobic glycolysis provides cancer cells with growth advantages (3–7). For example, limiting ATP production to the glycolytic pathway permits diversion of intermediates into anabolic pathways to synthesize the nucleic acids, proteins, and fatty acids needed for extensive cell proliferation (3–7).

Although this metabolic adaptation provides growth advantages to cancer cells, it also presents opportunities to exploit the peculiarities of tumor cell metabolism for therapeutic purposes. The proof-of-concept for targeting energy metabolism for cancer chemoprevention is provided by the fact that inhibition of glycolysis through dietary caloric restriction or treatment with energy restriction-mimetic agents (ERMA) such as 2-deoxyglucose (2-DG) suppresses the growth of tumor xenografts and carcinogenesis in various animal models (8–12). To date, most of the animal studies that have assessed the anti-cancer effects of ERMAs have focused on late stages of cancer development or tumor growth, whereas their effects on the development and progression of preneoplastic conditions, such as prostatic intraepithelial neoplasia (PIN), remain largely undefined.

The prostates of transgenic adenocarcinoma of the mouse prostate (TRAMP) mice undergo a series of pathologic changes that mirror those which occur in men (13–15). Lesions develop progressively following the testosterone-dependent activation of the rat probasin promoter and

Authors' Affiliations: [1]Division of Medicinal Chemistry, College of Pharmacy; [2]Department of Veterinary Biosciences, College of Veterinary Medicine; [3]Division of Medical Oncology, Department of Internal Medicine, College of Medicine; [4]Comparative Pathology & Mouse Phenotyping Shared Resource, Comprehensive Cancer Center, The Ohio State University, Columbus, Ohio; and [5]Institute of Basic Medical Sciences, National Cheng-Kung University, Tainan, Taiwan

Note: Supplementary data for this article are available at Cancer Prevention Research Online (http://cancerprevres.aacrjournals.org/).

Corresponding Author: Ching-Shih Chen, College of Pharmacy, 336 Parks Hall, The Ohio State University, 500 West 12th Avenue, Columbus, OH 43210. Phone: 614-688-4008; Fax: 614-688-8556; E-mail: chen.844@osu.edu

doi: 10.1158/1940-6207.CAPR-12-0057

Published OnlineFirst December 28, 2012; DOI:10.1158/1940-6207.CAPR-12-0057

expression of the SV40 large and small T antigens (T Ag) in the prostatic epithelium. Transgene expression results in inhibition of p53 and Rb tumor suppressors and development of prostate tumors (14–17). Prostates from 6-week-old intact TRAMP mice typically exhibit varying degrees of PIN with the development of well-differentiated adenocarcinomas by approximately 18 weeks of age (13, 14, 16, 18) and the emergence of poorly differentiated cancers with neuroendocrine differentiation at later time points. Although controversy exists about the histogenesis of the poorly differentiated carcinomas, that is, whether they originate from epithelial cells within PIN lesions or from a distinct neuroendocrine stem cell population (19, 20), this has little relevance to studies that focus on the PIN lesions in lieu of carcinomas.

Prostate epithelial proliferation in the PIN lesions of TRAMP mice has been shown to be amenable to modulation by dietary energy restriction. Specifically, calorically restricting 7-week-old intact male TRAMP mice for 4 weeks reduces prostate pathology and accessory sex gland weights (21). Therefore, we chose to use TRAMP mice to investigate the *in vivo* efficacy of the novel ERMA OSU-CG5 in modulating preexisting PIN lesions. Our hypothesis was that ERMA treatment would reduce the severity of lesions in the prostates of 10-week-old TRAMP mice.

OSU-CG5 is a derivative of OSU-CG12 (Fig. 1A), a previously described ERMA with a potency that is 3 orders of magnitude higher than that of 2-DG in inducing cell death (22). Both OSU-CG compounds elicit energy restriction-associated cellular responses by inhibiting glucose transporters in tumor cells (23). OSU-CG5 exhibits an improved potency relative to OSU-CG12 in suppressing the [^{3}H]2-deoxyglucose uptake (IC_{50}, 6 vs. 9 μmol/L) and viability of human LNCaP prostate cancer cells (IC_{50}, 4.5 vs. 6 μmol/L; refs. 23, 24). Here, we examine the ability of OSU-CG5 to suppress cancer cell energy production *in vitro* and the *in vivo* efficacy and safety of OSU-CG5 in the TRAMP mouse model system of prostate neoplasia at the preneoplastic stage.

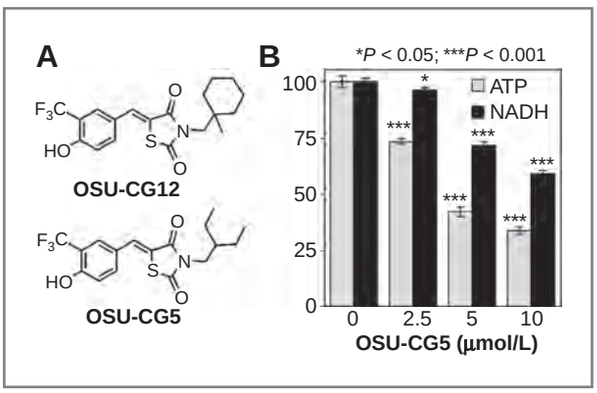

Figure 1. Evidence that OSU-CG5 reduces energy production. A, chemical structures of OSU-CG12 and OSU-CG5. B, dose-dependent suppressive effects of OSU-CG5 on ATP and NADH levels in LNCaP cells after 24 hours of treatment. The analyses were conducted in triplicate according to procedures described under Materials and Methods.

Materials and Methods

Cell cultures and reagents

Human LNCaP prostate cancer cells were obtained from the American Type Culture Collection and maintained with 10% FBS and 1% penicillin/streptomycin-supplemented RPMI-1640 medium (Invitrogen). No authentication of this cell line was conducted. All cells were cultured at 37°C in a humidified incubator containing 5% CO_2. OSU-CG5 was synthesized in our laboratory (data not shown). OSU-CG5 was dissolved in dimethyl sulfoxide (DMSO) and added to the culture medium with a final DMSO concentration of 0.1%.

ATP and NADH bioassays

The EnzyLight ATP Assay Kit (EATP-100) for rapid bioluminescent quantification of ATP and the EnzyChrom NAD+/NADH Assay Kit (E2ND-100) were obtained from BioAssay Systems. LNCaP cells were cultured in the presence of DMSO or OSU-CG5 at the indicated concentrations for 24 hours. Bioassays were conducted according to the manufacturer's instructions in triplicate.

In vivo study

TRAMP mice (C57BL/6 TRAMP × FvB) were bred and housed, and the presence of the transgene in each mouse was confirmed by PCR, as previously reported (25). Mice received a standard rodent diet and water *ad libitum*. All procedures were conducted in accordance with protocols approved by the Institutional Animal Care and Use Committee of The Ohio State University (Columbus, OH).

At 6 weeks of age, intact male transgenic mice were randomized to 2 groups that received either vehicle ($n = 20$) or 100 mg/kg/d of OSU-CG5 ($n = 19$). In addition, 6-week-old intact male wild-type littermates ($n = 6$/group) were also randomized into the same two groups. The test article was prepared as a suspension in sterile water containing 0.5% methylcellulose (w/v) and 0.1% Tween-80 (v/v). Suspensions of OSU-CG5 were prepared on a weekly basis and stored at room temperature. Mice received treatments once daily via oral gavage under isoflurane anesthesia for the duration of the study (4 weeks). Body weights were measured weekly and at necropsy. At the termination of the study (age 10 weeks), mice were euthanized via CO_2 approximately 2 to 4 hours after they had received their last dose, and complete necropsies were conducted. Urogenital tracts (UGT) were removed from all mice and weighed, after which relative UGT weights (UGT weight/terminal body weight × 100%) were determined. The livers, kidneys, hearts, spleens, and testes of each wild-type mouse were weighed, and relative organ weights were determined as described above for the UGT.

The individual lobes of the prostate were microdissected at necropsy and immersed in either RNAlater (Qiagen; transgenic mice only, $n = 9$ for vehicle; $n = 8$ for OSU-CG5) or PBS ($n = 11$ for each transgenic mouse treatment group, $n = 6$ for each wild-type mouse treatment group). The dorsal and lateral lobes of prostates microdissected in RNAlater were stored at 4°C overnight in RNAlater and then transferred to empty vials for storage at −80°C for

Published OnlineFirst December 28, 2012; DOI:10.1158/1940-6207.CAPR-12-0057

subsequent RNA extraction. The dorsal, lateral, ventral, and anterior lobes microdissected in PBS were weighed individually. One lobe of each pair was snap-frozen in liquid nitrogen and stored at −80°C until needed for Western blot analysis of relevant biomarkers, whereas the other was fixed in 10% neutral-buffered formalin (NBF). All other tissues were fixed in NBF.

At necropsy, serum was collected from 5 transgenic mice per group and submitted to Anilytics Inc. for determination of free and total testosterone concentrations via radioimmunoassay. Serum was also collected from 5 transgenic mice in the OSU-CG5 group and 4 transgenic mice in the vehicle-treated group for determination of liver enzyme values, including alanine aminotransferase (ALT), aspartate aminotransferase (AST), alkaline phosphatase (ALKP), and γ-glutamyl transpeptidase (GGT), and total bilirubin by the Comparative Pathology and Mouse Phenotyping Shared Resource (CPMPSR) at the Ohio State University. Serum was collected from 3 wild-type mice per group for determination of serum glucose, insulin-like growth factor (IGF)-1, and insulin concentrations. Serum glucose was measured by the CPMPSR. IGF-1 and insulin concentrations were determined using the IGF1 Mouse ELISA Kit (ab100695) from Abcam Inc and Insulin (Mouse) ELISA Kit (80-INSMS-E01) from ALPCO Diagnostics. Each ELISA was conducted according to the manufacturers' instructions in duplicate.

Histopathology and scoring of prostatic lesions in the TRAMP mice

Five-micrometer-thick, paraffin-embedded sections of the lobes of the prostate ($n = 11$ transgenic mice/group) as well as selected organs ($n = 5$ transgenic mice/group: liver, kidney, spleen, lung, heart, small intestine, testes, thymus, brain, eye, and bone marrow) were stained with hematoxylin and eosin (H&E) by standard procedures. All tissues were examined via light microscopy by a board-certified veterinary anatomic pathologist (LDBB) using an Olympus Model CHT research microscope (Olympus). The H&E-stained sections of the four lobes of the prostate of each transgenic mouse were evaluated and scored separately using a grading scheme (19) in which the most severe and most common lesions in each lobe were determined and assigned numerical scores. The sum of the scores of the most severe lesion and the most common lesion, termed the "sum of the adjusted lesion scores" (SALS), was then obtained for each lobe. The average SALS as well as the average most severe and average most common lesion scores of each lobe were compared between groups.

Immunohistochemistry

To evaluate prostate and small intestinal epithelial proliferation, 5-μm-thick, paraffin-embedded tissue sections of the lobes of the prostate and cross-sections of small intestine were immunostained for Ki67 using a commercially available rabbit anti-human monoclonal antibody (clone SP6; catalog#RM-9106-S0; Thermo Fisher Scientific). This primary antibody was applied at a dilution of 1:180. The immunohistochemistry staining protocol used the Avidin-Biotin Complex method with DakoCytomation Target Retrieval Solution and a Decloaking Chamber (Biocare Medical) according to the manufacturer's instructions, following the application of a protein block (DakoCytomation Serum-Free Protein Block, Dako). For each lobe of the prostate and section of small intestine, the number of Ki67-positive cells in 3 randomly selected 400× (i.e., high-power) fields was counted and divided by the total number of cells (Ki67-positive and -negative) in those fields ($n = 5$/group) to yield the percentage of Ki67-immunopositive cells.

RNA isolation and microarray analysis

Using a tissue homogenizer (Tissue Tearor, Model 985370-395; BioSpec Products, Inc.) and TRIzol reagent (Invitrogen), total RNA was isolated from the combined dorsal and lateral prostate lobes of control and OSU-CG5–treated transgenic mice ($n = 3$/group). After purification using the RNAeasy Mini Kit (Qiagen), the RNA was submitted to the Microarray Shared Resource at The Ohio State University Comprehensive Cancer Center (OSU-CCC) for RNA quantification and microarray analysis of gene expression using Affymetrix Genechip Mouse Genome 430 2.0 Arrays (Affymetrix). Microarray data were deposited in NCBI's Gene Expression Omnibus (GEO), and can be accessed via accession number GSE32422.

Protein isolation and Western blot analysis

For Western blot analysis of intraprostatic biomarkers, the dorsal and lateral prostate lobes of individual transgenic mice were combined and pulverized in liquid nitrogen ($n = 5$/group). SDS lysis buffer (1% SDS, 50 mmol/L Tris-HCl, pH 8.0, 10 mmol/L EDTA) containing 1× protease inhibitor cocktail (Sigma) and PhoSTOP phosphatase inhibitor cocktail (Roche) were added to the crushed tissue. The resulting lysates were sonicated until clear and centrifuged at 16,100 × g for 15 minutes. Protein concentrations in the supernatants were determined using the Micro BCA Protein Assay (Pierce Chemical). Proteins were separated by 1-dimensional electrophoresis in 8%–12% SDS-PAGE and transferred onto nitrocellulose membranes. After blocking with 5% nonfat milk, the membranes were incubated with primary antibodies (see below) at 1:1,000 dilution in TBS-Tween 20 overnight at 4°C. The protein bands were developed using horseradish peroxidase–conjugated secondary antibodies at 1:5,000 dilution in the same buffer for 1 hour at room temperature. Bands were visualized on X-ray film using an enhanced chemiluminescence system. Densitometric analysis of protein bands was conducted using ImageJ software to determine the relative intensities of protein expression in drug-treated samples versus those of vehicle-treated controls after normalization to the internal reference protein β-actin.

The target proteins and commercial sources of the antibodies for several biomarkers are given here. Mouse monoclonal antibodies directed against β-actin were from MP Biomedicals, Src from Calbiochem, or SV40 T Ag from Santa Cruz Biotechnology. Rabbit polyclonal antibodies came from 2 sources. Reagents directed against IGF-1 receptor

Published OnlineFirst December 28, 2012; DOI:10.1158/1940-6207.CAPR-12-0057

(IGF-1R), androgen receptor (AR), and proliferating cell nuclear antigen (PCNA) were acquired from Santa Cruz. Antibodies directed against Akt, p-Akt-Ser473, PTEN, c-Myc, glycogen synthase kinase 3β (GSK3β), and p-GSK3β were obtained from Cell Signaling.

Statistical analysis

Data were assessed for normality using the Shapiro–Wilk normality test. All data were found to be normally distributed except the Ki67 values for the ventral and anterior lobes of the prostate and the small intestine; the SALS for the dorsal, lateral, and anterior lobes of the prostates; the serum concentrations of total and free testosterone, glucose, IGF-1, and insulin; the serum activities of liver enzymes; and the relative weights of the heart, kidney, and spleen. For the normally distributed data, differences between group means were analyzed for statistical significance using the Student *t* test. For the data that were not normally distributed, statistical significance was evaluated using the Wilcoxon rank-sum test. Differences were considered to be significant at $P < 0.05$. Microarray data were submitted to The OSU-CCC Biomedical Informatics Shared Resource for statistical analysis, using the Bioconductor microarray analysis package, using the Student *t* test. Fold changes and differences in gene expression profiles were considered significant at $P < 0.05$. Microarray pathways were analyzed using Ingenuity Pathway Analysis (IPA) software (Ingenuity Systems). Only genes with greater than 1.5-fold up- or downregulation and $P < 0.05$ were selected for pathway analysis. All *P* values were 2-sided, except for *P* values from the Western blots, which were 1-sided.

Results

Suppressive effects of OSU-CG5 on LNCaP cell ATP and NADH production

Previously, we showed that OSU-CG5, a structurally optimized derivative of OSU-CG12, blocked glucose uptake in LNCaP cells by blocking glucose transporters (23, 24). The consequent effect on energy production was manifested by its ability to lower the levels of ATP and NADH in a dose-dependent manner after 24 hours of treatment. At 5 μmol/L, OSU-CG5 reduced ATP and NADH production by 58% ± 1% ($P < 0.0001$) and 28% ± 1% ($P < 0.0001$), respectively, relative to the DMSO control (Fig. 1B).

OSU-CG5 decreased prostate weight and prostate epithelial cell proliferation in transgenic TRAMP mice

To investigate the effect of OSU-CG5 on the progression of preneoplastic lesions, 6-week-old TRAMP mice were treated once daily with OSU-CG5 (100 mg/kg, *per os*, $n = 19$) or vehicle ($n = 20$) for 4 weeks. As UGT weight has previously been shown to correlate significantly with prostate lesion severity and progression (13, 26), the average UGT weights of each group were compared. OSU-CG5 treatment resulted in 12% and 11% reductions in the absolute UGT weight (332 ± 40 mg vs. 377 ± 37 mg in controls; $P = 0.001$) and relative UGT weight (1.24% ± 0.14% vs. 1.39% ± 0.11% in controls; $P = 0.001$; Fig. 2A). Moreover, the weights of the individual prostate lobes of the OSU-CG5–treated mice were decreased relative to vehicle controls ($n = 11$ mice/group): dorsal, 25.7% ($P = 0.013$); lateral, 31.5% ($P = 0.003$); ventral, 10% ($P = 0.413$); anterior, 16.5% ($P = 0.026$; Fig. 2B). Importantly, these reductions in weight were not associated

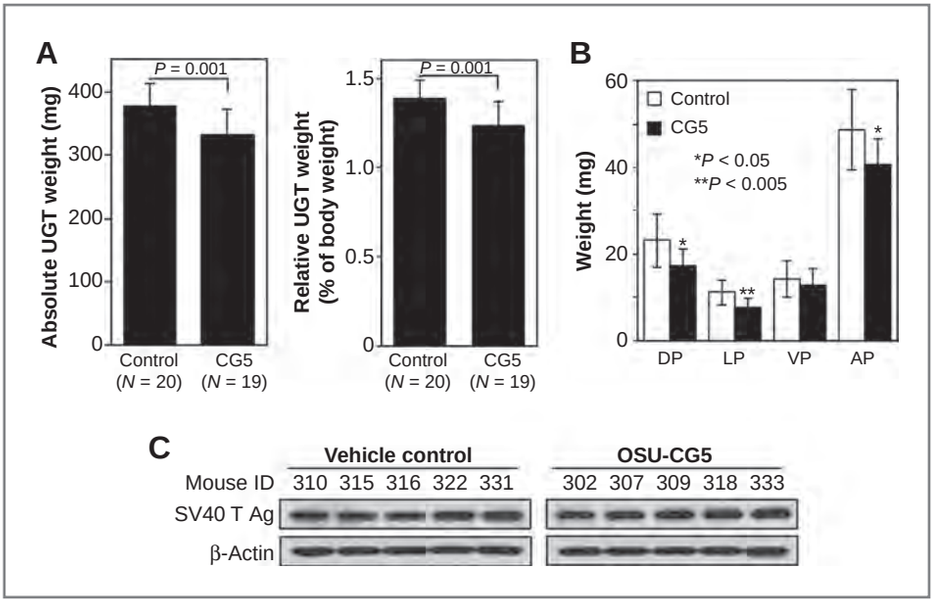

Figure 2. OSU-CG5 reduced prostate weight in TRAMP mice. Six-week-old intact male TRAMP mice were treated orally with OSU-CG5 (100 mg/kg) once daily for 4 weeks. The weights of the UGTs from each mouse were determined, as well as the weights of individual prostate lobes after microdissection. Treatment with OSU-CG5 caused statistically significant reductions in (A) absolute and relative UGT weights and (B) the weights of the dorsal, lateral, and anterior lobes of the prostate. C, drug treatment had no effect on the expression level of the SV40 large T antigen in the combined dorsal and lateral prostates (5 mice/group) as determined by Western blotting. In (A) and (B), bars represent the mean ± SD. AP, anterior lobe of the prostate; CG5, OSU-CG5; DP, dorsal lobe of the prostate; LP, lateral lobe of the prostate; VP, ventral lobe of the prostate.

Published OnlineFirst December 28, 2012; DOI:10.1158/1940-6207.CAPR-12-0057

with decreased SV40 large T Ag expression in the prostate ($n = 5$ mice/group), as Western blot analysis indicated that the amount of SV40 oncoprotein in the combined dorsal and lateral lobes was comparable in both treatment groups (Fig. 2C).

The suppressive effect of OSU-CG5 on the UGT weight was linked to its ability to inhibit the proliferation of prostate epithelial cells. OSU-CG5 treatment led to a marked decrease in the proliferation index, as indicated by Ki67 immunoreactivity, in all 4 lobes of the prostate ($P < 0.05$ for all lobes; $n = 5$ mice/group; Fig. 3A and B). Western blot analysis indicated that OSU-CG5 decreased the expression level of PCNA in the combined dorsal and lateral lobes by 32% ($P = 0.002$) relative to the vehicle ($n = 5$ mice/group; Fig. 3C).

Histopathologic examination and scoring of each lobe of the prostate was conducted ($n = 11$ mice/group), and the sum of the adjusted lesion score (SALS) for each lobe was determined. The average SALS of the dorsal, lateral, ventral, and anterior lobes of the prostates from the vehicle-treated mice were 9.5 ± 1.4, 9.0 ± 4.4, 6.0 ± 2.1, and 4.5 ± 3.0, respectively, whereas the average SALS for these lobes in OSU-CG5–treated mice were 9.1 ± 1.8, 7.5 ± 1.0, 5.6 ± 2.5, and 5.5 ± 3.0. No statistical differences were found in the average SALS of each lobe or the average scores for the most severe or most common lesions in each lobe (Supplementary Table S1).

Testosterone radioimmunoassays indicated that the serum concentrations of free and total testosterone were 0.21 ± 0.11 and 0.33 ± 0.09 ng/mL, respectively, for OSU-CG5–treated mice ($n = 5$ mice/group) versus 3.4 ± 4.6 and 1.6 ± 2.0 ng/mL, respectively, for vehicle-treated mice ($n = 5$ mice/group). Despite 93.7% and 79.7% decreases in the free and total testosterone, respectively, these reductions were not statistically significant ($P > 0.05$), in part, due to large variations in the testosterone concentrations of vehicle controls. This wide variation in the serum testosterone level, however, is in line with the reported range of 1 to 90 pg/mL in nude mice (27).

OSU-CG5 treatment was not associated with any evidence of systemic toxicity

No overt toxicity was noted with OSU-CG5, as the drug-treated transgenic group gained a similar amount of weight to that of the control group after 4 weeks of treatment (Table 1). Similarly, there were no significant changes in the absolute or relative weights of the UGT, liver, kidneys, hearts, or testes (Table 1), in the wild-type mice ($n = 6$ mice/group; $P > 0.05$). Histologic evaluation of H&E-stained sections of metabolically active organs

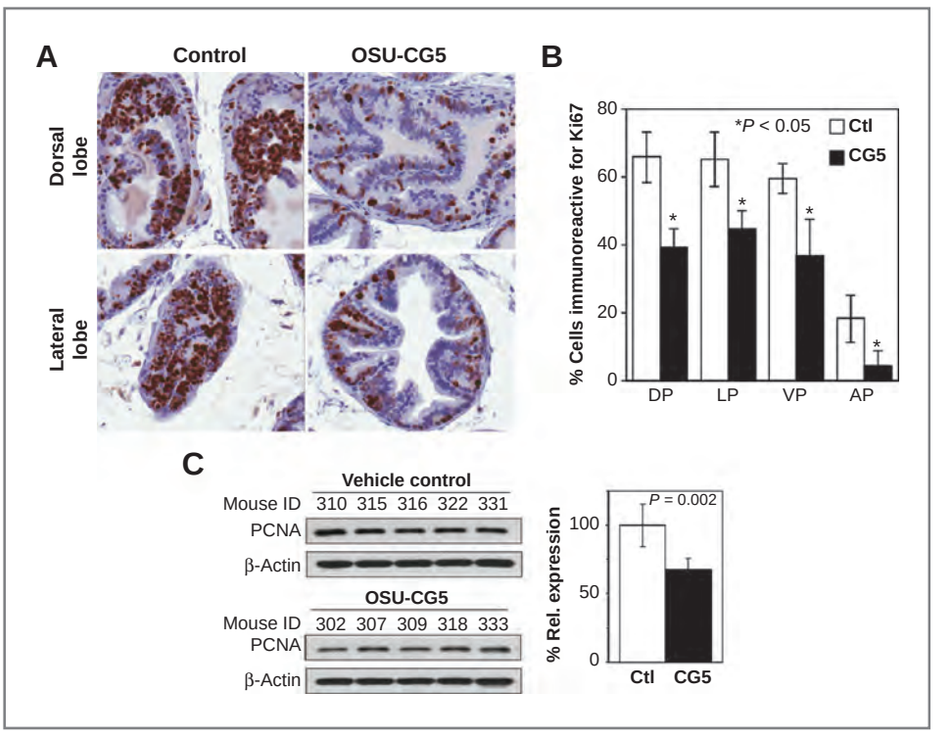

Figure 3. OSU-CG5 reduced prostate epithelial proliferation in TRAMP mice. Proliferation within the prostates of TRAMP mice treated with OSU-CG5 (100 mg/kg/d) or vehicle for 4 weeks was assessed by immunohistochemistry for Ki67 (A and B) and Western blotting for PCNA (C). A, photomicrographs showing Ki67 immunoreactivity in the dorsal and lateral lobes of representative vehicle- and OSU-CG5–treated TRAMP mice (×400). B, the percentages of cells that were immunopositive for Ki67 in each prostate lobe were reduced in OSU-CG5–treated TRAMP mice relative to vehicle-treated controls ($n = 5$ mice/group). C, Western blot analysis shows that OSU-CG5 treatment reduced the expression levels of PCNA in the combined dorsal and lateral lobes prostates of TRAMP mice relative to vehicle-treated controls (5 mice/group). In (B) and (C), bars represent the mean ± SD. AP, anterior lobe of the prostate; Ctl, vehicle control; CG5, OSU-CG5; DP, dorsal lobe of the prostate; LP, lateral lobe of the prostate; VP, ventral lobe of the prostate.

Published OnlineFirst December 28, 2012; DOI:10.1158/1940-6207.CAPR-12-0057

Table 1. Evidence that OSU-CG5 caused no systemic toxicity in young adult mice after 4 weeks of treatment

	Vehicle-treated	OSU-CG5–treated
TRAMP mice: body weight gain, g		
	2.0 ± 1.0 ($n = 20$)	2.2 ± 1.1 ($n = 19$)
Wild-type littermates of TRAMP mice: organ weight ($n = 6$ for both groups), mg		
UGT (% body weight)	351 ± 60 (1.31 ± 0.15)	355 ± 53 (1.29 ± 0.15)
Liver (% body weight)	1303 ± 124 (4.89 ± 0.31)	1,372 ± 124 (5.00 ± 0.33)
Kidney (% body weight)	408 ± 28 (1.54 ± 0.14)	450 ± 36 (1.64 ± 0.04)
Heart (% body weight)	164 ± 19 (0.62 ± 0.07)	173 ± 41 (0.63 ± 0.13)
Spleen (% body weight)	72 ± 6 (0.27 ± 0.02)	82 ± 8 (0.3 ± 0.02)
Testes (% body weight)	204 ± 21 (0.76 ± 0.07)	221 ± 16 (0.81 ± 0.09)
TRAMP mice: liver function ($n = 4$ for vehicle; $n = 5$ for OSU-CG5)		
ALT, U/L	22 ± 5	19 ± 2
AST, U/L	89 ± 75	50 ± 16
ALKP, U/L	54 ± 6	63 ± 12
GGT, U/L	4 ± 2	7 ± 2
Total bilirubin, mg/dL	0.3 ± 0.1	0.3 ± 0.1
TRAMP mice: cell proliferation[a] in nonneoplastic tissues ($n = 5$ for both groups)		
Small intestinal epithelium	48.2 ± 4.1	52.9 ± 6.8

NOTE: Statistically equivalent for OSU-CG5–treated and vehicle-treated mice, $P > 0.05$, for all values except absolute and relative weights of the spleen.

[a]Proliferation evaluated as percentage of Ki67-immunopositive cells.

including liver, kidney, spleen, lung, heart, small intestine, testes, thymus, brain, eye, and bone marrow ($n = 5$ mice/group) did not reveal any lesions consistent with systemic or organ-specific toxicity. Although OSU-CG5 treatment was associated with mild splenomegaly with slight increases in the average absolute and relative weights of the spleen ($P < 0.05$; Table 1), there were no associated histologic lesions. There was no biochemical evidence of hepatotoxicity as the concentrations of various hepatic biomarkers, including ALT, AST, ALKP, and GGT, and total bilirubin were not affected by 4 weeks of OSU-CG5 treatment (vehicle: $n = 4$ mice; OSU-CG5: $n = 5$ mice; Table 1). Moreover, analysis of the proliferation index of small intestinal epithelial cells found no significant differences in the percentage of Ki67-immunopositive cells between these 2 groups of mice ($n = 5$ mice/group; Table 1). Together, these findings indicate that OSU-CG5 treatment was not associated with any detectable systemic toxicity.

OSU-CG5–mediated suppression of prostate epithelial proliferation in transgenic TRAMP mice was associated with modulation of gene expression in the combined dorsal and lateral lobes of the prostate

Earlier studies indicate that caloric restriction and 2-DG suppress carcinogenesis by perturbing cellular signaling and/or gene expression profiles (9–10, 12, 28–30). Microarray analysis was conducted using RNA from the combined dorsal and lateral prostate lobes of OSU-CG5- and vehicle-treated animals ($n = 3$ mice/group). Using IPA software, the top 5 gene networks affected by OSU-CG5 treatment were identified (Supplementary Table S2). Of these, we focused on the "Cellular Assembly and Organization, Cellular Function and Maintenance, Gene Expression" because of the likely role of genes in this network in maintaining cellular homeostasis and suppression of tumorigenesis (Supplementary Table S2). The pathway network is shown in Fig. 4. *Akt* appeared to have a central role in this constellation, with 5 genes in the network interacting directly with *Akt* and 5 genes interacting indirectly with *Akt*. In light of this information and due to the fact that an earlier study showed upregulation of Akt signaling, as manifested by dramatically increased phosphorylation of Akt and GSK3β, in proliferative prostate epithelium in TRAMP mice with PIN (25), we investigated the phosphorylation status of Akt and GSK3β in the combined dorsal and lateral lobes of prostates of OSU-CG5- versus vehicle-treated mice. As shown in Fig. 5, OSU-CG5 treatment significantly reduced phospho-Ser473-Akt and phospho-GSK3β levels by 50% ($P = 0.012$) and 45% ($P = 0.043$), respectively, relative to the vehicle-treated controls.

The microarray data also showed changes in the expression of genes encoding proteins of potential therapeutic relevance for prostate cancer. OSU-CG5 exhibited suppressive effects on the expression of the Rous sarcoma

Published OnlineFirst December 28, 2012; DOI:10.1158/1940-6207.CAPR-12-0057

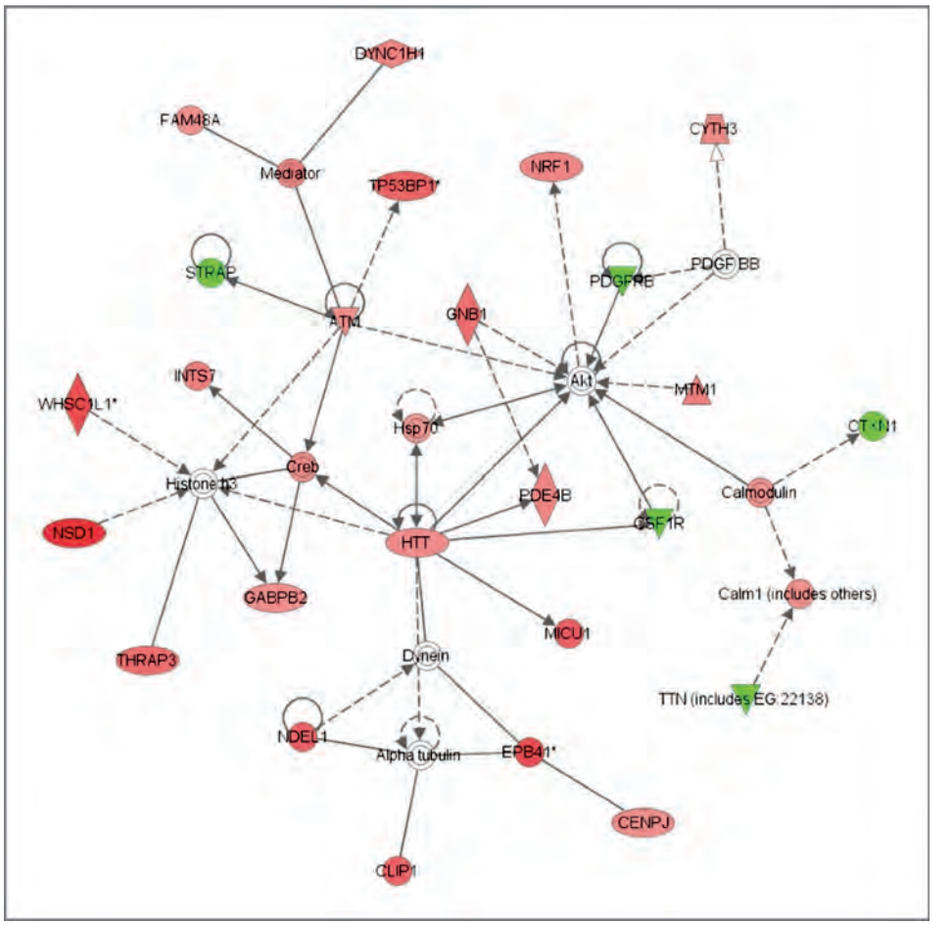

Figure 4. △ = Transporter, ◇ = Enzyme, ▽ = Kinase, △ = Phosphatase, ⬭ = Transcription regulator, ⊂ = Other, ◎ = Complex/group, ◇ = Peptidase. Gene network in the combined dorsal and lateral lobes of prostate of TRAMP mice treated for 4 weeks with 100 mg/kg/d of OSU-CG5 was created using Ingenuity pathway analysis software. We focused on the network that was described as being involved in "Cellular Assembly and Organization, Cellular Function and Maintenance, Gene Expression." *Akt* appears to have a central role in this pathway. Genes are represented as nodes, with upregulated genes colored red and downregulated genes colored green. The intensity of the color indicates the degree of up- or downregulation. Genes that are not colored were not in the analyzed data set. The biologic relationships between genes are indicated by lines; solid lines represent direct interactions whereas dashed lines represent indirect interactions. Arrowheads indicate the directionality of interaction, and lines without arrowheads indicate binding. Lines that begin and end at the same gene indicate autoregulation.

oncogene (*v-src*; −1.44-fold, $P = 0.007$), and its cellular counterpart, the proto-oncogene *c-src* (−1.36-fold, $P = 0.012$). Downregulation of *Src* represents a therapeutically relevant target in prostate cancer (31). In addition, OSU-CG5 decreased the expression of the Myc-like oncogene, *s-myc* (−1.32-fold, $P = 0.007$) and upregulated the expression of *PTEN* (1.25-fold, $P = 0.033$). Further review of the data revealed a number of other upregulated genes with central roles in suppressing tumorigenesis and downregulated genes with roles in tumor development and progression. These genes, categorized according to mechanism of action, are found in Supplementary Tables S3 and S4.

Considering the importance of Src, myc, and PTEN in prostate cancer pathogenesis, as well as the importance of growth factor signaling through IGF-1R and AR for prostate epithelial proliferation, we assessed the expression levels of these proteins by Western blotting ($n = 5$/group). OSU-CG5 significantly reduced the expression of Src, AR, and IGF-1R by 28% ($P = 0.001$), 26% ($P = 0.036$), and 47% ($P = 0.001$), respectively, whereas no significant changes were noted in the protein levels of PTEN or c-Myc (Fig. 5).

Despite reduced intraprostatic IGF-1R expression, OSU-CG5 did not affect glucose homeostasis, as no significant changes ($P > 0.05$) in the serum levels of glucose, IGF-1, or insulin were noted in drug-treated mice. Concentrations of these serum parameters in vehicle- and OSU-CG5–treated mice were as follows, respectively: glucose, 279 ± 11 and 288 ± 26 mg/dL; IGF-1, 2.7 ± 0 and 2.7 ± 0.1 ng/mL; insulin, 0.92 ± 0.23 and 0.94 ± 0.29 ng/mL. These results suggest that the ERMA activity of OSU-CG5 was restricted to the proliferating cells within the PIN lesions and did not affect whole-body energy metabolism.

Published OnlineFirst December 28, 2012; DOI:10.1158/1940-6207.CAPR-12-0057

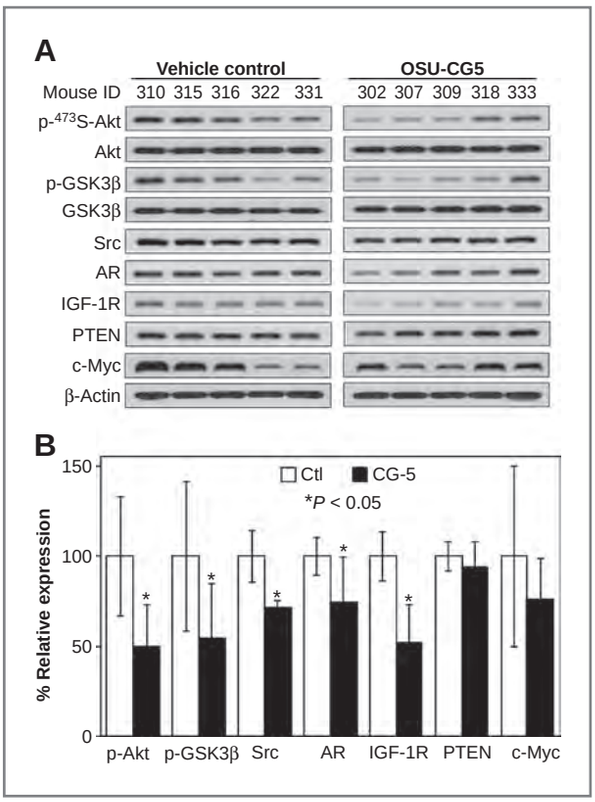

Figure 5. A, Western blot analysis of the effects of OSU-CG5 on the phosphorylation of Akt-Ser-473 and GSK3β and the expression of several prosurvival factors (Src, AR, IGF-1R, c-Myc) and a tumor suppressor (PTEN) in the combined dorsal and lateral lobes of prostates in TRAMP mice treated with OSU-CG5 (100 mg/kg/d) or vehicle for 4 weeks. B, densitometric analysis of protein bands was conducted to calculate relative phosphorylation/expression levels of individual proteins. Bars represent the mean ± SD. Ctl, vehicle control; CG5, OSU-CG5.

Discussion

The adaptation of cancer cells to preferentially use aerobic glycolysis is an early step in carcinogenesis and presents an opportunity for therapeutic exploitation. The efficacy of energy restriction as a chemotherapeutic or chemopreventive strategy has been shown by the finding that inhibiting glycolysis through dietary caloric restriction or by administration of 2-DG suppresses xenograft tumor growth and carcinogenesis in various animal models (8–12). However, dietary caloric restriction is not an easy intervention for human patients with cancer, and previous work by our laboratory has showed that 2-DG has relatively low *in vitro* cytotoxic activity (22). In addition, ERMAs currently in clinical trials have not been without serious side effects. For example, a clinical trial using 2-DG to treat advanced prostate cancer (NCT00633087) was stopped by the U.S. Food and Drug Administration because of concerns about hepatotoxicity (32). Therefore, new ERMAs with higher potency and improved *in vivo* safety are needed.

Although chronic dietary restriction (21, 33) or intermittent caloric restriction (34) has been shown to retard prostate lesion development in the TRAMP mouse model, we are aware of only one study that included an evaluation of caloric restriction on the progression of preneoplastic lesions (21). Studies in TRAMP mice have found that 20% caloric restriction initiated at approximately 7 weeks of age had a greater effect on the suppression of lesion development than 20% caloric restriction started at a later time point (20 weeks; refs. 21, 33). This result implies that the age at which the dietary intervention is initiated influences its effectiveness. In addition, intermittent caloric restriction delayed prostate tumor development longer than chronic caloric restriction when both were begun at the same age (34). Given the results from these studies, it seems logical to examine the effect that an ERMA administered beginning at puberty could have on the severity of PIN lesions.

In this study, we showcase the ability of OSU-CG5, a novel glucose transporter inhibitor (23, 24), to modify the early lesions of TRAMP mice. OSU-CG5 reduced the weights of the UGTs as well as the dorsal, lateral, and anterior lobes of prostates by suppressing prostate epithelial proliferation. As the UGT weight correlates with lesion severity and progression in TRAMP mice (13, 26), the effect of OSU-CG5 on UGT weights underscores this ERMA's ability to reduce the prostate pathology within these mice. The lack of statistically significant changes in the histopathologic lesion scores of the individual prostate lobes in this study likely reflects the fact that the traditional scoring criteria for mouse prostatic cancer models are weighted to the assessment of later-stage neoplastic lesions rather than to the early PIN changes.

Importantly, our data indicate that OSU-CG5 is well tolerated. Chronic oral administration of OSU-CG5 resulted in no untoward (i.e., "toxic") effects in metabolically active organs with naturally high glycolytic rates, including the liver, kidney, small intestine, brain, and eye, did not impact the proliferation of a nonneoplastic tissue (the small intestine) and did not induce elevations in serum activities of liver enzymes. Taken together, these animal data underscore the translational potential of OSU-CG5.

In this study, we also investigated multiple mechanisms by which OSU-CG5 acts to decrease prostate epithelial proliferation. For example, treatment with OSU-CG5 resulted in decreased AR expression, which accords well with our previous finding that the ERMA OSU-CG12 suppressed AR expression in LNCaP cells by downregulating expression of the transcription factor Sp1 (22). In light of the pivotal role of AR signaling in prostate carcinogenesis and tumor progression (35), downregulation of AR expression likely contributed, at least in part, to the decreased prostate epithelial proliferation observed in this study.

Despite decreased AR expression levels in the prostate, there was no evidence of testicular atrophy in OSU-CG5–treated wild-type mice as suggested by lack of histologic

Published OnlineFirst December 28, 2012; DOI:10.1158/1940-6207.CAPR-12-0057

lesions within the testes or changes in testicular weights. Together with the finding that OSU-CG5 did not reduce the wild-type UGT weights, these data imply that OSU-CG5 does not act as an anti-androgen. Although the decrease in serum testosterone concentrations in OSU-CG5–treated mice was not statistically significant due to a high degree of interindividual variability, caloric restriction has been reported to decrease circulating testosterone (36). Therefore, the decreased testosterone level in this study might represent a cellular response to OSU-CG5 as it mimics caloric restriction *in vivo*. Any decrease in serum testosterone may have potentiated the effect of the decreased AR. Further studies are needed to determine any effect that OSU-CG5 may have had on the hypothalamic–pituitary hormonal axis that control gonadal function, especially after prolonged therapy. Interestingly, lesion progression in TRAMP mice has previously been shown to be relatively resistant to reductions in serum testosterone, with 80% of TRAMP mice castrated by 12 weeks of age developing prostate tumors by 24 weeks of age (37).

Moreover, OSU-CG5 inhibited the IGF-1R/PI3K/Akt signaling axis in the combined dorsal and lateral lobes of prostates. The microarray data suggested a central role for Akt in the top network modulated by OSU-CG5, and we subsequently showed the suppressive effect of OSU-CG5 on phosphorylation of Akt and its target GSK3β. This finding is in accordance with a recent report that caloricallly restricting Hi-Myc transgenic mice reduces the incidence of prostatic adenocarcinomas and the phosphorylation level of Akt (38).

From a mechanistic perspective, the ability of OSU-CG5 to inhibit Akt signaling might, in part, be attributable to the observed downregulation of intraprostatic IGF-1R expression, which would have led to decreased IGF-1/IGF-1R signaling. Downregulation of IGF-1/IGF-1R signaling has been shown to be a major mechanism underlying the effect of caloric restriction on tumor suppression (39). Despite reduced intraprostatic IGF-1R expression, there was no significant change in the serum level of IGF-1 in the OSU-CG5–treated wild-type cohort. Together with the lack of changes in serum glucose and insulin, this finding lends credence to our hypothesis that OSU-CG5 targets neoplastic cell energy metabolism and does not affect global glucose homeostasis. There is also conflicting information about the effect of caloric restriction on IGF-1 levels in TRAMP mice. Although intermittent caloric restriction has been shown to reduce serum IGF-1 levels (34), no significant changes in serum IGF-1 were reported in TRAMP mice receiving chronic caloric restriction (33).

Although we believe that we have shown the efficacy of OSU-CG5 in suppressing PIN epithelial proliferation *in vivo*, our study was not without limitations. As the focus of this study was PIN and the mice were euthanized before tumors developed, we were unable to evaluate how OSU-CG5 treatment might influence prostate carcinoma development and the pattern and rate of metastasis. Such an investigation of late-stage neoplastic lesions is currently underway. In addition, the TRAMP model may not be the best transgenic mouse model in which to evaluate the development of prostate carcinomas as controversy exists about the exact histogenesis of the poorly differentiated carcinomas that represent the majority of end-stage tumors. Furthermore, although statistically significant, the effect of OSU-CG5 on the weights of UGT and prostate lobes were relatively modest compared with the effect on prostate epithelial cell proliferation (as determined by Ki67 and PCNA) and biomarker modulation. A possible explanation for this disconnect is that OSU-CG5–mediated changes in proliferation may precede more substantial differences in lobe weights. Further work is needed to define the regimen and manner in which ERMAs such as OSU-CG5 may be introduced into the clinical armamentarium for treating prostatic and other cancers.

In summary, our study showed that oral administration of OSU-CG5 suppressed the proliferation of prostate epithelial cells in TRAMP mice without evidence of toxicity or modulation of whole-body glucose homeostasis. Microarray and Western blotting data revealed that OSU-CG5 targeted proliferating preneoplastic cells via multiple mechanisms that include the modulation of cell survival and proliferation pathways and interference with cellular energy metabolism. This range of antitumor activities in the absence of toxicity suggested the translational potential of OSU-CG5 as a chemopreventive agent, warranting further investigation in this regard.

Disclosure of Potential Conflicts of Interest

No potential conflicts of interest were disclosed.

Authors' Contributions

Conception and design: L.-D. Berman-Booty, P.-C. Chu, B. Bolon, S.K. Clinton, C.-S. Chen
Development of methodology: L.-D. Berman-Booty, S.K. Clinton
Acquisition of data (provided animals, acquired and managed patients, provided facilities, etc.): L.-D. Berman-Booty, J.M. Thomas-Ahner, S.K. Clinton, C.-S. Chen
Analysis and interpretation of data (e.g., statistical analysis, biostatistics, computational analysis): L.-D. Berman-Booty, P.-C. Chu, S.K. Clinton, S.K. Kulp, C.-S. Chen
Writing, review, and/or revision of the manuscript: L.-D. Berman-Booty, J.M. Thomas-Ahner, B. Bolon, S.K. Clinton, S.K. Kulp, C.-S. Chen
Administrative, technical, or material support (i.e., reporting or organizing data, constructing databases): T. Yang, S.K. Clinton, C.-S. Chen
Study supervision: S.K. Clinton, C.-S. Chen
Provided chemicals for this study: D. Wang

Acknowledgments

The authors thank Daphne Pringle for her help with pathway analysis of the microarray data and Dr. Jie Zhang for statistical analysis of the microarray data.

Grant Support

This work was supported by a T-32 Institutional National Research Service Award in Mouse Models of Human Disease (Ruth L. Kirschstein-NRSA; T32RR007073) and NIH grant K01 OD010463 to LDBB and NIH grant CA112250 and Department of Defense Prostate Cancer Research Program grant W81XWH-09-0198 to C.-S. Chen.

The costs of publication of this article were defrayed in part by the payment of page charges. This article must therefore be hereby marked *advertisement* in accordance with 18 U.S.C. Section 1734 solely to indicate this fact.

Received February 7, 2012; revised November 21, 2012; accepted December 18, 2012; published OnlineFirst December 28, 2012.

Published OnlineFirst December 28, 2012; DOI:10.1158/1940-6207.CAPR-12-0057

References

1. Chesney J. 6-phosphofructo-2-kinase/fructose-2,6-bisphosphatase and tumor cell glycolysis. Curr Opin Clin Nutr Metab Care 2006;9:535–9.
2. Warburg O. On the origin of cancer cells. Science 1956;123:309–14.
3. Kroemer G, Pouyssegur J. Tumor cell metabolism: cancer's Achilles' heel. Cancer Cell 2008;13:472–82.
4. Kim JW, Dang CV. Cancer's molecular sweet tooth and the Warburg effect. Cancer Res 2006;66:8927–30.
5. Vander Heiden MG, Cantley LC, Thompson CB. Understanding the Warburg effect: the metabolic requirements of cell proliferation. Science 2009;324:1029–33.
6. Hsu PP, Sabatini DM. Cancer cell metabolism: Warburg and beyond. Cell 2008;134:703–7.
7. Kaelin WG Jr, Thompson CB. Q&A: Cancer: clues from cell metabolism. Nature 2010;465:562–4.
8. Kritchevsky D. Caloric restriction and experimental carcinogenesis. Toxicol Sci 1999;52:13–6.
9. Jiang W, Zhu Z, Thompson HJ. Dietary energy restriction modulates the activity of AMP-activated protein kinase, Akt, and mammalian target of rapamycin in mammary carcinomas, mammary gland, and liver. Cancer Res 2008;68:5492–9.
10. Hursting SD, Lavigne JA, Berrigan D, Perkins SN, Barrett JC. Calorie restriction, aging, and cancer prevention: mechanisms of action and applicability to humans. Annu Rev Med 2003;54:131–52.
11. Berrigan D, Perkins SN, Haines DC, Hursting SD. Adult-onset calorie restriction and fasting delay spontaneous tumorigenesis in p53-deficient mice. Carcinogenesis 2002;23:817–22.
12. Mukherjee P, Sotnikov AV, Mangian HJ, Zhou JR, Visek WJ, Clinton SK. Energy intake and prostate tumor growth, angiogenesis, and vascular endothelial growth factor expression. J Natl Cancer Inst 1999;91:512–23.
13. Kaplan-Lefko PJ, Chen TM, Ittman MM, Barrios RJ, Ayala GE, Huss WJ, et al. Pathobiology of autochthonous prostate cancer in a preclinical transgenic mouse model. Prostate 2003;55:219–37.
14. Gingrich JR, Barrios RJ, Foster BA, Greenberg NM. Pathologic progression of autochthonous prostate cancer in the TRAMP model. Prostate Cancer Prostatic Dis 1999;2:70–5.
15. Greenberg NM, DeMayo F, Finegold MJ, Medina D, Tilley WD, Aspinall JO, et al. Prostate cancer in a transgenic mouse. Proc Natl Acad Sci USA 1995;92:3439–43.
16. Gingrich JR, Barrios RJ, Morton RA, Boyce BF, DeMayo FJ, Finegold MJ, et al. Metastatic prostate cancer in a transgenic mouse. Cancer Res 1996;56:4096–102.
17. Greenberg NM, DeMayo FJ, Sheppard PC, Barrios R, Lebovitz R, Finegold M, et al. The rat probasin gene promoter directs hormonally- and developmentally-regulated expression of a heterologous gene specifically to the prostate in transgenic mice. Mol Endocrinol 1994;8:230–9.
18. Greenberg NM. Transgenic models for prostate cancer research. Urol Oncol 1996;2:119–22.
19. Berman-Booty LD, Sargeant AM, Rosol TJ, Rengel RC, Clinton SK, Chen CS, et al. A Review of the existing grading schemes and a proposal for a modified grading scheme for prostatic lesions in TRAMP mice. Toxicol Pathol 2012;40:5–17.
20. Chiaverotti T, Couto SS, Donjacour A, Mao JH, Nagase H, Cardiff RD, et al. Dissociation of epithelial and neuroendocrine carcinoma lineages in the transgenic adenocarcinoma of mouse prostate model of prostate cancer. Am J Pathol 2008;172:236–46.
21. Suttie A, Nyska A, Haseman JK, Moser GJ, Hackett TR, Goldsworthy TL. A grading scheme for the assessment of proliferative lesions of the mouse prostate in the TRAMP model. Toxicol Pathol 2003;31:31–8.
22. Wei S, Kulp SK, Chen CS. Energy restriction as an antitumor target of thiazolidinediones. J Biol Chem 2010;285:9780–91.
23. Wang D, Chu PC, Yang CN, Yan R, Chuang YC, Kulp SK, et al. Development of a novel class of glucose transporter inhibitors. J Med Chem 2012;55:3827–36.
24. Lin HY, Kuo YC, Weng YI, Lai IL, Huang TH, Lin SP, et al. Activation of silenced tumor suppressor genes in prostate cancer cells by a novel energy restriction-mimetic agent. Prostate 2012;72:1767–78.
25. Sargeant AM, Klein RD, Rengel RC, Clinton SK, Kulp SK, Kashida Y, et al. Chemopreventive and bioenergetic signaling effects of PDK1/Akt pathway inhibition in a transgenic mouse model of prostate cancer. Toxicol Pathol 2007;35:549–61.
26. Kee K, Foster BA, Merali S, Kramer DL, Hensen ML, Diegelman P, et al. Activated polyamine catabolism depletes acetyl-CoA pools and suppresses prostate tumor growth in TRAMP mice. J Biol Chem 2004;279:40076–83.
27. van Steenbrugge GJ, van Dongen JJ, Reuvers PJ, de Jong FH, Schroeder FH. Transplantable human prostatic carcinoma (PC-82) in athymic nude mice: I. Hormone dependence and the concentration of androgens in plasma and tumor tissue. Prostate 1987;11:195–210.
28. Kritchevsky D. Caloric restriction and experimental carcinogenesis. Hybrid Hybridomics 2002;21:147–51.
29. Zhu Z, Jiang W, McGinley JN, Thompson HJ. 2-Deoxyglucose as an energy restriction mimetic agent: effects on mammary carcinogenesis and on mammary tumor cell growth in vitro. Cancer Res 2005;65:7023–30.
30. Liao Z, Wang S, Wiegers BS, Clinton SK. Energy balance alters dunning R3327-H prostate tumor architecture, androgen receptor expression, and nuclear morphometry in rats. Prostate 2006;66:945–53.
31. Fizazi K. The role of Src in prostate cancer. Ann Oncol 2007;18:1765–73.
32. Omar HA, Berman-Booty L, Kulp SK, Chen CS. Energy restriction as an antitumor target. Future Oncol 2010;6:1675–9.
33. Suttie AW, Dinse GE, Nyska A, Moser GJ, Goldsworthy TL, Maronpot RR. An investigation of the effects of late-onset dietary restriction on prostate cancer development in the TRAMP mouse. Toxicol Pathol 2005;33:386–97.
34. Bonorden MJ, Rogozina OP, Kluczny CM, Grossmann ME, Grambsch PL, Grande JP, et al. Intermittent calorie restriction delays prostate tumor detection and increases survival time in TRAMP mice. Nutr Cancer 2009;61:265–75.
35. Dutt SS, Gao AC. Molecular mechanisms of castration-resistant prostate cancer progression. Future Oncol 2009;5:1403–13.
36. Levay EA, Tammer AH, Penman J, Kent S, Paolini AG. Calorie restriction at increasing levels leads to augmented concentrations of corticosterone and decreasing concentrations of testosterone in rats. Nutr Res 2010;30:366–73.
37. Gingrich JR, Barrios RJ, Kattan MW, Nahm HS, Finegold MJ, Greenberg NM. Androgen-independent prostate cancer progression in the TRAMP model. Cancer Res 1997;57:4687–91.
38. Blando J, Moore T, Hursting S, Jiang G, Saha A, Beltran L, et al. Dietary energy balance modulates prostate cancer progression in Hi-Myc mice. Cancer Prev Res 2011;4:2002–14.
39. Powolny AA, Wang S, Carlton PS, Hoot DR, Clinton SK. Interrelationships between dietary restriction, the IGF-I axis, and expression of vascular endothelial growth factor by prostate adenocarcinoma in rats. Mol Carcinog 2008;47:458–65.